PERFORMANCE EVALUATION / DOWNTIME ANALYSIS OF A FLOATING LIQUEFIED NATURAL GAS FACILITY

A Thesis

by

YONG SUK CHO

Submitted to the Office of Graduate and Professional Studies of
Texas A&M University
in partial fulfillment of the requirements for the degree of

MASTER OF SCIENCE

Chair of Committee,	Moo-Hyun Kim
Committee Members,	Robert E. Randall
	Achim Stoessel
Head of Department,	Robin Autenreith

August 2015

Major Subject: Ocean Engineering

ABSTRACT

Numerical modeling of a particular Floating Liquefied Natural Gas (FLNG) facility, targeting on Prelude FLNG, was done to find an appropriate design of the FLNG including downtime in the specific field conditions. Hull/mooring coupled FLNG models with different vertical mass distributions (represented by the center of gravity's vertical coordinates, ZCGs) are tested under complex environmental conditions of sea-wave, wind, current, and swell.

WAMIT is used for the hydrodynamic analysis in frequency domain, and the time-series of motions under swell-excluded conditions are obtained by using CHARM3D. The time-series of linear swell-induced motions are separately obtained from the Response Amplitude Operators (RAOs, results form WAMIT). The consequential time-series of motions for the combined conditions are obtained by linearly superposing the two separate results.

Each of the two split environmental conditions shows very distinct effects on roll motion about the varied ZCGs. Thus, the test results enable to estimate the proper natural periods for the floating system, which provides a reference model for further analyses of several modifications under practical assumptions.

One scenario assumes a design modification with reduced weight in the topside facilities, which roughly reflects a conceptual design of the FLNG introduced by Shell. The other scenario is more practical, assuming an operational stage of less stored volume, by simply reducing the hull weight. The motional characteristics differentiated by these

two scenarios are investigated through their annual performances based on two heading strategies.

Performance evaluation can be done by estimating the downtime of the FLNG. In this study, the typical operation limits for topside facilities of FLNGs, 2° of roll/pitch, are compared with the maximum magnitudes of the roll/pitch angles during 3-hour time series of motion. From a sample of metocean data, only dominant waves that can cause downtime are employed to check the possibility of downtime, while the minor wave system's joint conditions are excluded. Once the excessive weather conditions that induce downtime are defined by the combinations of Tp (peak period of waves) and Hs (significant wave height), the total downtime periods including recovery hours can be estimated throughout a year.

As a result, the operability of the FLNG was very sensitive to the variation of topside weights, whereas the lighter-hull assumption brought negligible differences. These outcomes consequently demonstrate that the natural periods of an offshore system should be properly tuned based on the local sea states, and any modification of topside designs that includes nontrivial weight changes requires careful analysis. Moreover, the FLNG heading strategy by Dynamic Positioning (DP) system may have great impact on the operability, and seasonally-varied heading strategies are recommended for the FLNG to minimize downtime.

DEDICATION

To my wife, Jiyoung

ACKNOWLEDGEMENTS

I wish to express my sincere gratitude to Dr. M.H. Kim, for his guidance and unceasing inspiration throughout the course of this research. I also deeply appreciate my committee members, Dr. Randall, and Dr. Stössell, for their encouragement and valuable advice.

Thanks also go to my friends and colleagues and the department faculty and staff for sharing their ideas and knowledge, and for making my time at Texas A&M University a great experience. I also want to extend my appreciation to KOGAS, which allowed me this great opportunity; I sincerely thank Dr. H.M. Lee and all other members in Samcheok Terminal.

Last but not least, heartfelt thanks to my wife and our parents, for their patience and love during the last two years.

TABLE OF CONTENTS

Page

LIST OF FIGURES

Page

LIST OF TABLES

Page

CHAPTER I

INTRODUCTION

1.1. Background and Motivation

The oil and gas industry is approaching a new era of LNG FPSO (Floating Production, Storage and Offloading unit), which is widely called FLNG, Floating Liquefied Natural Gas. Figure 1 shows the LNG value chain when FLNG is introduced, comparing with the conventional value chain. FLNG is an integrated offshore system of production, liquefaction, storage and offloading for the upstream of LNG business. Because of the wide functionality, performance of an FLNG should be carefully studied during its design phases. This gives a good reason for studies on performance evaluation of an FLNG in practice.

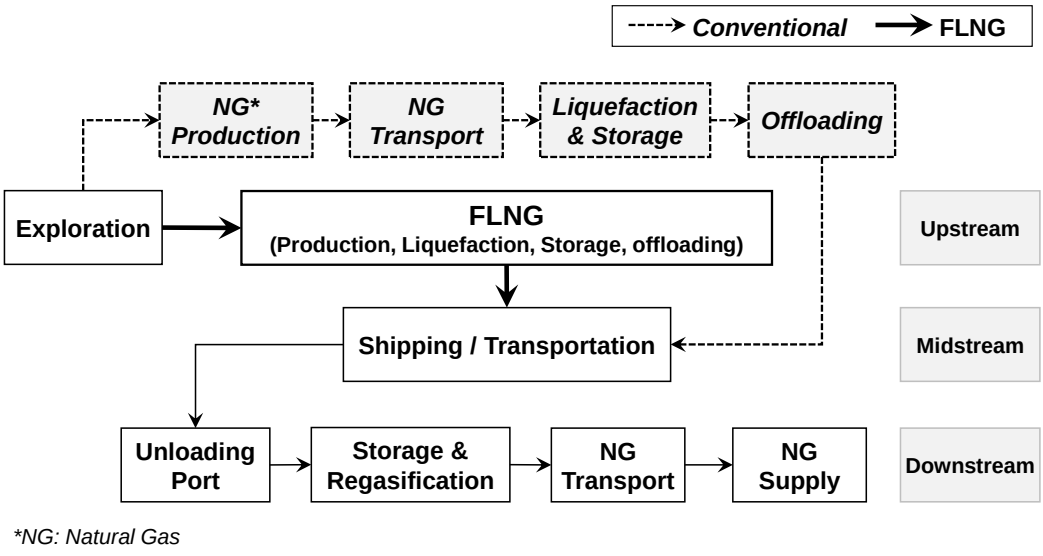

Figure 1. LNG value chain (Conventional vs. FLNG), revised from McDonald, L. (IBC Energy), 2013, 7th Annual FLNG Conference, Seoul, Korea.

Performance of a floating system can be typically evaluated by estimating its downtime. Because an FLNG is a combined system from production to offloading, downtime analysis of an FLNG can be done in various aspects. While large motion at topside facilities is one of the typical causes of the production downtime due to harsh weather conditions (Rice, 1985), another reason that leads to shutdown is exceedance of storage capacity due to offloading delay. The shutdown due to excessive storage is so-called "tank top," and is typically studied during the design phase to assess required storage capacity of the FLNG. Additionally, the maintenance, breakdown, or unexpected composition of the feed-gas may cause downtime.

However, this study is mainly focusing on the downtime due to severe weather conditions, which is often called 'weather downtime'. More specifically, the malfunction of the topside process due to excessive tilting motions is only considered through this study.

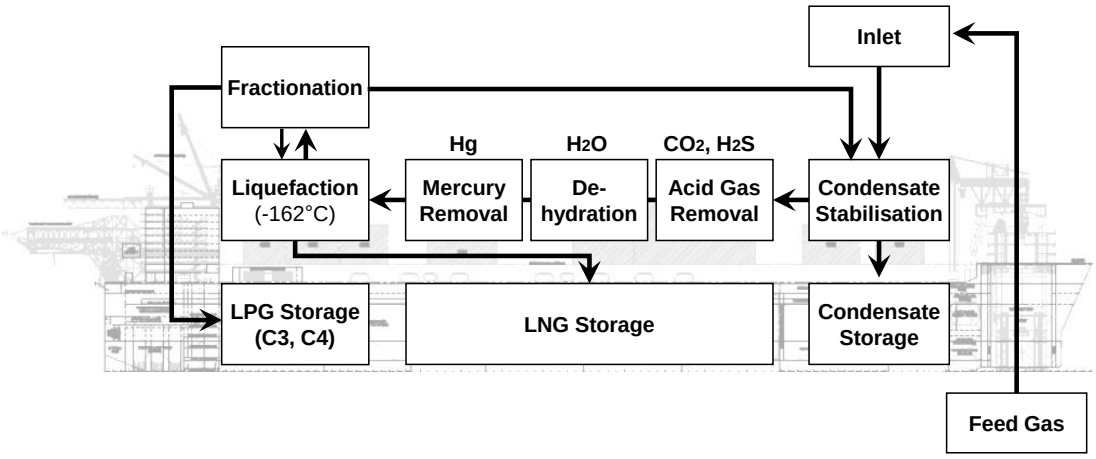

Figure 2. Schematic process flow of FLNGs (Background image source: Pek, B. and Velder, H.v.d., 2013, LNG 17, Houston, U.S.A.)

The overall topside process of FLNGs (Figure 2) should be similar to that of FPSOs except some liquefaction-related systems. Having a fractionating column, which is known as the most sensitive to body motion in general, the typical operation limits for FLNGs are 2 degrees of roll/pitch angles, and 5 degrees for FPSOs (Xia, 2012, and Khaw, 2005). These are the typical maximum limits of the operable conditions if the specific limiting-criterion are not given for the particular topside facilities but what is better is to find those values by specified experiments during engineering phases. The maximum angles are considered together with another limit of the static angles (1 degree of mean roll/pitch), known as much important as the maximum tilts, as double thresholds for the operability.

In order to conduct downtime analysis, the first step is to target one specific project. Currently there is no FLNG in operational states but only a few projects are under construction at particular regions (Figure 3).

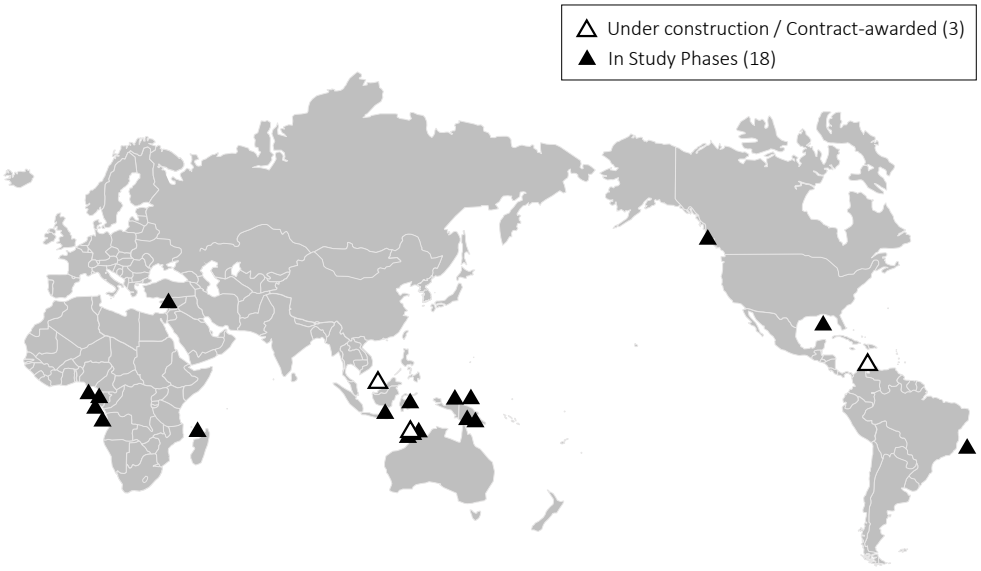

Figure 3. Locations of ongoing FLNG projects, reproduced from the presentation given by Paul C. Young (EXMAR), 7th Annual FLNG Conference, Seoul, 2013

While the West Africa and the Timor Sea are the most popular regions for the ongoing FLNG projects, the Prelude FLNG is targeted for this study. Prelude FLNG is going to be located in the offshore field approximately 200km off North West Australia (water depth: 250m, latitude: 13°47’25.53”S, longitude: 123°19’55.09”E), and beginning its operation in 2016. By targeting this project, which is known as the world-first FLNG project, enough information was expected to be available. However, even if there is any inaccessible key-information, it may also be a good subject of study to fill out the missing information by evaluating different designs of the FLNG in practice.

1.2. Research Objectives

The main purpose of the present study is to learn how to evaluate performance of an FLNG by estimating its downtime and operability. But the operability of the targeted FLNG cannot be accurately predicted without a validation from experience, unless sufficient background data is provided. Nevertheless, the existing FPSOs give us valuable lessons about a design philosophy to minimize downtime in adverse weather conditions (Xia, 2012). Taking the given lessons into account, differences in performance of varied FLNG designs from hypothetical scenarios are going to be studied based on the methodology of downtime analysis.

Consequently, the effect of design changes in general aspects, and a proper design of an FLNG for the specific field-condition are also expected to be learned. The following steps are taken through this study on these purposes.

1) Numerical modeling of hull/mooring coupled system

- Geometry of submerged body surface into discretized panels
- Calculation of mass matrices differentiated by vertical weight distributions
- Mooring lines coupled with the body, with drag plates and wind area sets

2) Simplification of the environmental condition

- Obtaining a sample data set of sea-wave, swell-wave, wind and current
- Wave scatter diagrams of least variables to define downtime conditions

3) Hydrodynamic analysis

- Frequency-domain analysis by using WAMIT
- Time-domain analysis of hull/mooring coupled system by using CHARM3D

Examples of performance evaluation on a weathervaning FLNG/FPSO are found from the offshore-engineering industry. Vestbostad et al (2002) presented a method to predict extreme roll motions using semi-empirical RAOs and statistics, focusing on varied heading strategies. They linearly superposed the roll motions separately induced by wind-sea and swell, and several extreme conditions were considered rather than estimating downtime. Ewans et al (2003, 2006) focused more on the weather condition, accurately decomposed into wind-sea and swell. Responses of an FLNG were taken from a look-up table provided by Maritime Research Institute Netherlands (MARIN), based on model tests.

On the other hand, direct time domain analysis was applied to estimate downtime of a Floating Storage and Regasification Unit (FSRU) by Wilde et al (2009), mainly focusing on accurate motions including non-linearity (second order calculation). They used 200 PCs as a computer cluster to run more than 17,000 cases of 4-hour time-simulations, representing offloading work during 6 years of North Sea environment. Taking the complete work scenarios into account, the study shows more complex analysis in realistic traces of time.

More recently, application of downtime analysis for a comparative study on roll-suppression device for an LNG FPSO was presented by Lee et al (2010). Wave scatter diagrams were used for describing joint-occurrences of non-exceedance levels, by comparing the typical roll limit (max. 2°) to the response, calculated by multiplying the RAOs and the corresponding wave spectra about varied directions.

The schematic approach of the present study is similar to the way of downtime analysis, applied for the comparative study, by Lee et al (2010). However, in this study, the environmental condition is decomposed into wind-sea and swell, in order to reflect the typical conditions in the Southern Hemisphere. Also, time-simulations including nonlinear effects are conducted so that the dynamic motions are more accurately obtained. Moreover, recovery-hours will be considered by analyzing the sequence of downtime conditions throughout a 1-year data.

CHAPTER II

NUMERICAL MODEL

2.1. Introduction

In this chapter, the FLNG is modeled based on the information collected from open sources including reasonable assumptions for some parts of its detail. Even though the numerical models created in this chapter are not perfectly replicating the targeted FLNG, they provide enough basis not only for the comparative study but also to investigate the design in regard to the field-specific environmental condition, on the research purposes.

2.2. Geometric Data

First, a body-fixed coordinate system with its origin at the mid-point of the waterline length is defined so the rotational axis of the turret is defined as (x, y)=(211, 0). Figure 4 shows the coordinate system and sign convention used throughout this study.

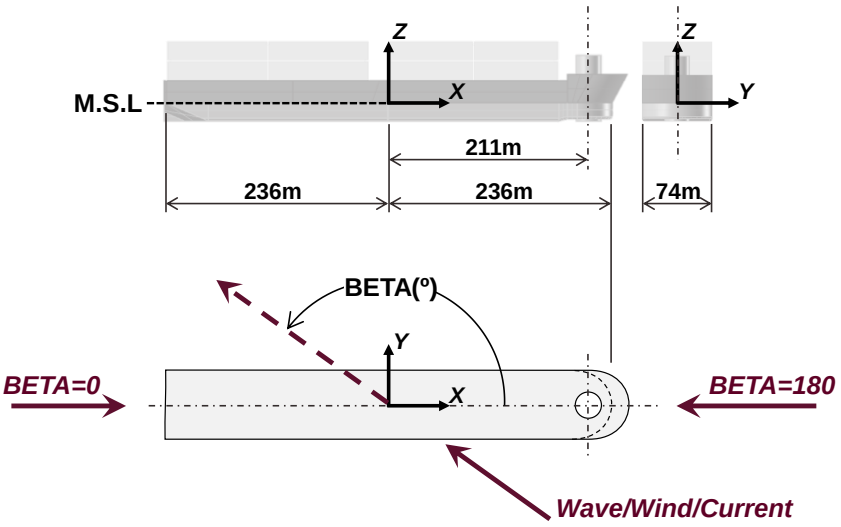

Figure 4. Definition of the body-fixed coordinate system (top) and the sign convention of environmental forces in WAMIT and CHARM3D (bottom)

The information of the water depth at the project location, and the principal dimensions of the FLNG are collected. The displacement of the FLNG is known as around 600,000 m^3, and up to 661,400 m^3 when it is fully laden (media-release by Shell), and the draft is known as in the range between 17m and 20m. The details of the FLNG's body structure are approximated by targeting the maximum displacement with the maximum draft (20m) following the collected information. Then, again, targeting the displacement within the given range, a constant draft (19m) is assumed for this research as a design draft for the FLNG. Then, the displacement and the total weight are calculated from the 3D model of the submerged hull structure. The main particulars of the FLNG's hull obtained from the pre-described steps above are presented in Table 1.

Table 1. Main particulars of the FLNG hull

Designation	*Symbol*	*Quantity*	*Unit*	*Source*
Overall Length		488.00	m	Pek et al. (Shell), 2013 LNG 17 Conference
Length between perpendiculars	L	472.00	m	
Breadth	B	74.00	m	
Depth of Hull	D	43.00	m	
Draft	T	19.00	m	given: 17~20m
Displacement	V	627,904.00	m^3	3D surface modeling
Center of Buoyancy above Base	FB	9.71	m	
Water Plane Area	A	34,332.75	m^2	
Length/Beam Ratio	L/B	6.38		
Draft/Length Ratio	T/L	0.04		
Beam/Draft Ratio	B/T	3.89		
Beam/Depth Ratio	B/D	1.72		
Block Coefficient	Cb	0.95		Cb=V/(L·B·T)
Water Plane Coefficient	Cw	0.98		Cw=A/(L·B)

The wetted surface of the submerged hull is then meshed by 3,096 panels (Figure 5) to set the body boundary condition for the hydrodynamic analysis, and the coordinates of the panels' vertices are collected to form a set of geometric data as an input to WAMIT.

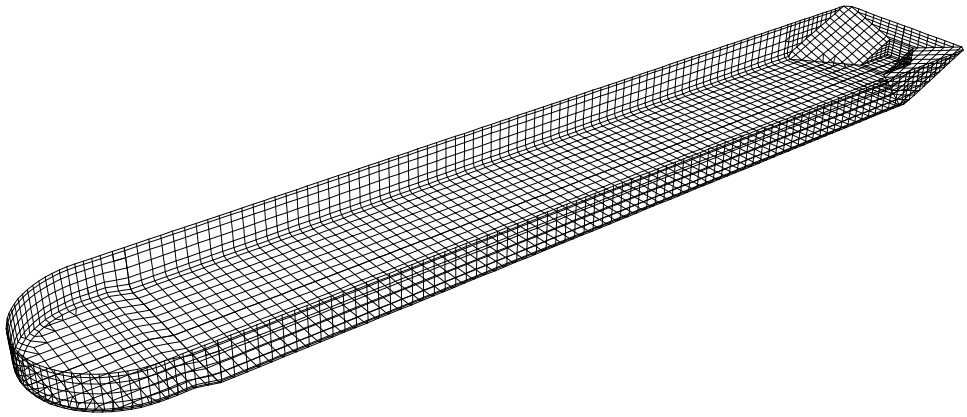

Figure 5. The wetted surface discretized into 3,096 panels for the FLNG of 19m-draft

On the other hand, the information about its weight distribution, or the center of gravity (CG) is not accessible but the turret weight, and the light weight are roughly informed. Since the missing information is one of the key-parameters that may determine its motion, it should not be just roughly assumed but more careful investigation is required. Thus, in order to find an appropriate design, FLNG models of varied mass distributions are going to be modeled in this chapter so that they can be compared later from the numerical test of simulations.

2.3. Mass Matrices

A mass matrix, *M*, which consists of 10 independent parameters including mass, center of gravity's coordinates, and products of inertia. It is defined as follows.

$$M = \begin{bmatrix} m & 0 & 0 & 0 & mz_{B,g} & -my_{B,g} \\ 0 & m & 0 & -mz_{B,g} & 0 & mx_{B,g} \\ 0 & 0 & m & my_{B,g} & -mx_{B,g} & 0 \\ 0 & -mz_{B,g} & my_{B,g} & (I_{YY}^{B} + I_{ZZ}^{B}) & -I_{YX}^{B} & -I_{ZX}^{B} \\ mz_{B,g} & 0 & -mx_{B,g} & -I_{XY}^{B} & (I_{ZZ}^{B} + I_{XX}^{B}) & -I_{ZY}^{B} \\ -my_{B,g} & mx_{B,g} & 0 & -I_{XZ}^{B} & -I_{YZ}^{B} & (I_{XX}^{B} + I_{YY}^{B}) \end{bmatrix} \quad \textbf{(1)}$$

where

$\vec{x}_{B,g} = (x_{B,g}, y_{B,g}, z_{B,g})$ are the center of gravity's coordinates about the body-fixed coordinate system, The center of gravity's coordinates can be defined as follows.

$$x_{B,g} = \frac{\iiint_{V_B} x_B \, dm}{\iiint_{V_B} dm} \qquad y_{B,g} = \frac{\iiint_{V_B} y_B \, dm}{\iiint_{V_B} dm} \qquad z_{B,g} = \frac{\iiint_{V_B} z_B \, dm}{\iiint_{V_B} dm} \quad \textbf{(2)}$$

$(I_{XX}^{B}, I_{YY}^{B}, I_{ZZ}^{B}, I_{XY}^{B} = I_{YX}^{B}, I_{XZ}^{B} = I_{YZ}^{B}, I_{ZY}^{B})$ are the products of inertia relative to the body-fixed coordinate system, which can be defined as follows.

$$I_{XX}^{B} = \iiint_{V_B} x_B^2 \, dm \qquad I_{XY}^{B} = I_{YX}^{B} = \iiint_{V_B} x_B y_B \, dm$$

$$I_{YY}^{B} = \iiint_{V_B} y_B^2 \, dm \qquad I_{XZ}^{B} = I_{ZX}^{B} = \iiint_{V_B} x_B z_B \, dm \quad \textbf{(3)}$$

$$I_{ZZ}^{B} = \iiint_{V_B} z_B^2 \, dm \qquad I_{YZ}^{B} = I_{ZY}^{B} = \iiint_{V_B} y_B z_B \, dm$$

Discretizing the whole body into *N* components, volume moments of each part can be calculated. Assuming the density of each component of the body is uniformly distributed, mass distribution and the center of gravity of the body can be manipulated by changing the density of each part. In order to make a mass matrix, the products of inertia can be obtained by adding up each volume moment multiplied by its corresponding density as follows.

$$I_{XY}^{B} = I_{YX}^{B} = \iiint_{V_B} x_B y_B \, dm = \iiint_{V_B} x_B y_B \, dV \frac{dm}{dV} \equiv \sum_{i=1}^{N} \left({I'}_{XY,i}^{B} \times \frac{m_i}{V_i} \right)$$

$$I_{XZ}^{B} = I_{ZX}^{B} = \iiint_{V_B} x_B z_B \, dm = \iiint_{V_B} x_B z_B \, dV \frac{dm}{dV} \equiv \sum_{i=1}^{N} \left({I'}_{XZ,i}^{B} \times \frac{m_i}{V_i} \right) \quad \textbf{(4)}$$

$$I_{YZ}^{B} = I_{ZY}^{B} = \iiint_{V_B} y_B z_B \, dm = \iiint_{V_B} y_B z_B \, dV \frac{dm}{dV} \equiv \sum_{i=1}^{N} \left({I'}_{YZ,i}^{B} \times \frac{m_i}{V_i} \right)$$

where ${I'}_{XY,i}^{B}$ is the volume product moment of i_{th} component of the body. N is the number of discretized components of the body, m_i is the mass of i_{th} component of the body, and V_i is the volume of i_{th} component of the body.

Based on the available information, several models of different vertical mass distributions can be considered for the FLNG designs. In order to generate the FLNG models of varied ZCG (z-coordinate of CG), excluding any other contribution but the effect of vertical distribution of the mass, the FLNG model is intentionally discretized into the 5 components of sub-volumes as described in Figure 6. It is assumed that the each

component of the body has uniform density so that the mass distribution of the body can be manipulated by adjusting the densities of the body components.

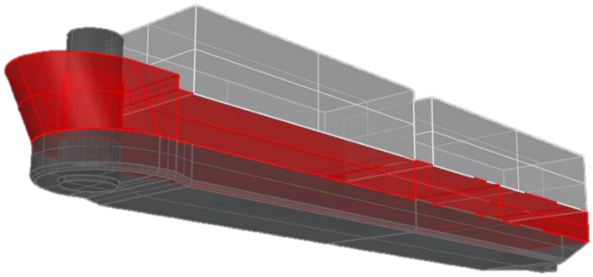

Figure 6. Volume distribution into 5 parts (3D drawing by using Rhino): Lower hull, Upper hull, Topside front, Topside back, and Turret

In this study, the weights of the topside (front + back) and the turret are fixed at approximated values based on the collected information. Figure 6 shows the volume model that consists of five sub-volumes; each weight of the body components is assumed to be uniformly distributed. The vertical position of the center of gravity can be controlled by adjusting the weight distribution between the upper hull and the lower hull, while the weight distribution between the two topsides can be used for maintaining the horizontal position of the CG at the same position as the center of buoyancy's.

By utilizing the constant values of the volume product moments and the centroids, total 8 mass models are generated by targeting ZCGs of the FLNG from 4m to 11m by every 1m. The volume properties, which are fixed through the 8 different cases of modeling, is presented in Table 2, followed by the mass products of inertia calculation results for the FLNG models varied by their vertical mass distributions (Table 3~10).

Table 2. Discretized volume properties (draft=19m)

		Upper Hull	*Lower Hull*	*Topside Front*	*Topside Back*	*Turret*	*Total*
Volume Centroid	***X***	1.170	-4.542	89.770	-126.613	211	
	Y	0.000	0.000	0.000	0.000	0	
	Z	11.943	-9.301	44.000	44.000	15.25	
Volume [m3]		8.0680E+05	6.1782E+05	5.5801E+05	6.6271E+05	3.7781E+04	2.6831E+06
Volume product moments	$I'^{B}_{XX,i}$	1.5131E+10	1.0157E+10	5.9957E+09	1.3135E+10	1.6837E+09	
	$I'^{B}_{YY,i}$	3.6851E+08	2.7704E+08	2.5464E+08	3.0241E+08	1.6582E+06	
	$I'^{B}_{ZZ,i}$	1.5430E+08	7.1675E+07	1.1623E+09	1.3804E+09	2.3560E+07	
	$I'^{B}_{XY,i}$	-1.2159E+01	-9.8608E+00	1.1950E-03	-3.7298E-02	0.0000E+00	
	$I'^{B}_{YZ,i}$	-9.2088E-01	5.0000E-01	6.3618E-03	1.7163E-02	0.0000E+00	
	$I'^{B}_{ZX,i}$	8.9256E+07	2.2047E+07	2.2041E+09	-3.6919E+09	1.2157E+08	

Table 3. Mass distribution of the FLNG with ZCG=4m

		Upper Hull	*Lower Hull*	*Topside Front*	*Topside Back*	*Turret*	*Total*
Center of Gravity	***XCG***	1.170	-4.542	89.770	-126.613	211	**-0.833851**
	YCG	0.000	0.000	0.000	0.000	0	**0.000000**
	ZCG	11.943	-9.301	44.000	44.000	15.25	**4.000000**
Fixed weight %		84.60%		14.00%		1.41%	100.00%
weight %		25.87%	58.73%	7.53%	6.47%	1.40%	100.00%
mass [kg]		1.6648E+08	3.7800E+08	4.8491E+07	4.1613E+07	9.0104E+06	6.4360E+08
mass/volume		206.349	611.839	86.900	62.793	238.492	239.871
Mass Products of Inertia	I^{B}_{XX}	3.1223E+12	6.2143E+12	5.2103E+11	8.2476E+11	4.0155E+11	**1.1084E+13**
	I^{B}_{YY}	7.6042E+10	1.6950E+11	2.2128E+10	1.8990E+10	3.9547E+08	**2.8706E+11**
	I^{B}_{ZZ}	3.1840E+10	4.3854E+10	1.0101E+11	8.6680E+10	5.6187E+09	**2.6900E+11**
	I^{B}_{XY}	-2.5089E+03	-6.0332E+03	1.0385E-01	-2.3420E+00	0.0000E+00	**-8.5444E+03**
	I^{B}_{YZ}	-1.9002E+02	3.0592E+02	5.5284E-01	1.0777E+00	0.0000E+00	**1.1753E+02**
	I^{B}_{ZX}	1.8418E+10	1.3489E+10	1.9153E+11	-2.3183E+11	2.8993E+10	**2.0608E+10**

Table 4. Mass distribution of the FLNG with ZCG=5m

		Upper Hull	*Lower Hull*	*Topside Front*	*Topside Back*	*Turret*	*Total*
Center of Gravity	***XCG***	1.170	-4.542	89.770	-126.613	211	**-0.833851**
	YCG	0.000	0.000	0.000	0.000	0	**0.000000**
	ZCG	11.943	-9.301	44.000	44.000	15.25	**5.000000**
Fixed weight %		84.60%		14.00%		1.41%	100.00%
weight %		30.57%	54.03%	7.41%	6.59%	1.40%	100.00%
mass [kg]		1.9678E+08	3.4771E+08	4.7691E+07	4.2413E+07	9.0104E+06	6.4360E+08
mass/volume		243.899	562.803	85.467	64.000	238.492	239.871
Mass Products of Inertia	I^B_{XX}	3.6905E+12	5.7163E+12	5.1244E+11	8.4061E+11	4.0155E+11	**1.1161E+13**
	I^B_{YY}	8.9879E+10	1.5592E+11	2.1763E+10	1.9354E+10	3.9547E+08	**2.8731E+11**
	I^B_{ZZ}	3.7635E+10	4.0339E+10	9.9341E+10	8.8346E+10	5.6187E+09	**2.7128E+11**
	I^B_{XY}	-2.9655E+03	-5.5497E+03	1.0213E-01	-2.3870E+00	0.0000E+00	**-8.5175E+03**
	I^B_{YZ}	-2.2460E+02	2.8140E+02	5.4372E-01	1.0984E+00	0.0000E+00	**5.8442E+01**
	I^B_{ZX}	2.1769E+10	1.2408E+10	1.8838E+11	-2.3628E+11	2.8993E+10	**1.5265E+10**

Table 5. Mass distribution of the FLNG with ZCG=6m

		Upper Hull	*Lower Hull*	*Topside Front*	*Topside Back*	*Turret*	*Total*
Center of Gravity	***XCG***	1.170	-4.542	89.770	-126.613	211	**-0.833851**
	YCG	0.000	0.000	0.000	0.000	0	**0.000000**
	ZCG	11.943	-9.301	44.000	44.000	15.25	**6.000000**
Fixed weight %		84.60%		14.00%		1.41%	100.00%
weight %		35.28%	49.32%	7.29%	6.71%	1.40%	100.00%
mass [kg]		2.2707E+08	3.1741E+08	4.6892E+07	4.3213E+07	9.0104E+06	6.4360E+08
mass/volume		281.449	513.767	84.034	65.206	238.492	239.871
Mass Products of Inertia	I^B_{XX}	4.2587E+12	5.2182E+12	5.0385E+11	8.5645E+11	4.0155E+11	**1.1239E+13**
	I^B_{YY}	1.0372E+11	1.4233E+11	2.1398E+10	1.9719E+10	3.9547E+08	**2.8756E+11**
	I^B_{ZZ}	4.3429E+10	3.6824E+10	9.7675E+10	9.0012E+10	5.6187E+09	**2.7356E+11**
	I^B_{XY}	-3.4220E+03	-5.0662E+03	1.0042E-01	-2.4320E+00	0.0000E+00	**-8.4905E+03**
	I^B_{YZ}	-2.5918E+02	2.5688E+02	5.3461E-01	1.1191E+00	0.0000E+00	**-6.4401E-01**
	I^B_{ZX}	2.5121E+10	1.1327E+10	1.8522E+11	-2.4074E+11	2.8993E+10	**9.9227E+09**

Table 6. Mass distribution of the FLNG with ZCG=7m

		Upper Hull	*Lower Hull*	*Topside Front*	*Topside Back*	*Turret*	*Total*
Center of Gravity	***XCG***	1.170	-4.542	89.770	-126.613	211	**-0.833851**
	YCG	0.000	0.000	0.000	0.000	0	**0.000000**
	ZCG	11.943	-9.301	44.000	44.000	15.25	**7.000000**
Fixed weight %		84.60%		14.00%		1.41%	100.00%
weight %		39.99%	44.61%	7.16%	6.84%	1.40%	100.00%
mass [kg]		2.5737E+08	2.8712E+08	4.6092E+07	4.4012E+07	9.0104E+06	6.4360E+08
mass/volume		318.999	464.731	82.601	66.413	238.492	239.871
Mass Products of Inertia	I^B_{XX}	4.8268E+12	4.7202E+12	4.9525E+11	8.7230E+11	4.0155E+11	**1.1316E+13**
	I^B_{YY}	1.1755E+11	1.2875E+11	2.1033E+10	2.0084E+10	3.9547E+08	**2.8782E+11**
	I^B_{ZZ}	4.9223E+10	3.3310E+10	9.6010E+10	9.1677E+10	5.6187E+09	**2.7584E+11**
	I^B_{XY}	-3.8786E+03	-4.5826E+03	9.8708E-02	-2.4770E+00	0.0000E+00	**-8.4636E+03**
	I^B_{YZ}	-2.9376E+02	2.3237E+02	5.2549E-01	1.1398E+00	0.0000E+00	**-5.9730E+01**
	I^B_{ZX}	2.8473E+10	1.0246E+10	1.8206E+11	-2.4519E+11	2.8993E+10	**4.5799E+09**

Table 7. Mass distribution of the FLNG with ZCG=8m

		Upper Hull	*Lower Hull*	*Topside Front*	*Topside Back*	*Turret*	*Total*
Center of Gravity	***XCG***	1.170	-4.542	89.770	-126.613	211	**-0.833851**
	YCG	0.000	0.000	0.000	0.000	0	**0.000000**
	ZCG	11.943	-9.301	44.000	44.000	15.25	**8.000000**
Fixed weight %		84.60%		14.00%		1.41%	100.00%
weight %		44.70%	39.90%	7.04%	6.96%	1.40%	100.00%
mass [kg]		2.8766E+08	2.5682E+08	4.5292E+07	4.4812E+07	9.0104E+06	6.4360E+08
mass/volume		356.549	415.694	81.168	67.619	238.492	239.871
Mass Products of Inertia	I^B_{XX}	5.3950E+12	4.2221E+12	4.8666E+11	8.8815E+11	4.0155E+11	**1.1393E+13**
	I^B_{YY}	1.3139E+11	1.1516E+11	2.0668E+10	2.0449E+10	3.9547E+08	**2.8807E+11**
	I^B_{ZZ}	5.5017E+10	2.9795E+10	9.4344E+10	9.3343E+10	5.6187E+09	**2.7812E+11**
	I^B_{XY}	-4.3352E+03	-4.0991E+03	9.6995E-02	-2.5220E+00	0.0000E+00	**-8.4367E+03**
	I^B_{YZ}	-3.2834E+02	2.0785E+02	5.1637E-01	1.1605E+00	0.0000E+00	**-1.1882E+02**
	I^B_{ZX}	3.1824E+10	9.1650E+09	1.7890E+11	-2.4964E+11	2.8993E+10	**-7.6284E+08**

Table 8. Mass distribution of the FLNG with ZCG=9m

		Upper Hull	*Lower Hull*	*Topside Front*	*Topside Back*	*Turret*	*Total*
Center of Gravity	***XCG***	1.170	-4.542	89.770	-126.613	211	**-0.833851**
	YCG	0.000	0.000	0.000	0.000	0	**0.000000**
	ZCG	11.943	-9.301	44.000	44.000	15.25	**9.000000**
Fixed weight %		84.60%		14.00%		1.41%	100.00%
weight %		49.40%	35.20%	6.91%	7.09%	1.40%	100.00%
mass [kg]		3.1796E+08	2.2653E+08	4.4493E+07	4.5611E+07	9.0104E+06	6.4360E+08
mass/volume		394.099	366.658	79.735	68.826	238.492	239.871
Mass Products of Inertia	I^B_{XX}	5.9632E+12	3.7241E+12	4.7807E+11	9.0400E+11	4.0155E+11	**1.1471E+13**
	I^B_{YY}	1.4523E+11	1.0158E+11	2.0304E+10	2.0814E+10	3.9547E+08	**2.8832E+11**
	I^B_{ZZ}	6.0811E+10	2.6280E+10	9.2679E+10	9.5009E+10	5.6187E+09	**2.8040E+11**
	I^B_{XY}	-4.7917E+03	-3.6156E+03	9.5283E-02	-2.5671E+00	0.0000E+00	**-8.4097E+03**
	I^B_{YZ}	-3.6292E+02	1.8333E+02	5.0726E-01	1.1812E+00	0.0000E+00	**-1.7790E+02**
	I^B_{ZX}	3.5176E+10	8.0839E+09	1.7574E+11	-2.5410E+11	2.8993E+10	**-6.1056E+09**

Table 9. Mass distribution of the FLNG with ZCG=10m

		Upper Hull	*Lower Hull*	*Topside Front*	*Topside Back*	*Turret*	*Total*
Center of Gravity	***XCG***	1.170	-4.542	89.770	-126.613	211	**-0.833851**
	YCG	0.000	0.000	0.000	0.000	0	**0.000000**
	ZCG	11.943	-9.301	44.000	44.000	15.25	**10.000000**
Fixed weight %		84.60%		14.00%		1.41%	100.00%
weight %		54.11%	30.49%	6.79%	7.21%	1.40%	100.00%
mass [kg]		3.4825E+08	1.9623E+08	4.3693E+07	4.6411E+07	9.0104E+06	6.4360E+08
mass/volume		431.649	317.622	78.302	70.033	238.492	239.871
Mass Products of Inertia	I^B_{XX}	6.5314E+12	3.2260E+12	4.6948E+11	9.1985E+11	4.0155E+11	**1.1548E+13**
	I^B_{YY}	1.5907E+11	8.7994E+10	1.9939E+10	2.1179E+10	3.9547E+08	**2.8857E+11**
	I^B_{ZZ}	6.6605E+10	2.2766E+10	9.1013E+10	9.6674E+10	5.6187E+09	**2.8268E+11**
	I^B_{XY}	-5.2483E+03	-3.1320E+03	9.3571E-02	-2.6121E+00	0.0000E+00	**-8.3828E+03**
	I^B_{YZ}	-3.9750E+02	1.5881E+02	4.9814E-01	1.2019E+00	0.0000E+00	**-2.3699E+02**
	I^B_{ZX}	3.8527E+10	7.0028E+09	1.7258E+11	-2.5855E+11	2.8993E+10	**-1.1448E+10**

Table 10. Mass distribution of the FLNG with ZCG=11m

		Upper Hull	*Lower Hull*	*Topside Front*	*Topside Back*	*Turret*	*Total*
Center of Gravity	***XCG***	1.170	-4.542	89.770	-126.613	211	**-0.833851**
	YCG	0.000	0.000	0.000	0.000	0	**0.000000**
	ZCG	11.943	-9.301	44.000	44.000	15.25	**11.000000**
Fixed weight %		84.60%		14.00%		1.41%	100.00%
weight %		58.82%	25.78%	6.66%	7.34%	1.40%	100.00%
mass [kg]		3.7855E+08	1.6594E+08	4.2894E+07	4.7211E+07	9.0104E+06	6.4360E+08
mass/volume		469.199	268.586	76.869	71.239	238.492	239.871
Mass Products of Inertia	I^B_{XX}	7.0995E+12	2.7280E+12	4.6089E+11	9.3570E+11	4.0155E+11	**1.1626E+13**
	I^B_{YY}	1.7290E+11	7.4409E+10	1.9574E+10	2.1544E+10	3.9547E+08	**2.8883E+11**
	I^B_{ZZ}	7.2399E+10	1.9251E+10	8.9347E+10	9.8340E+10	5.6187E+09	**2.8496E+11**
	I^B_{XY}	-5.7048E+03	-2.6485E+03	9.1858E-02	-2.6571E+00	0.0000E+00	**-8.3559E+03**
	I^B_{YZ}	-4.3208E+02	1.3429E+02	4.8902E-01	1.2227E+00	0.0000E+00	**-2.9607E+02**
	I^B_{ZX}	4.1879E+10	5.9216E+09	1.6942E+11	-2.6301E+11	2.8993E+10	**-1.6791E+10**

The resultant mass matrices for the FLNG models calculated by varied targets of the vertical mass distributions, represented by ZCGs (4~11m), are collected below.

When

- ZCG=4m,

$$M = \begin{bmatrix} 6.436E+08 & 0 & 0 & 0 & 2.574E+09 & 0 \\ 0 & 6.436E+8 & 0 & -2.574E+09 & 0 & -5.367E+08 \\ 0 & 0 & 6.436E+08 & 0 & 5.367E+08 & 0 \\ 0 & -2.574E+9 & 0 & 5.561E+11 & 8.544E+03 & -2.061E+10 \\ 2.574E+09 & 0 & 5.367E+8 & 8.544E+03 & 1.135E+13 & -1.175E+02 \\ 0 & -5.367E+8 & 0 & -2.061E+10 & -1.175E+02 & 1.137E+13 \end{bmatrix}$$

- ZCG=5m,

$$M = \begin{bmatrix} 6.436E+08 & 0 & 0 & 0 & 3.218E+09 & 0 \\ 0 & 6.436E+08 & 0 & -3.218E+09 & 0 & -5.367E+08 \\ 0 & 0 & 6.436E+08 & 0 & 5.367E+08 & 0 \\ 0 & -3.218E+09 & 0 & 5.586E+11 & 8.517E+03 & -1.527E+10 \\ 3.218E+09 & 0 & 5.367E+08 & 8.517E+03 & 1.143E+13 & -5.844E+01 \\ 0 & -5.367E+08 & 0 & -1.527E+10 & -5.844E+01 & 1.145E+13 \end{bmatrix}$$

- ZCG=6m,

$$M = \begin{bmatrix} 6.436E+08 & 0 & 0 & 0 & 3.862E+09 & 0 \\ 0 & 6.436E+08 & 0 & -3.862E+09 & 0 & -5.367E+08 \\ 0 & 0 & 6.436E+08 & 0 & 5.367E+08 & 0 \\ 0 & -3.862E+09 & 0 & 5.611E+11 & 8.491E+03 & -9.923E+09 \\ 3.862E+09 & 0 & 5.367E+08 & 8.491E+03 & 1.151E+13 & 6.440E-01 \\ 0 & -5.367E+08 & 0 & -9.923E+09 & 6.440E-01 & 1.153E+13 \end{bmatrix}$$

- ZCG=7m,

$$M = \begin{bmatrix} 6.436E+08 & 0 & 0 & 0 & 4.505E+09 & 0 \\ 0 & 6.436E+08 & 0 & -4.505E+09 & 0 & -5.367E+08 \\ 0 & 0 & 6.436E+08 & 0 & 5.367E+08 & 0 \\ 0 & -4.505E+09 & 0 & 5.637E+11 & 8.464E+03 & -4.580E+09 \\ 4.505E+09 & 0 & 5.367E+08 & 8.464E+03 & 1.159E+13 & 5.973E+01 \\ 0 & -5.367E+08 & 0 & -4.580E+09 & 5.973E+01 & 1.160E+13 \end{bmatrix}$$

- ZCG=8m,

$$M = \begin{bmatrix} 6.436E+08 & 0 & 0 & 0 & 5.149E+09 & 0 \\ 0 & 6.436E+08 & 0 & -5.149E+09 & 0 & -5.367E+08 \\ 0 & 0 & 6.436E+08 & 0 & 5.367E+08 & 0 \\ 0 & -5.149E+09 & 0 & 5.662E+11 & 8.437E+03 & 7.628E+08 \\ 5.149E+09 & 0 & 5.367E+08 & 8.437E+03 & 1.167E+13 & 1.188E+02 \\ 0 & -5.367E+08 & 0 & 7.628E+08 & 1.188E+02 & 1.168E+13 \end{bmatrix}$$

- ZCG=9m,

$$M = \begin{bmatrix} 6.436E+08 & 0 & 0 & 0 & 5.792E+09 & 0 \\ 0 & 6.436E+08 & 0 & -5.792E+09 & 0 & -5.367E+08 \\ 0 & 0 & 6.436E+08 & 0 & 5.367E+08 & 0 \\ 0 & -5.792E+09 & 0 & 5.687E+11 & 8.410E+03 & 6.106E+09 \\ 5.792E+09 & 0 & 5.367E+08 & 8.410E+03 & 1.175E+13 & 1.779E+02 \\ 0 & -5.367E+08 & 0 & 6.106E+09 & 1.779E+02 & 1.176E+13 \end{bmatrix}$$

- ZCG=10m,

$$M = \begin{bmatrix} 6.436E+08 & 0 & 0 & 0 & 6.436E+09 & 0 \\ 0 & 6.436E+08 & 0 & -6.436E+09 & 0 & -5.367E+08 \\ 0 & 0 & 6.436E+08 & 0 & 5.367E+08 & 0 \\ 0 & -6.436E+09 & 0 & 5.713E+11 & 8.383E+03 & 1.145E+10 \\ 6.436E+09 & 0 & 5.367E+08 & 8.383E+03 & 1.183E+13 & 2.370E+02 \\ 0 & -5.367E+08 & 0 & 1.145E+10 & 2.370E+02 & 1.184E+13 \end{bmatrix}$$

- ZCG=11m,

$$M = \begin{bmatrix} 6.436E+08 & 0 & 0 & 0 & 7.080E+09 & 0 \\ 0 & 6.436E+08 & 0 & -7.080E+09 & 0 & -5.367E+08 \\ 0 & 0 & 6.436E+08 & 0 & 5.367E+08 & 0 \\ 0 & -7.080E+09 & 0 & 5.738E+11 & 8.356E+03 & 1.679E+10 \\ 7.080E+09 & 0 & 5.367E+08 & 8.356E+03 & 1.191E+13 & 2.961E+02 \\ 0 & -5.367E+08 & 0 & 1.679E+10 & 2.961E+02 & 1.191E+13 \end{bmatrix}$$

2.4. Mooring Lines

The mooring line configuration is taken from the approximate information given in the project's bidding notification of the 'Mooring Pre-lay Installation' package, closed by April 2013. The horizontal arrangement of the lines and the anchor positions are also approximated by the information collected from the Environmental Impact Statement (EIS, 2009, by Shell) Chapter 1, and relevant articles.

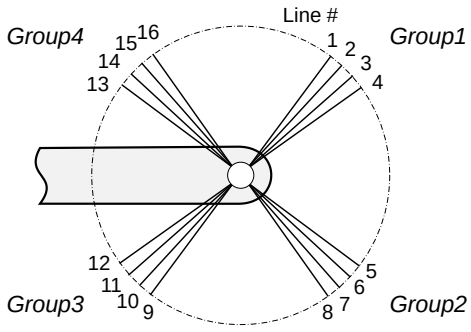

Figure 7. Mooring line configuration and the horizontal arrangement

The material properties of the chain and wire are calculated based on "Guide to Single Point Moorings" by Dr. Wichers (2013), and MIT Opencourse materials (2011), respectively. The properties, used as input data for CHARM3D simulations, are presented in Table 11. The catenary formation of mooring lines can be automatically adjusted during static analysis in CHARM3D, but a few properties have to be initially defined in the input data, which is a set of the fairlead position with unit vector, the anchor position, and the mooring tension for each line. In order to set this input, the catenary equations from "Sea Loads on Ships and Offshore Structures" by Dr. Faltinsen (1990) were used; Table 12 shows primary parts of the results.

Table 11. Mooring line material property (bending stiffness is zero)

	symbol	*unit*	*Chain (R4, Studless)*	*Wire (Strand)*
Diameter	D	mm	175	160
Outer diameter of equivalent line	OD	mm	315	160
Axial stiffness	AE	kN	2,615,375	2,304,000
Mass per unit length	RHOL	kg/m	609.44	132.86
Displaced mass per unit length	RHOA	kg/m	80.09	20.61
Inertia force per unit length	CI	N/m	159.76	41.22
Drag force per unit length	CD	N/m	395.52	200.90
Cross sectional area	AS	m^2	0.048	0.020

Table 12. Mooring line configuration assumed for CHARM3D inputs

	material	*length (m)*	*number of segments*	*length per segment (m)*	*initial tension at top segment (N)*
1. Bottom chain	chain	220	2	110	2,181,902
2. Ground Wire	wire	500	5	100	2,181,902
3. Touch down chain	chain	770	10	77	2,687,022
4. Mid water wire	wire	280	5	70~20	2,864,251
5. Top chain	chain	50	3	20~10	3,030,467
Total		1,820	25		

2.5. Drag Plates and Wind Areas

The submerged part of the transversal section is discretized into 3 plates along y-axis, and 20 plates were made from the longitudinal section along x-axis as shown in Figure 8. A uniform drag coefficient (Cd=2.0) is simply used for all directional cases. Collecting the geometric information and a drag term of each plate, the input data set for 19m-draft hull is all ready, in Table 13.

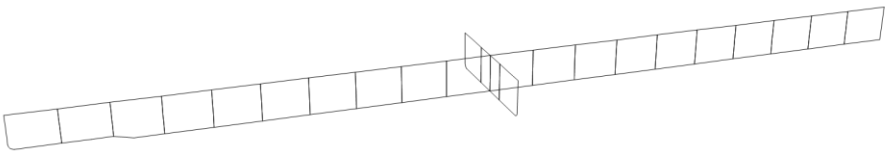

Figure 8. Drag plates in the submerged part of the FLNG (draft=19m)

Table 13. Drag plates information of the FLNGs (draft=19m)

Plate No.	$\frac{1}{2}\rho C_D A$	*center coordinates*			*unit normal vector*
		x	*y*	*z*	
1	465913.01	0.000	-24.964	-9.472	(1, 0, 0)
2	506350.00	0.000	0.000	-9.500	(1, 0, 0)
3	465913.01	0.000	24.964	-9.472	(1, 0, 0)
4	407324.14	224.159	0.000	-8.421	(0, 1, 0)
5	408817.53	200.600	0.000	-8.450	(0, 1, 0)
6	449895.70	176.812	0.000	-9.310	(0, 1, 0)
7	459610.00	153.400	0.000	-9.500	(0, 1, 0)
8	459610.00	129.800	0.000	-9.500	(0, 1, 0)
9	459610.00	106.200	0.000	-9.500	(0, 1, 0)
10	459610.00	82.600	0.000	-9.500	(0, 1, 0)
11	459610.00	59.000	0.000	-9.500	(0, 1, 0)
12	459610.00	35.400	0.000	-9.500	(0, 1, 0)
13	459610.00	11.800	0.000	-9.500	(0, 1, 0)
14	459610.00	-11.800	0.000	-9.500	(0, 1, 0)
15	459610.00	-35.400	0.000	-9.500	(0, 1, 0)
16	459610.00	-59.000	0.000	-9.500	(0, 1, 0)
17	459610.00	-82.600	0.000	-9.500	(0, 1, 0)
18	459610.00	-106.200	0.000	-9.500	(0, 1, 0)
19	459610.00	-129.800	0.000	-9.500	(0, 1, 0)
20	459610.00	-153.400	0.000	-9.500	(0, 1, 0)
21	459610.00	-177.000	0.000	-9.500	(0, 1, 0)
22	459610.00	-200.600	0.000	-9.500	(0, 1, 0)
23	459610.00	-224.200	0.000	-9.500	(0, 1, 0)

Projected areas above mean sea level, and the center coordinates for the wind direction 180°, 150°, 120°, and 90° are measured from the 3D surface model to represent the wind areas. The wind areas and input data sets for the representative wind directions are shown in Table 13 and Table 14, respectively. The other directional data of the areas and the center coordinates are interpolated, and a simplified drag coefficient (Cd=1.0) is used for all directions.

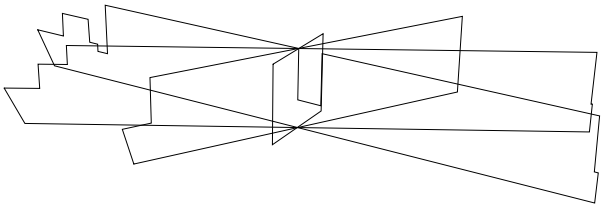

Figure 9. Wind areas of the direction 180°, 150°, 120°, and 90° in the order from the smallest area to the largest area

Table 14. Wind area information of the FLNGs (draft=19m)

BETA	*Area* (m^2)	*center coordinates*		
		x	*y*	*z*
180	4810.00	0.00	0.00	32.50
150	18131.73	-4.51	-7.81	31.99
120	27351.50	-8.74	-5.05	31.82
90	28423.41	-7.86	0.00	31.11

CHAPTER III

NUMERICAL TEST

3.1. Introduction

The hull/mooring coupled FLNG models of varied CG positions are tested in both frequency-domain and time-domain. By taking comparison of the responses under sea-wave/wind/current/swell combined condition, proper ranges of the design characteristics for the FLNG can be found, or evaluated when they are already given.

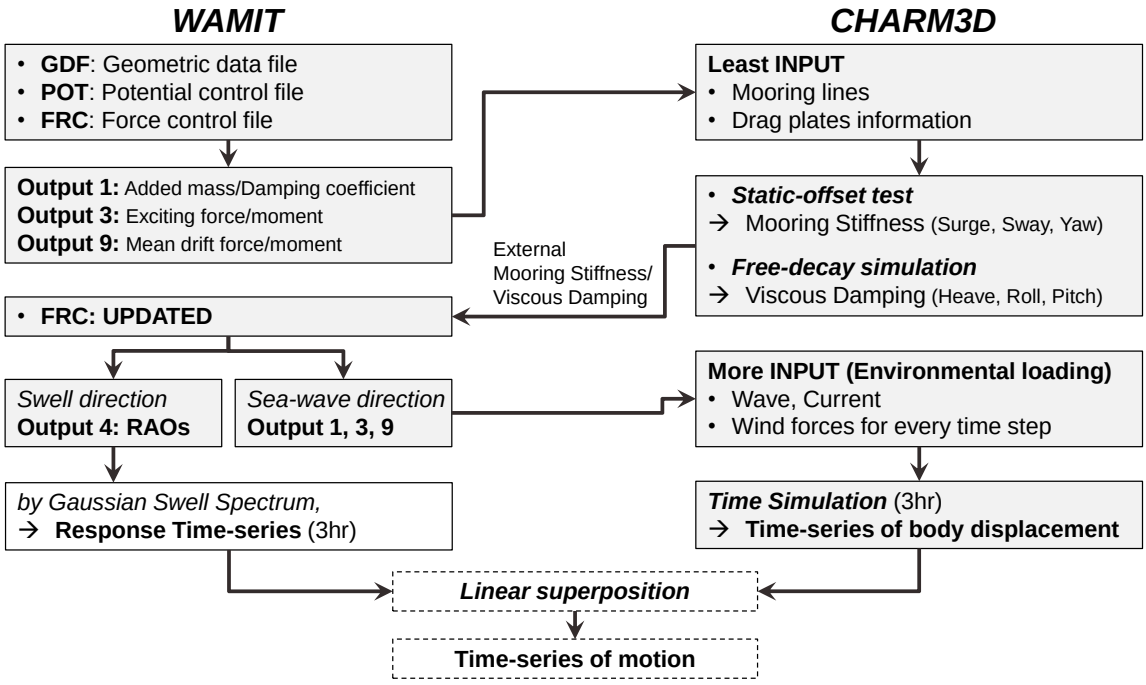

Figure 10. Procedure of numerical simulation specified for this study

In order to derive the time-series of motion under two wave conditions, swell-induced motion is separately obtained by linear theory and later superposed with the result from time-simulation of sea/wind/current-induced motion. The entire procedure specified

for this study is presented in Figure 10. This procedure is repeated for all of the numerical models of FLNG having varied CG positions, and under different environmental conditions.

3.2. Static-offset Test and Free-decay Simulation

Equivalent mooring stiffness of horizontal modes and viscous damping of heave/roll/pitch can be individually estimated by conducting static-offset tests and free-decay simulations, respectively. Taking the estimated mooring stiffness and damping coefficients as external stiffness and damping matrices back into WAMIT, more accurate results can be obtained.

Static-offset tests on the horizontal modes (surge, sway, and yaw) are conducted for one model (Figure 11) and the same results are taken for all of the other models regardless of the vertical mass distribution.

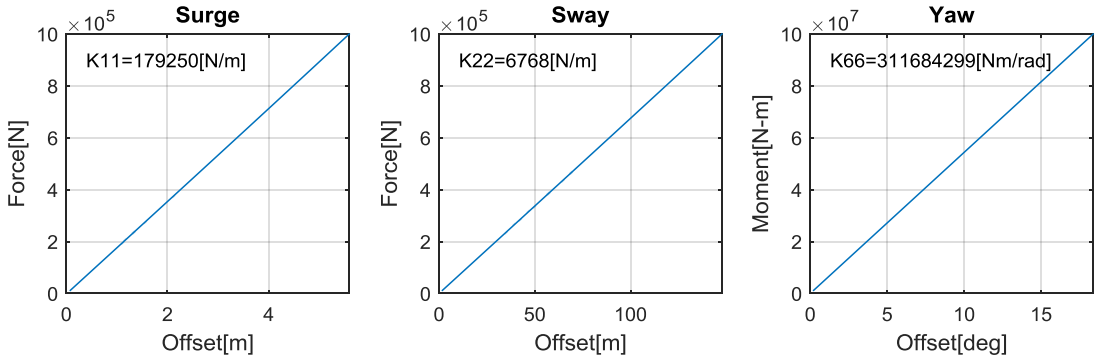

Figure 11. Static-offset tests

As a result of the static offset-tests, the equivalent mooring stiffness in those horizontal modes (K_{11}, K_{22}, K_{66}) are individually obtained by the slopes of the lines in Figure 11. Finally, the external stiffness matrix, *EXSTIF*, to update the input (force control file) in WAMIT is set as follows:

$$EXSTIF = \begin{bmatrix} 1.79e05 & & & & & \\ & 6.77e03 & & & & \\ & & 0 & & & \\ & & & 0 & & \\ & & & & 0 & \\ & & & & & 3.12e08 \end{bmatrix} \quad \textbf{(5)}$$

Meanwhile, free-decay simulations in the other three modes (Heave, Roll, and Pitch) are individually conducted to estimate the viscous damping, which is uncoupled. Below, the principal of a free-decay simulation and the interpretations of the outcomes are described, based on the course materials of OCEN676 (Dynamics of Offshore Structures) by Dr. Mercier.

The equation of motion for a viscously-damped free-vibration of a linear single-degree-of-freedom system can be described as $m\ddot{X} + b\dot{X} + kX = 0$, where the second term, $b\dot{X}$, represents the viscous damping force during free vibration. Then, the equation of motion can be expressed as follows when divided by the mass, *m*.

$$\ddot{X} + 2\zeta\omega_n\dot{X} + \omega_n^2 X = 0 \quad \textbf{(6)}$$

where

$$\omega_n = \sqrt{k/m} \ \ (k \text{ is the hydrostatic stiffness}) \quad \textbf{(7)}$$

$$\zeta = \frac{b}{2m\omega_n} = \frac{b}{b_r} = damping\ ratio \quad \textbf{(8)}$$

$$b_r = 2m\omega_n = 2\sqrt{km} = \frac{2k}{\omega_n} = critical\ damping\ coefficient \quad \textbf{(9)}$$

Substituting an exponential function about time as a general solution for the equation (6) lets the envelope of the displacement to become as follows.

$$X(t) = \pm\rho \cdot \exp(-\zeta\omega_n t) \quad \textbf{(10)}$$

where ρ is the amplitude of an un-damped vibration, which is

$$\rho = \sqrt{X(0)^2 + \left(\frac{\dot{X}(0) + \rho\omega_n X(0)}{\omega_D}\right)^2} \quad \textbf{(11)}$$

Noting that the peaks of a damped vibration meet the envelope curve, the ratio of the displacement-envelope about time can be matched with the ratio of the displacement's successive peaks.

$$\frac{X(t)}{X(t+T_D)} = \exp(\zeta\omega_n T_D) = \exp\left(\frac{2\pi\zeta}{\sqrt{1-\zeta^2}}\right) \quad \textbf{(12)}$$

where T_D is the damped period as follows:

$$T_D = \frac{2\pi}{\omega_D} = \frac{2\pi}{\omega_n\sqrt{1-\zeta^2}} \quad \textbf{(13)}$$

Then, its logarithmic decrement (δ) estimated by measuring the damped period and the peak displacements can be expressed in terms of the damping ratio.

$$\delta = \ln\left(\frac{X(t)}{X(t+N\cdot T_D)}\right) = \ln X(t) - \ln X(t+N\cdot T_D) = \frac{2\pi\zeta}{\sqrt{1-\zeta^2}} \quad \textbf{(14)}$$

where *N* is the number of cycle measured from the vibration.

Lastly, the damping ratio and the damping coefficient can be obtained from the following equations.

$$\zeta = \frac{\delta}{\sqrt{4\pi^2 + \delta^2}} \qquad b = 2m\omega_n\zeta = 2\zeta\sqrt{mk} \qquad \textbf{(15)}$$

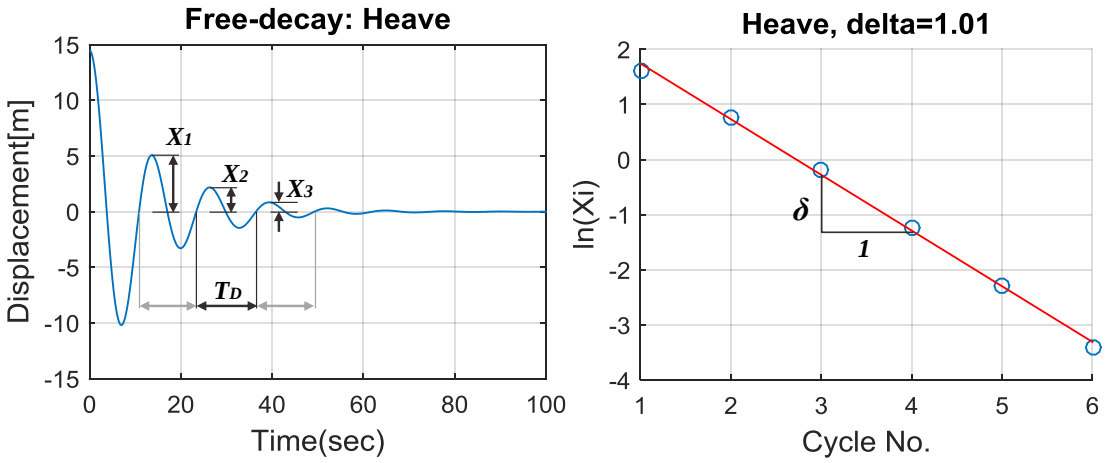

Figure 12. An example of heave free-decay simulations

For the free-decay simulations of the FLNG models (ZCG=4m~11m), the initial force/moment is set as $10^9 N$ for heave, $10^9 N \cdot m$ for roll, and $10^{12} N \cdot m$ for pitch. Releasing the force/moment lets the body freely oscillate with diminishing amplitude. Figure 12 shows an example of the free-decay simulations.

Finally, the characteristics of the FLNG models varied by mass-distributions are obtained. The most distinct parameters were found to be about roll motion. The results of the test process up to free-decay simulations for heave/roll/pitch modes are presented below, beginning with the hydrostatic stiffness of the models.

The hydrostatic stiffness, or the restoring coefficient of the FLNGs, *K*, are calculated from the frequency-domain analysis by using WAMIT prior to the free-decay simulations. The uncoupled roll stiffness (K44) is the only component of the restoring coefficients that shows visible changes of its size based on the difference of vertical mass distribution represented by varied ZCGs. The K matrices obtained from WAMIT are presented below; in addition, Figure 13~20 follows the K matrices to show the all results of heave/roll/pitch free-decay simulations for the ZCG-varied FLNGs.

When

- ZCG=4m,

$$K = \begin{bmatrix} 0 & 0 & 0 & 0 & 0 & 0 \\ 0 & 0 & 0 & 0 & 0 & 0 \\ 0 & 0 & 0.345E+09 & -0.552E+04 & 0.133E+10 & 0 \\ 0 & 0 & -0.552E+04 & \mathbf{0.705E+11} & -0.898E+05 & 0.199E+07 \\ 0 & 0 & 0.133E+10 & -0.898E+05 & 0.612E+13 & -0.197E+06 \\ 0 & 0 & 0 & 0 & 0 & 0 \end{bmatrix}$$

- ZCG=5m,

$$K = \begin{bmatrix} 0 & 0 & 0 & 0 & 0 & 0 \\ 0 & 0 & 0 & 0 & 0 & 0 \\ 0 & 0 & 0.345E+09 & -0.552E+04 & 0.133E+10 & 0 \\ 0 & 0 & -0.552E+04 & \mathbf{0.642E+11} & -0.898E+05 & 0.199E+07 \\ 0 & 0 & 0.133E+10 & -0.898E+05 & 0.612E+13 & -0.197E+06 \\ 0 & 0 & 0 & 0 & 0 & 0 \end{bmatrix}$$

- ZCG=6m,

$$K = \begin{bmatrix} 0 & 0 & 0 & 0 & 0 & 0 \\ 0 & 0 & 0 & 0 & 0 & 0 \\ 0 & 0 & 0.345E+09 & -0.552E+04 & 0.133E+10 & 0 \\ 0 & 0 & -0.552E+04 & \mathbf{0.578E+11} & -0.898E+05 & 0.199E+07 \\ 0 & 0 & 0.133E+10 & -0.898E+05 & 0.612E+13 & -0.197E+06 \\ 0 & 0 & 0 & 0 & 0 & 0 \end{bmatrix}$$

- ZCG=7m,

$$K = \begin{bmatrix} 0 & 0 & 0 & 0 & 0 & 0 \\ 0 & 0 & 0 & 0 & 0 & 0 \\ 0 & 0 & 0.345E+09 & -0.552E+04 & 0.133E+10 & 0 \\ 0 & 0 & -0.552E+04 & \mathbf{0.515E+11} & -0.898E+05 & 0.199E+07 \\ 0 & 0 & 0.133E+10 & -0.898E+05 & 0.610E+13 & -0.197E+06 \\ 0 & 0 & 0 & 0 & 0 & 0 \end{bmatrix}$$

- ZCG=8m,

$$K = \begin{bmatrix} 0 & 0 & 0 & 0 & 0 & 0 \\ 0 & 0 & 0 & 0 & 0 & 0 \\ 0 & 0 & 0.345E+09 & -0.552E+04 & 0.133E+10 & 0 \\ 0 & 0 & -0.552E+04 & \mathbf{0.452E+11} & -0.898E+05 & 0.199E+07 \\ 0 & 0 & 0.133E+10 & -0.898E+05 & 0.610E+13 & -0.197E+06 \\ 0 & 0 & 0 & 0 & 0 & 0 \end{bmatrix}$$

- ZCG=9m,

$$K = \begin{bmatrix} 0 & 0 & 0 & 0 & 0 & 0 \\ 0 & 0 & 0 & 0 & 0 & 0 \\ 0 & 0 & 0.345E+09 & -0.552E+04 & 0.133E+10 & 0 \\ 0 & 0 & -0.552E+04 & \mathbf{0.389E+11} & -0.898E+05 & 0.199E+07 \\ 0 & 0 & 0.133E+10 & -0.898E+05 & 0.609E+13 & -0.197E+06 \\ 0 & 0 & 0 & 0 & 0 & 0 \end{bmatrix}$$

- ZCG=10m,

$$K = \begin{bmatrix} 0 & 0 & 0 & 0 & 0 & 0 \\ 0 & 0 & 0 & 0 & 0 & 0 \\ 0 & 0 & 0.345E+09 & -0.552E+04 & 0.133E+10 & 0 \\ 0 & 0 & -0.552E+04 & \mathbf{0.326E+11} & -0.898E+05 & 0.199E+07 \\ 0 & 0 & 0.133E+10 & -0.898E+05 & 0.608E+13 & -0.197E+06 \\ 0 & 0 & 0 & 0 & 0 & 0 \end{bmatrix}$$

- ZCG=11m,

$$K = \begin{bmatrix} 0 & 0 & 0 & 0 & 0 & 0 \\ 0 & 0 & 0 & 0 & 0 & 0 \\ 0 & 0 & 0.345E+09 & -0.552E+04 & 0.133E+10 & 0 \\ 0 & 0 & -0.552E+04 & \mathbf{0.263E+11} & -0.898E+05 & 0.199E+07 \\ 0 & 0 & 0.133E+10 & -0.898E+05 & 0.608E+13 & -0.197E+06 \\ 0 & 0 & 0 & 0 & 0 & 0 \end{bmatrix}$$

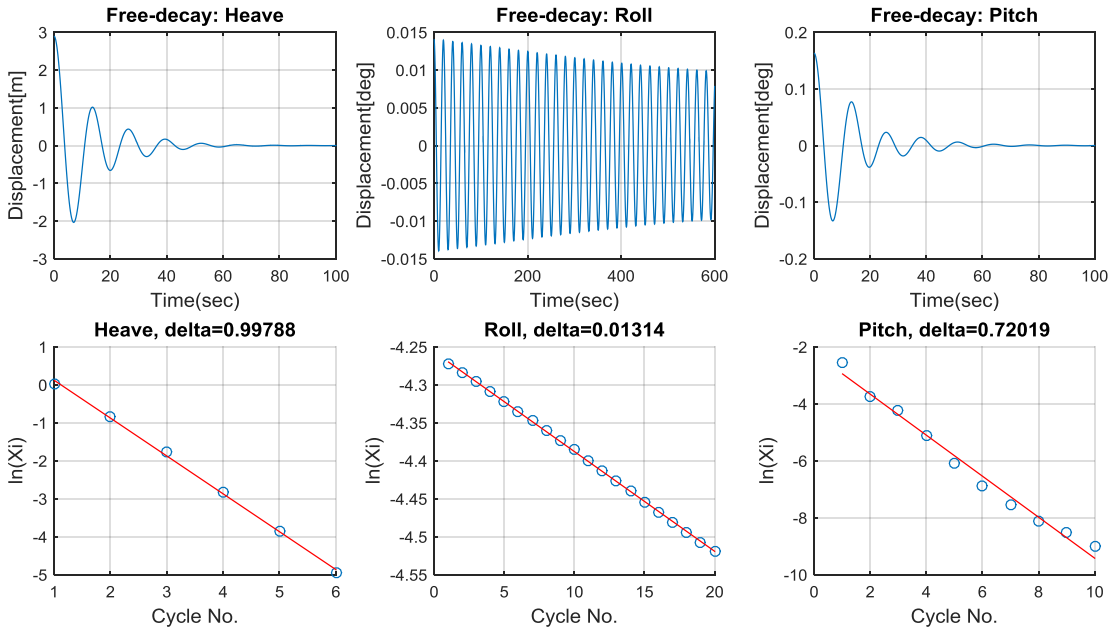

Figure 13. Free-decay simulations for the FLNG model of ZCG=4m

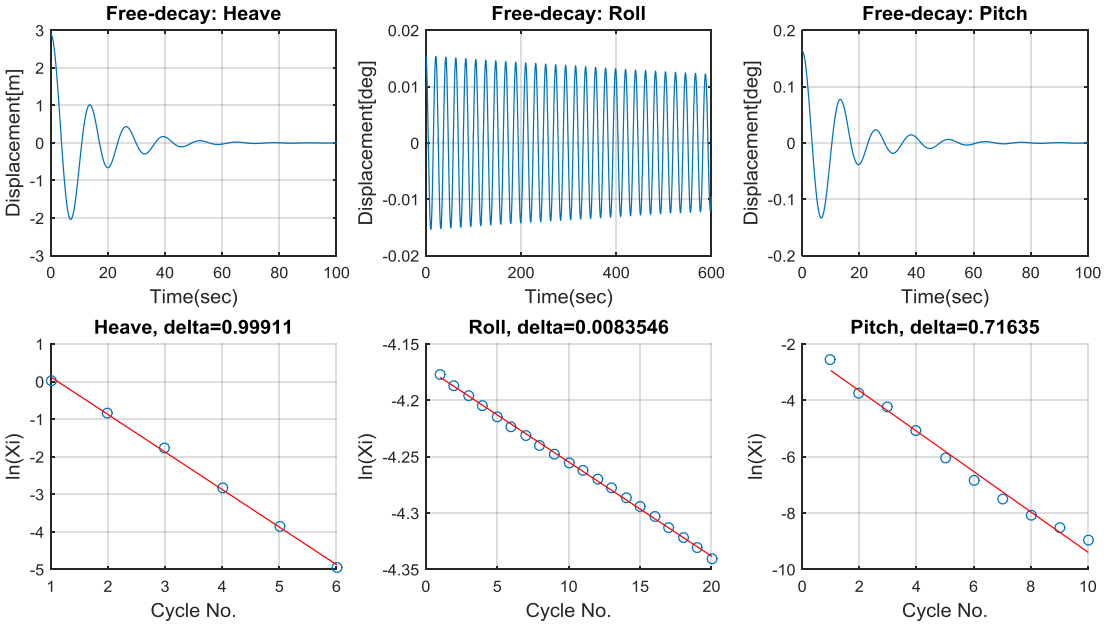

Figure 14. Free-decay simulations for the FLNG model of ZCG=5m

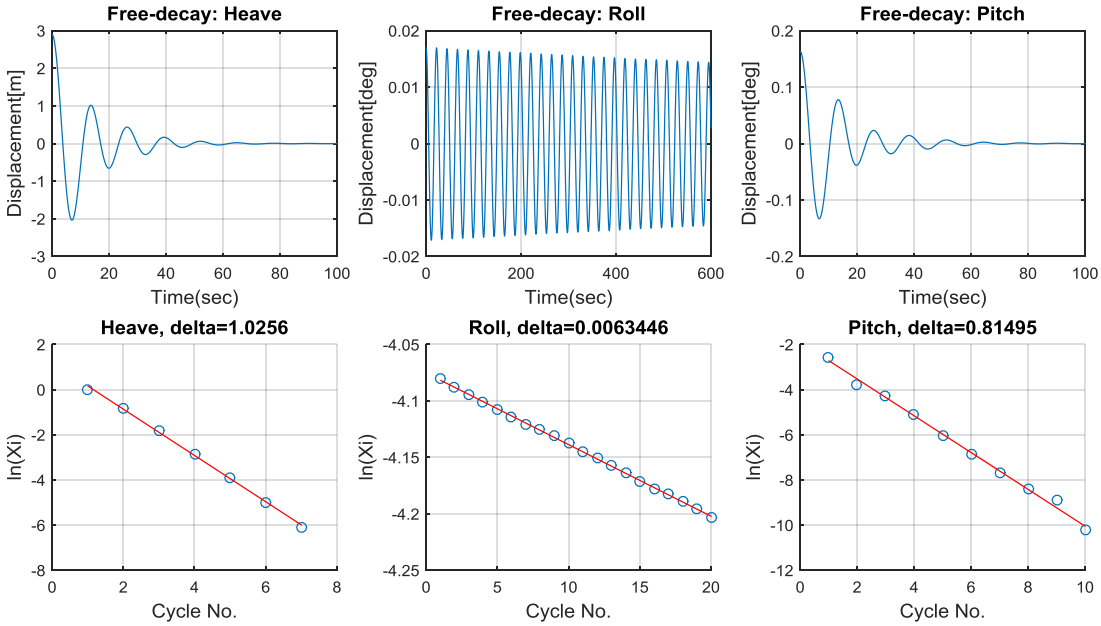

Figure 15. Free-decay simulations for the FLNG model of ZCG=6m

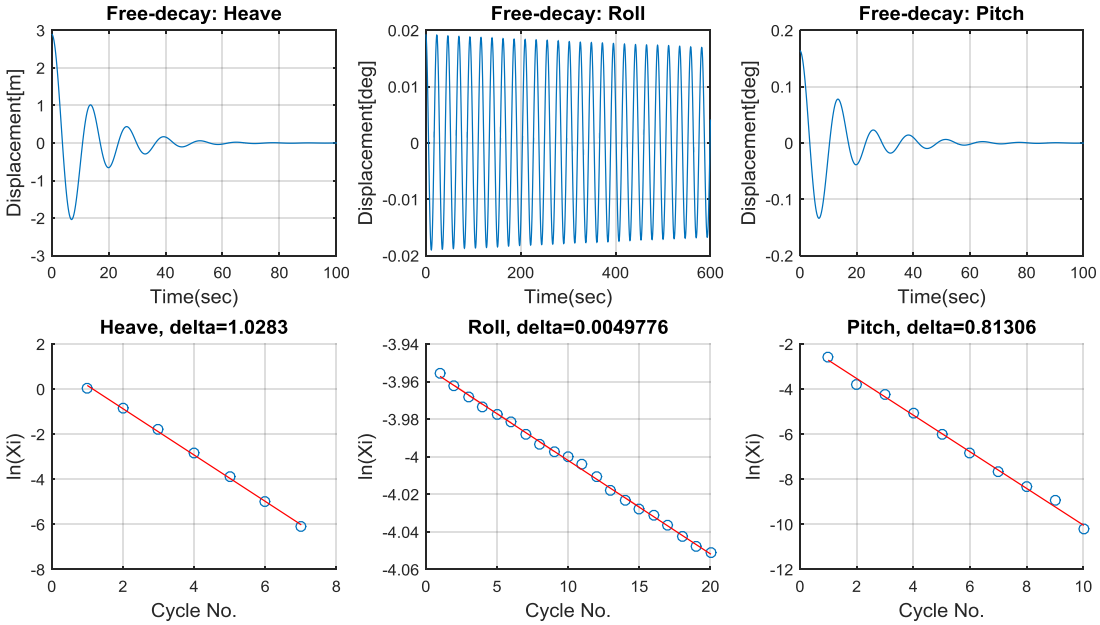

Figure 16. Free-decay simulations for the FLNG model of ZCG=7m

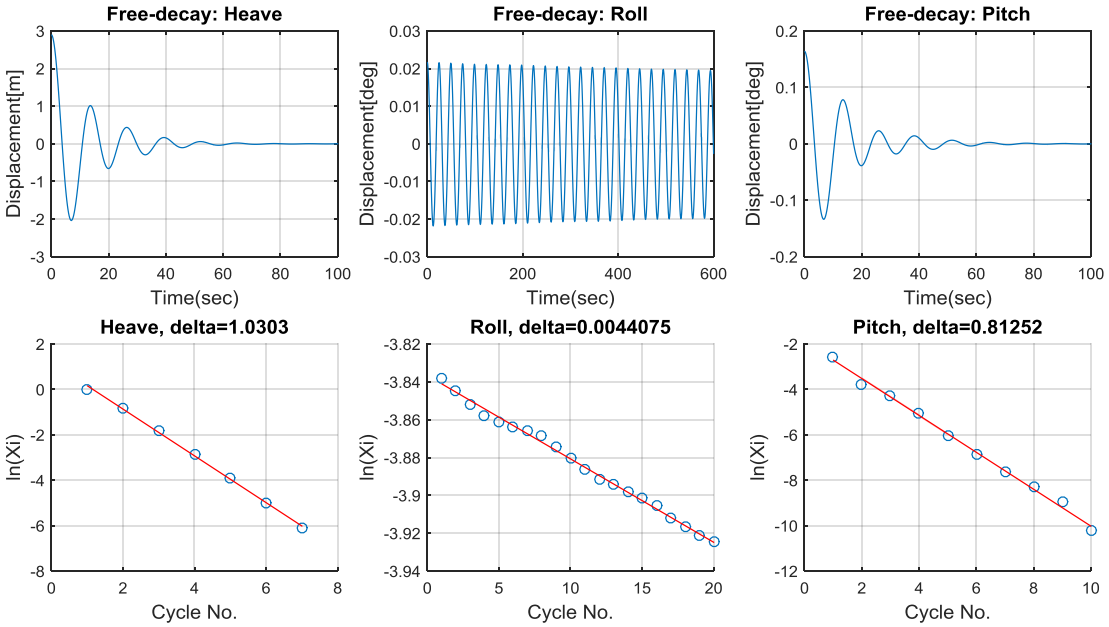

Figure 17. Free-decay simulations for the FLNG model of ZCG=8m

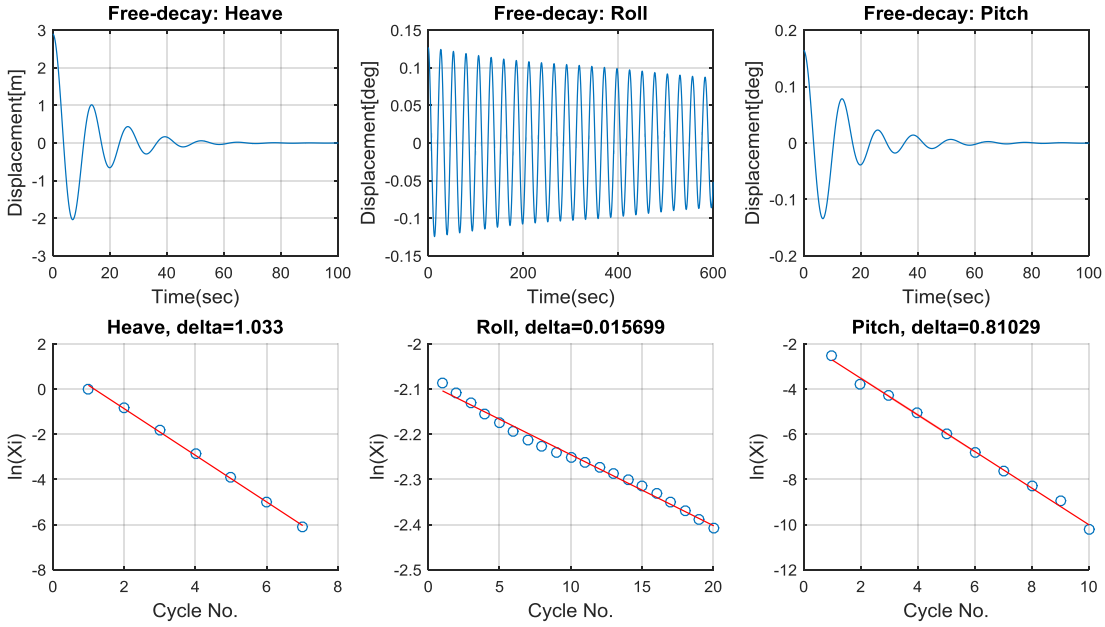

Figure 18. Free-decay simulations for the FLNG model of ZCG=9m

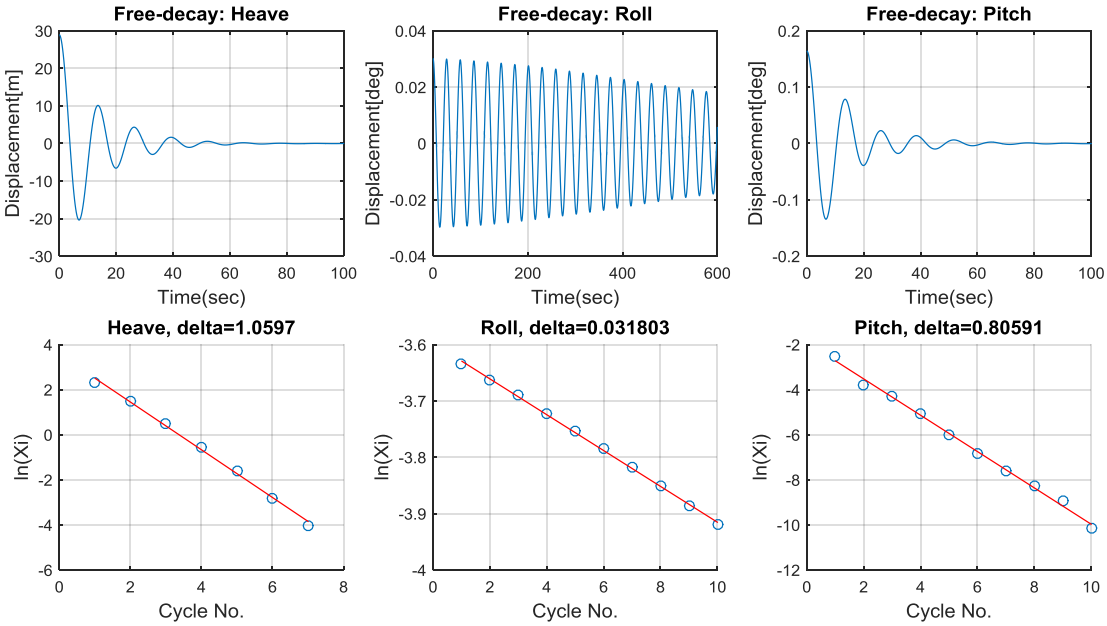

Figure 19. Free-decay simulations for the FLNG model of ZCG=10m

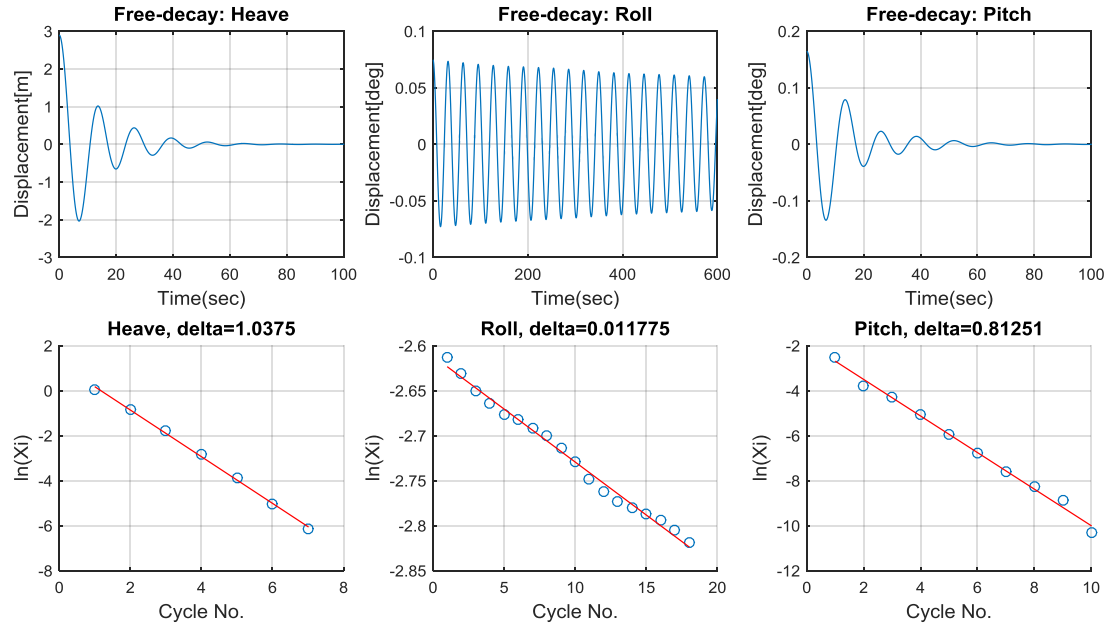

Figure 20. Free-decay simulations for the FLNG model of ZCG=11m

Table 15. Heave free-decay simulation results for varied ZCGs

ZCG	T_D	ω_D	δ	ζ	ω_n	T_n	k	b_r	b
4m	12.900	0.487	0.998	15.69%	0.493	12.740	3.450E+08	1.399E+09	2.195E+08
5m	12.900	0.487	0.999	15.70%	0.493	12.740	3.450E+08	1.399E+09	2.197E+08
6m	12.857	0.489	1.026	16.11%	0.495	12.689	3.450E+08	1.393E+09	2.245E+08
7m	12.857	0.489	1.028	16.15%	0.495	12.688	3.450E+08	1.393E+09	2.251E+08
8m	12.857	0.489	1.030	16.18%	0.495	12.688	3.450E+08	1.393E+09	2.255E+08
9m	12.857	0.489	1.033	16.22%	0.495	12.687	3.450E+08	1.393E+09	2.260E+08
10m	12.914	0.487	1.060	16.63%	0.493	12.734	3.450E+08	1.398E+09	2.326E+08
11m	12.829	0.490	1.037	16.29%	0.496	12.657	3.450E+08	1.390E+09	2.264E+08

Table 16. Roll free-decay simulation results for varied ZCGs

ZCG	T_D	ω_D	δ	ζ	ω_n	T_n	k	b_r	b
4m	20.070	0.313	0.013	0.21%	0.313	20.070	7.050E+10	4.504E+11	9.436E+08
5m	20.980	0.299	0.008	0.13%	0.299	20.980	6.420E+10	4.287E+11	5.701E+08
6m	22.050	0.285	0.006	0.10%	0.285	22.050	5.780E+10	4.057E+11	4.097E+08
7m	23.260	0.270	0.005	0.08%	0.270	23.260	5.150E+10	3.813E+11	3.021E+08
8m	24.720	0.254	0.004	0.07%	0.254	24.720	4.520E+10	3.557E+11	2.495E+08
9m	26.500	0.237	0.016	0.25%	0.237	26.500	3.890E+10	3.281E+11	8.199E+08
10m	28.860	0.218	0.032	0.51%	0.218	28.860	3.260E+10	2.995E+11	1.516E+09
11m	31.811	0.198	0.012	0.19%	0.198	31.811	2.630E+10	2.663E+11	4.991E+08

Table 17. Pitch free-decay simulation results for varied ZCGs

ZCG	T_D	ω_D	δ	ζ	ω_n	T_n	k	b_r	b
4m	13.220	0.475	0.720	11.39%	0.478	13.134	6.120E+12	2.559E+13	2.914E+12
5m	13.220	0.475	0.716	11.33%	0.478	13.135	6.120E+12	2.559E+13	2.898E+12
6m	12.780	0.492	0.815	12.86%	0.496	12.674	6.110E+12	2.465E+13	3.171E+12
7m	12.840	0.489	0.813	12.83%	0.493	12.734	6.100E+12	2.473E+13	3.173E+12
8m	12.840	0.489	0.813	12.82%	0.493	12.734	6.100E+12	2.473E+13	3.171E+12
9m	12.860	0.489	0.810	12.79%	0.493	12.754	6.090E+12	2.472E+13	3.162E+12
10m	12.860	0.489	0.806	12.72%	0.493	12.756	6.080E+12	2.469E+13	3.141E+12
11m	14.920	0.421	0.813	12.82%	0.425	14.797	6.080E+12	2.864E+13	3.673E+12

The most significant trend that can be found from Table 15~17 is the increasing roll natural period as the ZCG gets bigger, and that the roll damping ratios are negligibly small when compared to the heave and pitch damping ratios.

Taking the heave/roll/pitch damping coefficients (b) estimated from the free-decay simulations as viscous damping, the external damping matrices, *EXDAMP*, to update the input (force control file) in WAMIT are set for the different FLNG models.

When

- ZCG=4m,

$$EXDAMP = \begin{bmatrix} 0 & & & & & \\ & 0 & & & & \\ & & 2.195e8 & & & \\ & & & 9.436e8 & & \\ & & & & 2.914e12 & \\ & & & & & 0 \end{bmatrix}$$

- ZCG=5m,

$$EXDAMP = \begin{bmatrix} 0 & & & & & \\ & 0 & & & & \\ & & 2.197e8 & & & \\ & & & 5.701e8 & & \\ & & & & 2.898e12 & \\ & & & & & 0 \end{bmatrix}$$

- ZCG=6m,

$$EXDAMP = \begin{bmatrix} 0 & & & & & \\ & 0 & & & & \\ & & 2.245e8 & & & \\ & & & 4.097e8 & & \\ & & & & 3.171e12 & \\ & & & & & 0 \end{bmatrix}$$

- ZCG=7m,

$$EXDAMP = \begin{bmatrix} 0 & & & & & \\ & 0 & & & & \\ & & 2.251e8 & & & \\ & & & 3.021e8 & & \\ & & & & 3.173e12 & \\ & & & & & 0 \end{bmatrix}$$

- ZCG=8m,

$$EXDAMP = \begin{bmatrix} 0 & & & & & \\ & 0 & & & & \\ & & 2.255e8 & & & \\ & & & 2.495e8 & & \\ & & & & 3.171e12 & \\ & & & & & 0 \end{bmatrix}$$

- ZCG=9m,

$$EXDAMP = \begin{bmatrix} 0 & & & & & \\ & 0 & & & & \\ & & 2.260e8 & & & \\ & & & 8.199e8 & & \\ & & & & 3.162e12 & \\ & & & & & 0 \end{bmatrix}$$

- ZCG=10m,

$$EXDAMP = \begin{bmatrix} 0 & & & & & \\ & 0 & & & & \\ & & 2.326e8 & & & \\ & & & 1.516e9 & & \\ & & & & 3.141e12 & \\ & & & & & 0 \end{bmatrix}$$

- ZCG=11m,

$$EXDAMP = \begin{bmatrix} 0 & & & & & \\ & 0 & & & & \\ & & 2.264e8 & & & \\ & & & 4.991e8 & & \\ & & & & 3.673e12 & \\ & & & & & 0 \end{bmatrix}$$

3.3. RAO Comparison

Consequently, the RAOs (Response Amplitude Operators) under several incident wave headings (BETAs), calculated by using WAMIT with taking the external damping and stiffness into account, are presented in Figure 21~24.

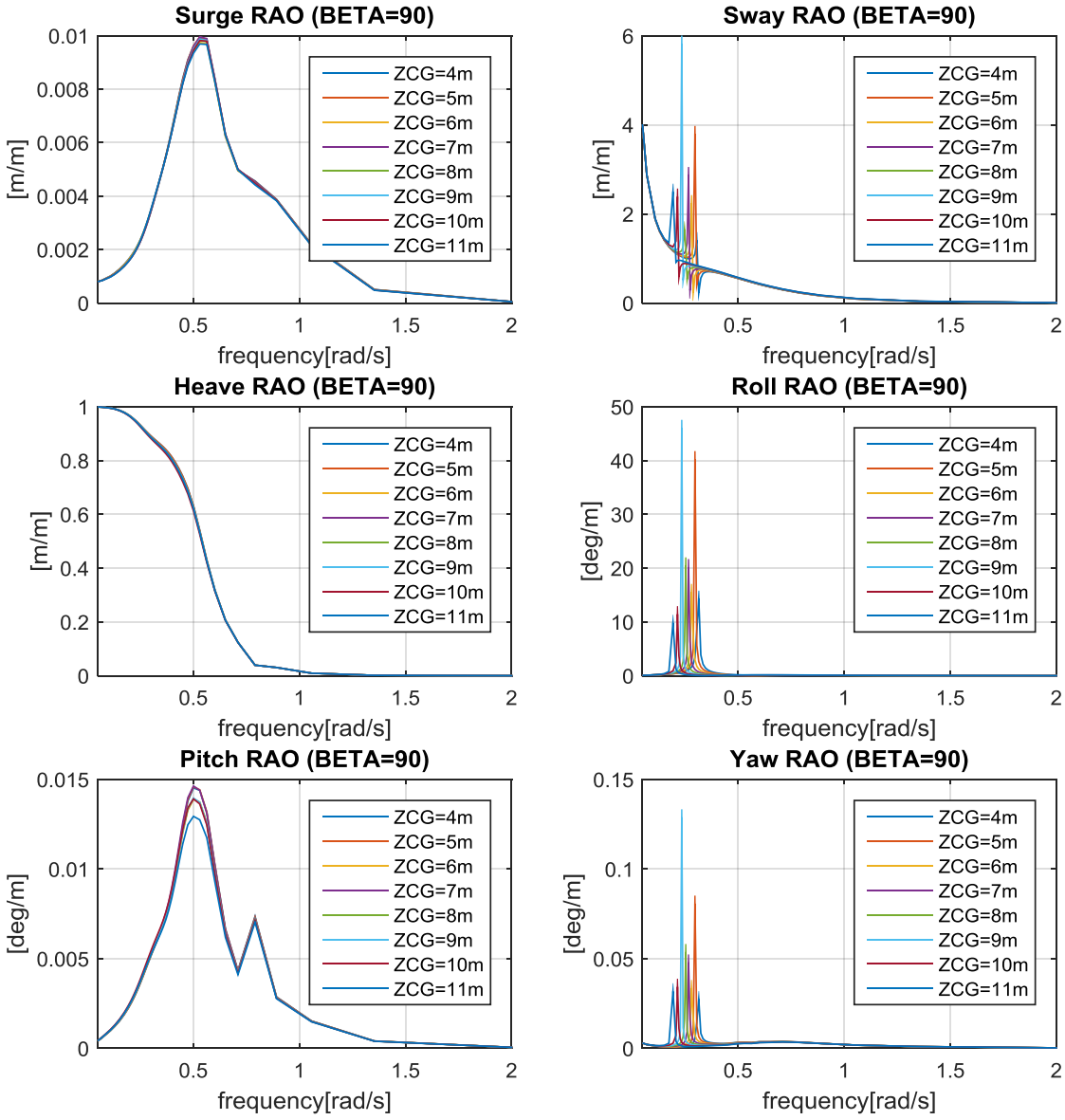

Figure 21. RAOs for the FLNGs of varied ZCGs (BETA=90)

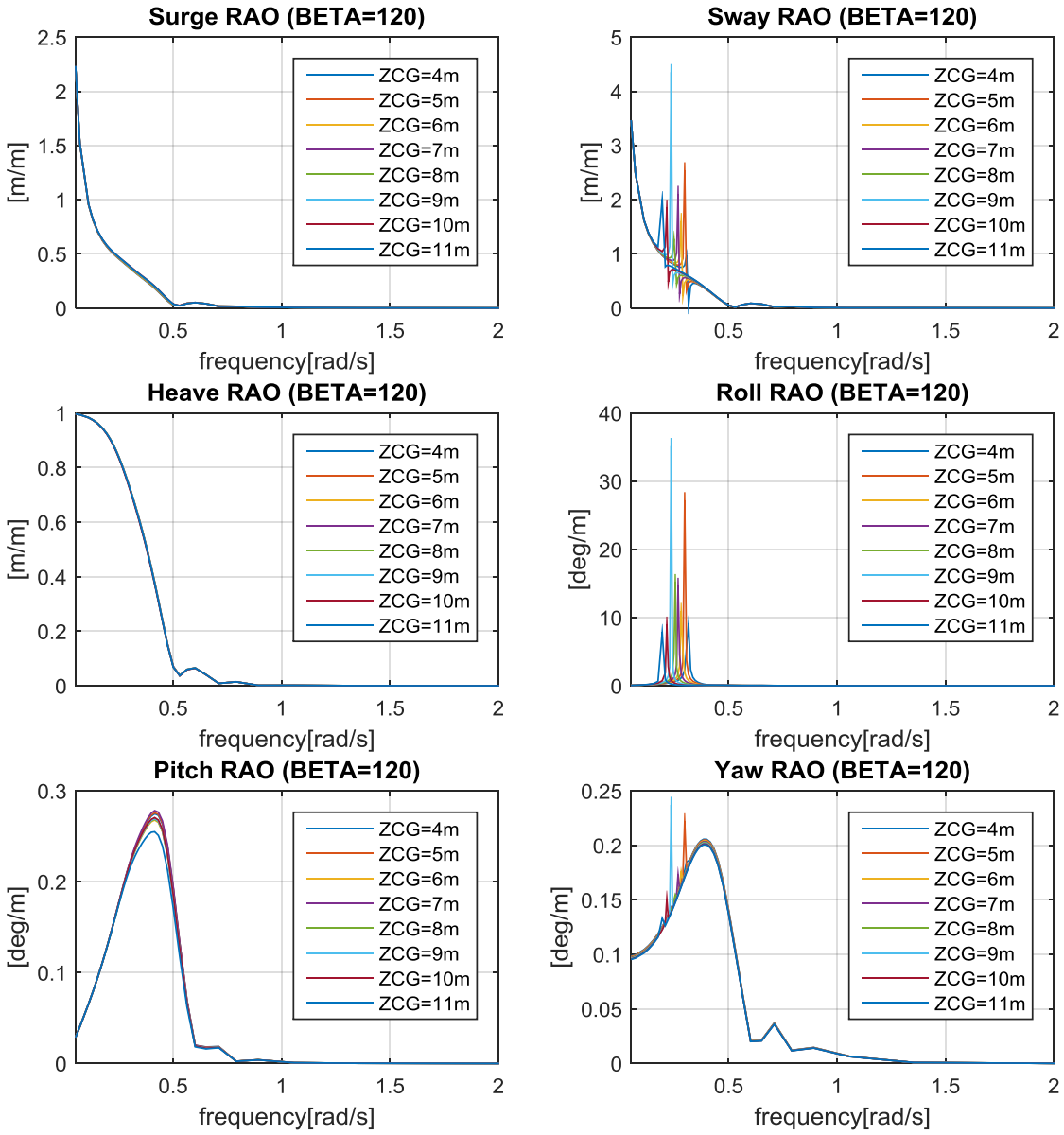

Figure 22. RAOs for the FLNGs of varied ZCGs (BETA=120)

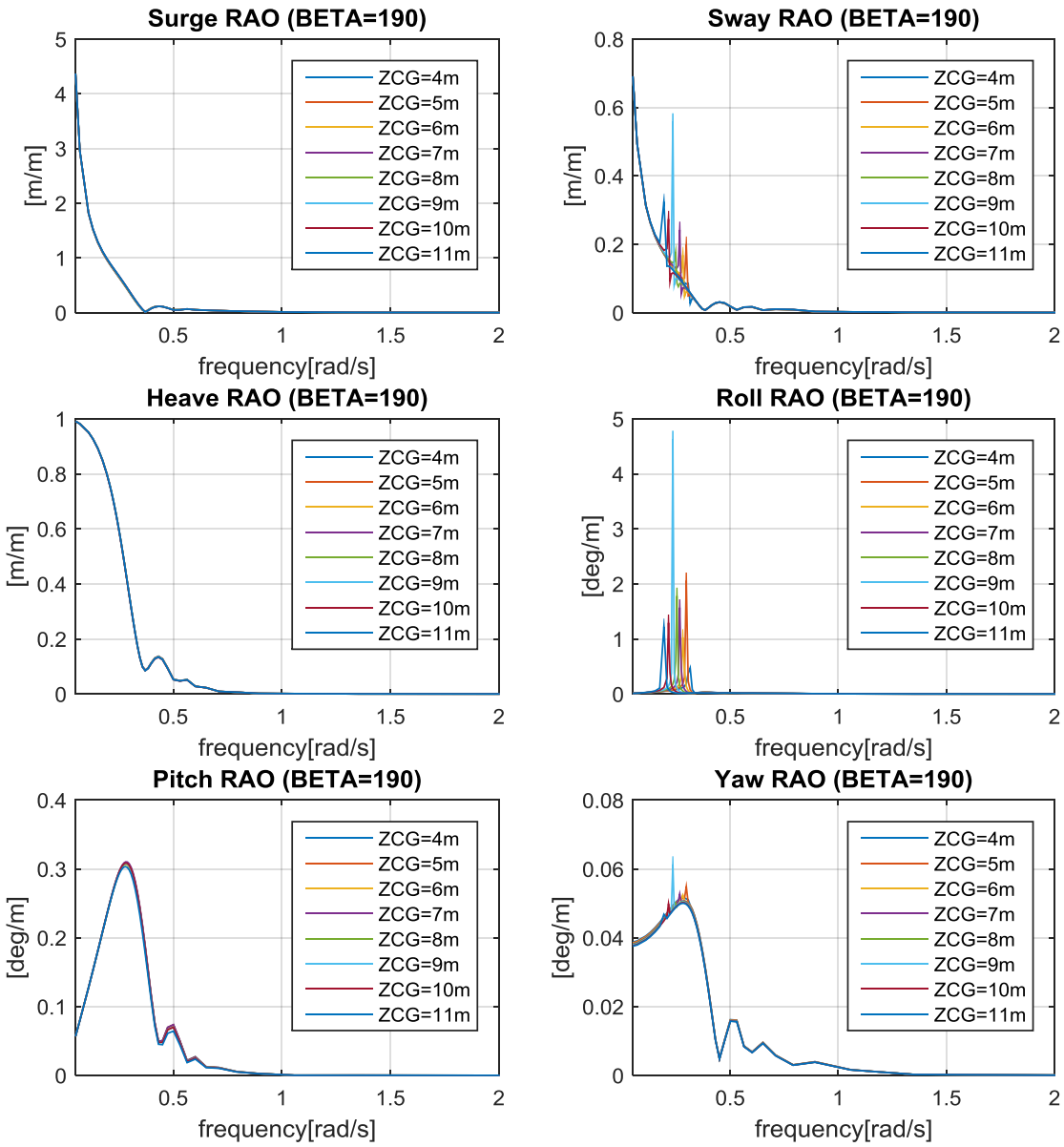

Figure 23. RAOs for the FLNGs of varied ZCGs (BETA=190, equivalent with BETA=170)

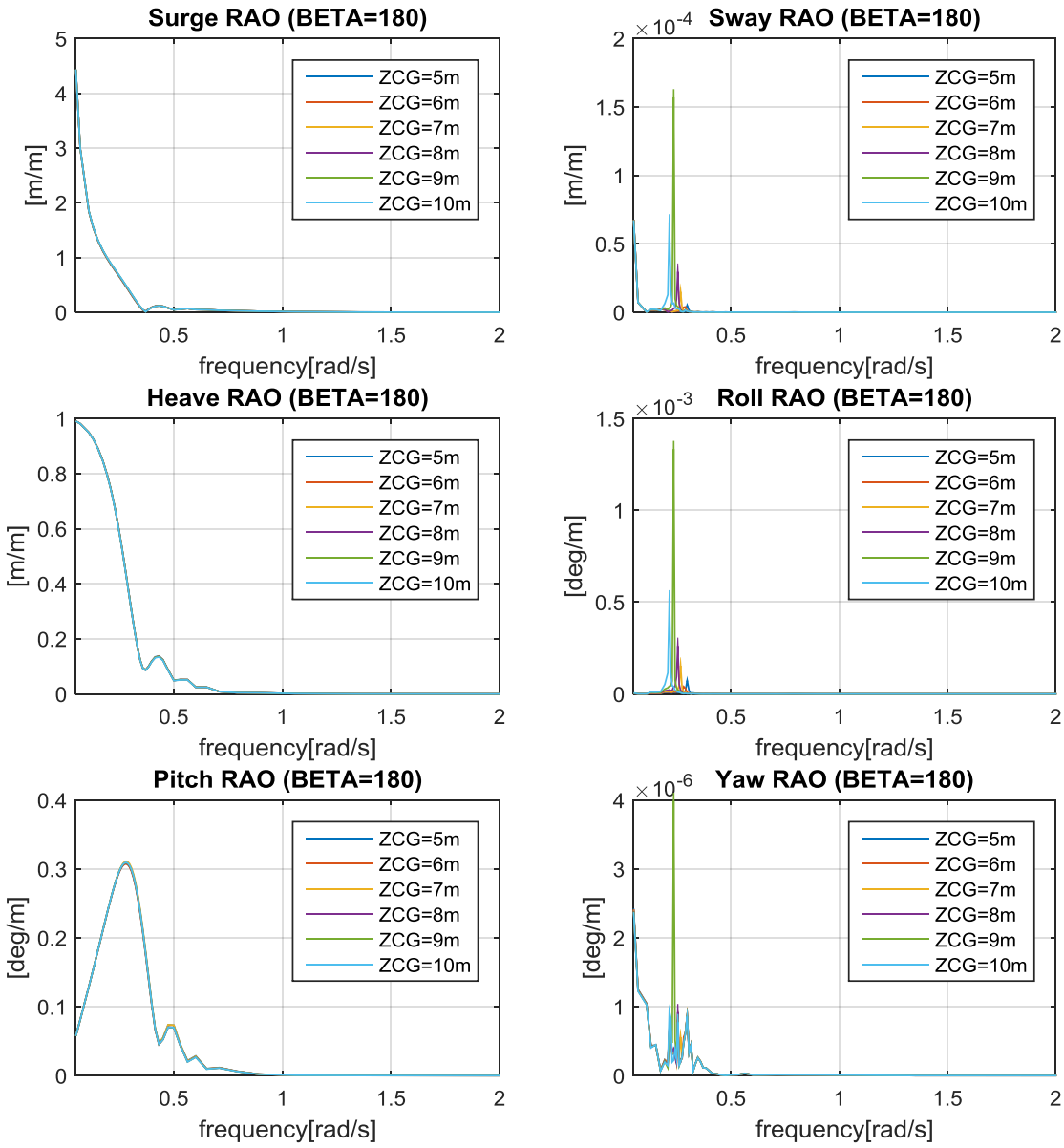

Figure 24. RAOs for the FLNGs of varied ZCGs (BETA=180)

Characteristics of the FLNGs differentiated by the ZCG variation are found under different heading conditions of the incident wave. While the surge/heave/pitch RAOs are almost identical for the different ZCGs, the other modes' RAOs show significant difference in their peak frequencies based on the differentiated ZCGs. Figure 25 shows the roll and pitch RAOs compared by different CG positions.

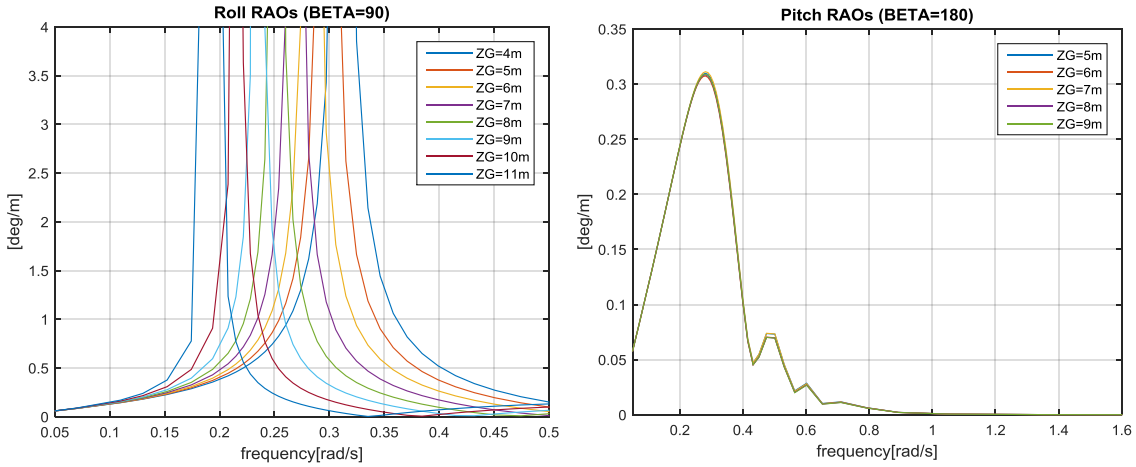

Figure 25. Roll RAOs (left, BETA=90) and Pitch RAOs in head-sea (right, BETA=180) for the FLNGs of varied ZCGs in closer view

Considering the sway-roll-yaw coupling effect, which is clearly observed through the analysis as presented in Figure 21~24, it should be worth focusing on roll response that is known as one of the critical motions that govern the topside operability of an FLNG having a fractionation column. The plots of roll RAOs in a closer look about the incident wave periods (second) are presented in Figure 26.

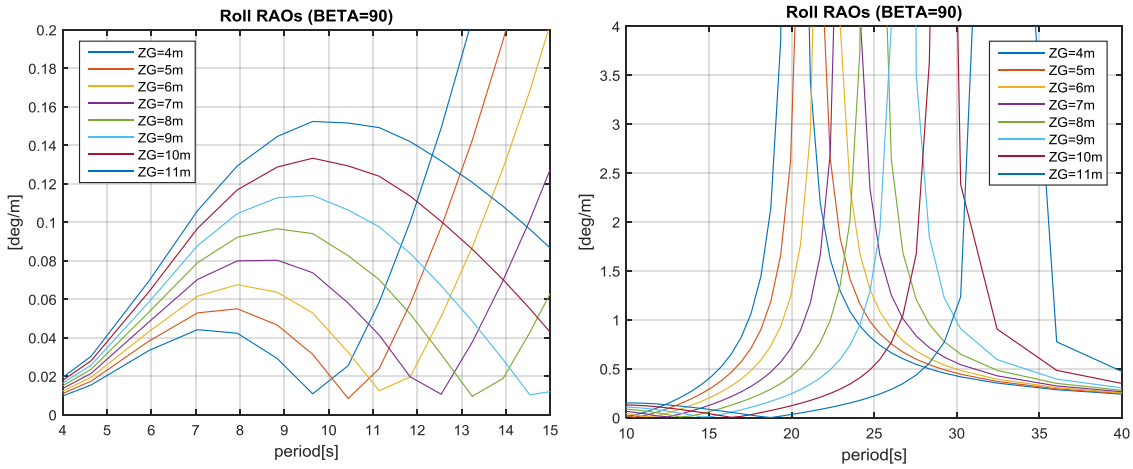

Figure 26. Roll RAOs (BETA=90) in the short period region (left) and in the long period region (right) for the FLNGs of varied ZCGs

The correlation between ZCG and roll RAO is very different based on the frequency regions. In the short period region (high frequency), the roll response of amplitude increases as ZCG increases. However, in the long period region (low frequency) up to the peak, the roll amplitude decreases as ZCG increases. Although the roll RAOs in the short period region is relatively very small, considering that practical wave periods are normally smaller than 18 seconds, the difference of RAOs in the short period region would not be trivial; thus, different effects of wave periods on the response of the FLNGs with varied ZCGs are expected.

3.4. Linear Swell-induced Motion

Swell is one of the long-period waves, propagating from distance without having correlation with local wind. In general, swell waves are initiated from storm-induced waves and travel a far distance without significant loss of energy but having the steepness

of the wave profile reduced. Swell waves, in long-crested shapes, propagate toward certain directions without gaining more energy from local wind, and consequently form so-called "wave trains" in different directions.

Considering a long-crested wave, far from wave breaking, irregular waves can be obtained by simply superposing regular waves. From the linear theory, swell-induced motions can be obtained by superposing separately-induced motions together (Ha, 2011).

In the present study, 80 frequencies are randomly selected from normal distribution varied by peak frequency and standard deviation (ω_p, σ) of swell-waves for every case running. Then, the amplitude of a wave component can be obtained by following equation.

$$a_j = \sqrt{2S(\omega_j)\Delta\omega_j} \quad \textbf{(16)}$$

where

ω_j is j_{th} component of the random wave frequencies.

$\Delta\omega_j$ is the width for j_{th} random frequency so the accumulation of the all $\Delta\omega_j$ can represent the whole frequency region of non-zero spectrum.

$S(\omega_j)$ is a wave spectrum.

The wave spectrum that typically represents swell waves is Gaussian swell spectrum, which can be described as follows (Wichers, 2013).

$$S(\omega) = \frac{\left(\frac{H_s}{4}\right)^2}{\sigma\omega_p\sqrt{2\pi}} \exp\left[-\frac{(\omega-\omega_p)^2}{2\sigma^2\omega_p^2}\right] \quad \textbf{(17)}$$

Taking random phase angles from uniform distribution within the range $[-\pi\ +\pi]$, the consequent response of motion can be finally obtained as follows.

$$\sum_{j=1}^{N} a_j \left|H(\omega_j)\right| \sin\left(\omega_j t + \epsilon_j\right) \qquad \textbf{(18)}$$

where

N is the total number of wave components

ϵ_j is the phase angle for j_{th} wave component

$\left|H(\omega_j)\right|$, the transfer function, is the RAO (Response Amplitude Operator).

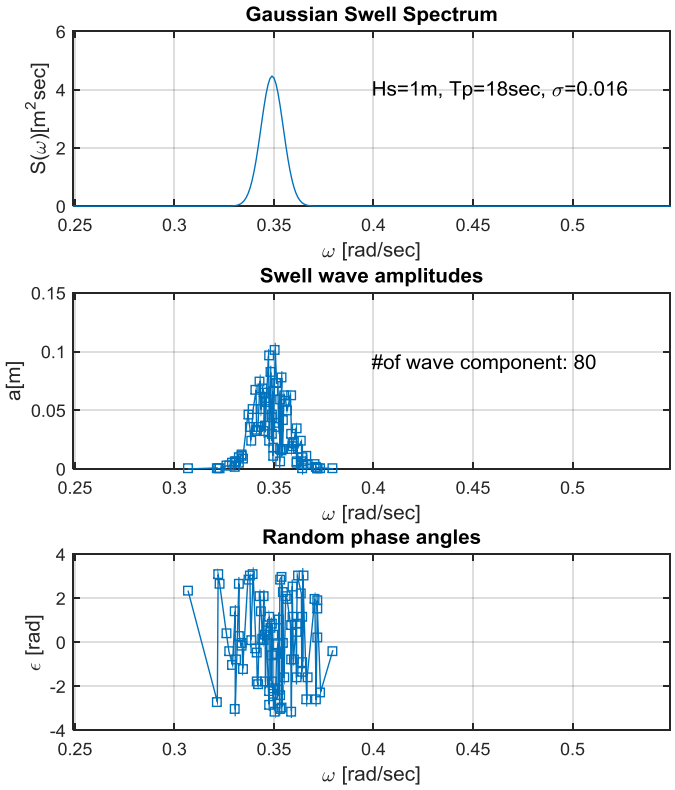

Figure 27. An example of Gaussian swell spectrum (Hs=1m, Tp=18sec, $\boldsymbol{\sigma}$=0.016), the amplitudes of randomly chosen 80 waves, and random phase angles

An example of Gaussian swell spectrum, including the random properties for its generation, is presented in Figure 27. Meanwhile, an irregular wave profile as a result of superposing random wave components can be obtained by the following equation.

$$\eta(t) = \sum_{j=1}^{N} a_j \sin\left(\omega_j t + \epsilon_j\right) \qquad \textbf{(19)}$$

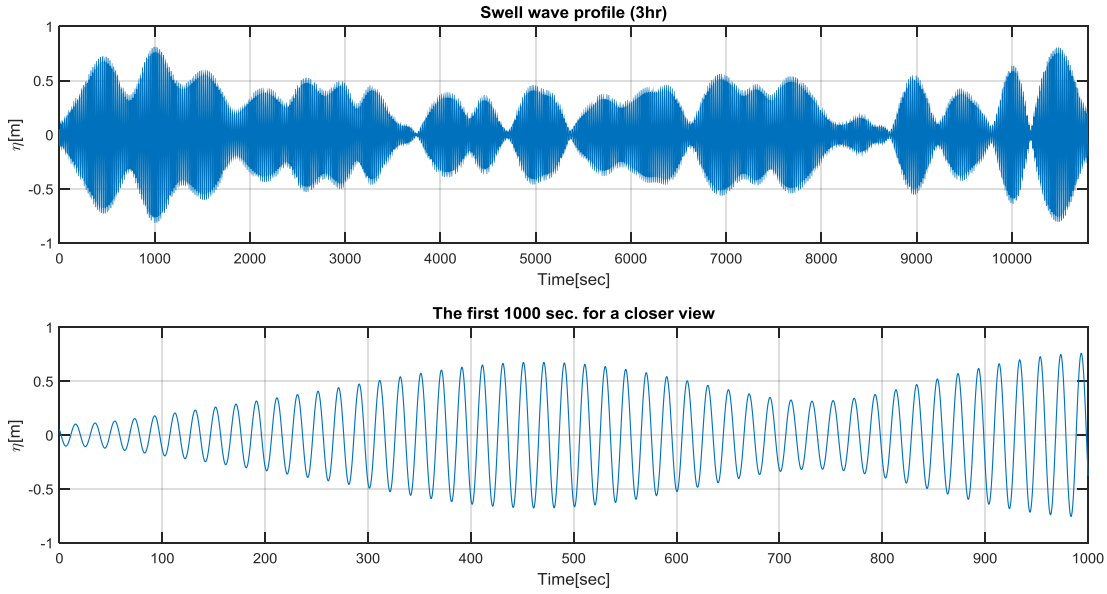

Figure 28. An example of swell wave profile (Hs=1m, Tp=20sec, $\boldsymbol{\sigma}$=0.016, time step: 0.02sec, total time period: 3 hours)

A swell wave profile, for an example, is presented in Figure 28. Again, a new irregular swell wave is randomly generated for every case of simulation in this study, following the pre-described steps up to this point.

3.5. Simulation Plan

Extreme cases and a simple heading configuration of environmental forces are used for the comparison of the FLNG models varied by vertical mass distribution, represented by their z-coordinates of the center of gravity. The directional configuration is as shown in Figure 29.

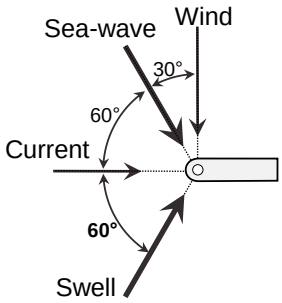

Figure 29. Heading configuration of the environmental forces considered in the model tests under extreme conditions

The extreme conditions of sea-waves and wind speeds are collected from the EIS (Environmental Impact Statement, by Shell), and the maximum speed of the surface current reported in the EIS is also taken for the simulations. The significant wave height of swell is averaged from a historical data, and the peak period of 18 seconds is suggested as a 1-year beam-on swell condition for the Northwest Australian Shelf by Xia, 2012. The 10-year peak period of swell (20 seconds) is roughly assumed while the maximum wave period during last 25 years is about 23.5 seconds.

The time-series of body motions are obtained by superposing two separate results from Part 1 and Part 2 as described in Table 18. This separation is intended for the simplification by considering only one wave system in a CHARM3D time-simulation.

Swell waves can be considered as independent of the local environmental conditions; thus, they are taken out of the whole environmental conditions and analyzed separately as previously mentioned.

Table 18. Separate environmental conditions (swell heading case #1) for numerical tests

Part 1	*Sea wave**			*Wind*		*Current*	
	BETA (deg.)	*Hs (m)*	*Tp (sec)*	*BETA (deg.)*	*U10 (m/s)*	*BETA (deg.)*	*Speed (m/s)*
1-yr	120	5.2	10.0	90	15.3	180	0.6
10-yr	120	7.2	12.1	90	25.8	180	0.6

*JONSWAP (γ=3.3)

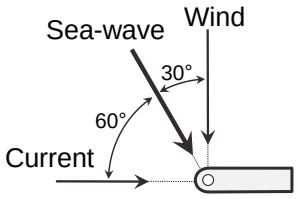

Part 2	*Swell wave***		
	BETA (deg.)	*Hs (m)*	*Tp (sec)*
1-yr	120 (eq.240)	1.0	18.0
10-yr	120 (eq.240)	1.0	20.0

**Gaussian Swell Spectrum (σ=0.016)

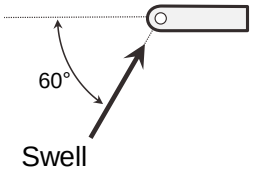

In addition, an artificial yaw stiffness is introduced to restrict the FLNG's heading to the planned direction during time-simulations with acceptable deviations. The artificial restriction of yaw motion is necessary because the simulations are under swell-missing environmental conditions, and variances of roll motion due to the coupling effect with yaw can be minimized by the restriction. The yaw stiffness is simply added to the hydrostatic stiffness matrix, more particularly to the 6^{th} component of the diagonal terms, which is initially zero. The magnitude of the artificial yaw stiffness is determined by

iterating time-simulations while targeting the mean yaw angle on around 10° and limited up to 15°, so it can be considered as practical behavior within the maximum-allowable deviation of wave headings in CHARM3D simulation.

From the free-decay simulation results for different FLNG models of varied ZCGs, as presented in Table 1, the roll natural period has been distinguished as the most critical parameter that is differentiated by the vertical distribution of the mass. In general, as mentioned earlier, sizing and designing of FLNGs should begin with targeting proper natural periods of heave/roll/pitch.

To evaluate the design of each model in connection with its natural periods and its operability, the tilting motions of the FLNG models with different designs in extreme sea states are to be compared. Accordingly, as a test result in this chapter, the maximum roll and pitch displacements during 3-hour simulations are collected for the models of varied ZCGs.

3.6. Simulation Result of Numerical Model

For convenience, only two sets of the results are shown in this section as an example of two cases of the environmental conditions; the entire sets of the simulation results for various ZCGs are presented in Appendix 2.

Each set of the results consist of two figures. The time-series of 6 DOF motions at the origin of the body-fixed coordinate system from Part 1 (CHARM3D simulation under sea wave, wind, and current) are presented first. Then, a figure that includes the time-series from each part, and the superposed time-series of roll/pitch motions follows up in

the every set of the test results. The random frequencies and the phase angles for calculating the linear swell-induced motions are independently selected for each case of the tests, but only two representative cases (when the peak period of swell wave is 18sec, or 20sec) are presented to show the difference of the wave spectra.

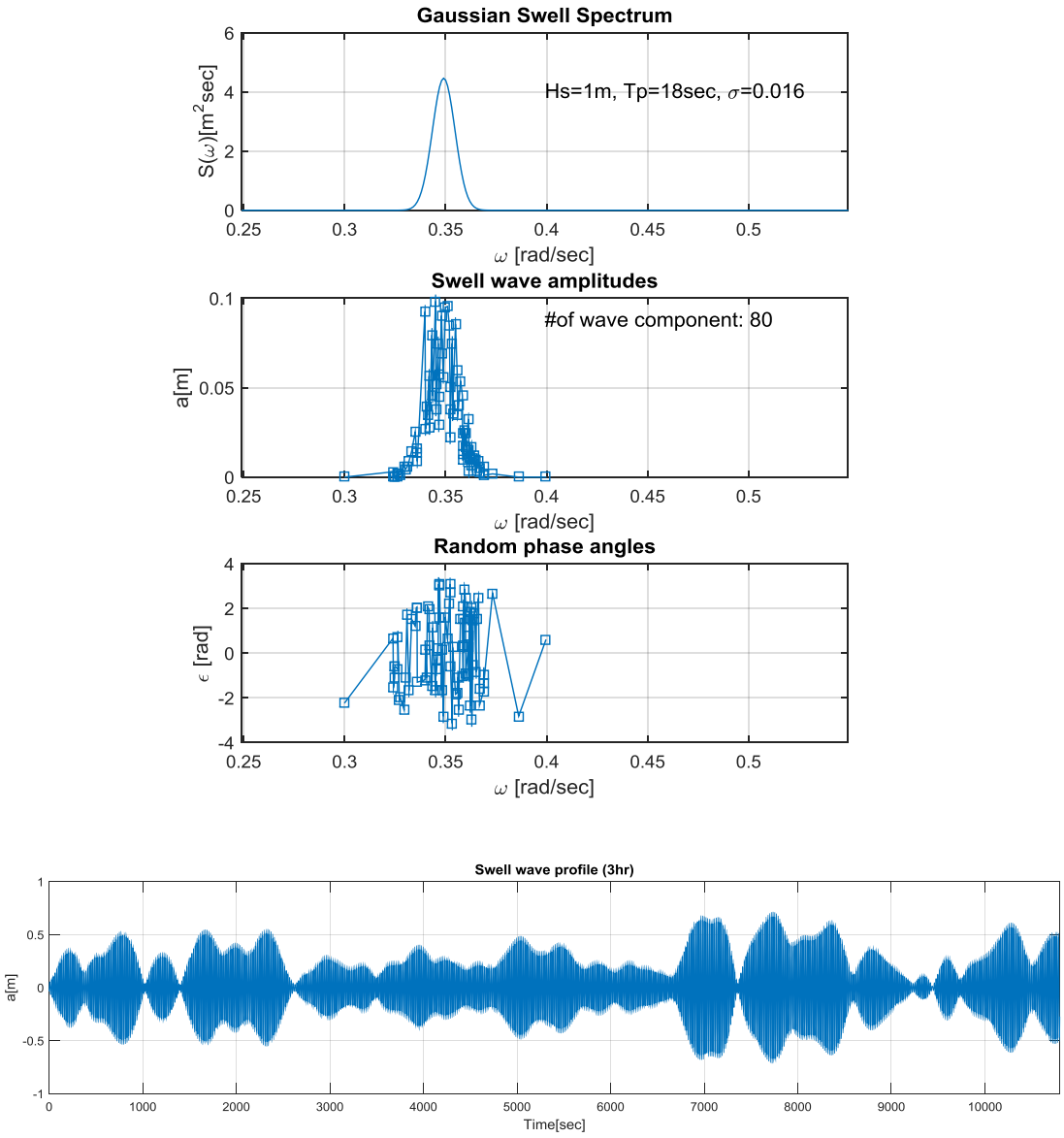

Figure 30. Random swell-wave generation (Hs=1m, Tp=18sec) for the test case of ZCG=4m under 1-year extreme condition

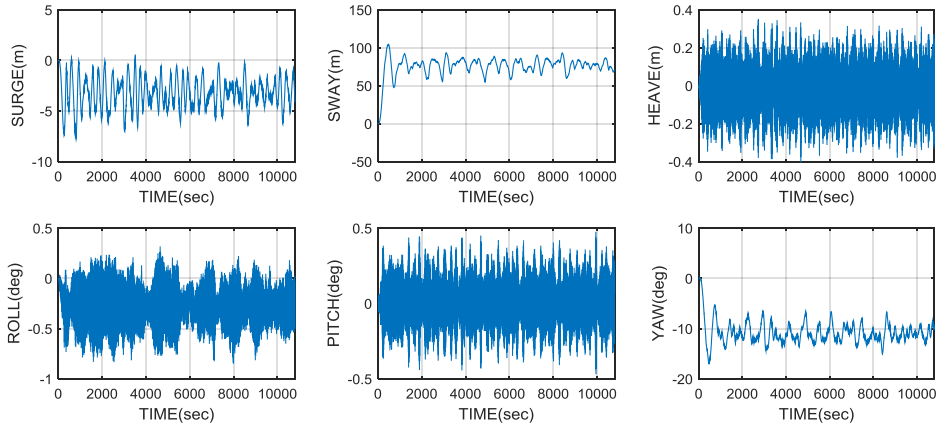

Figure 31. Test result: ZCG=4m under 1-year extreme condition (Part 1)

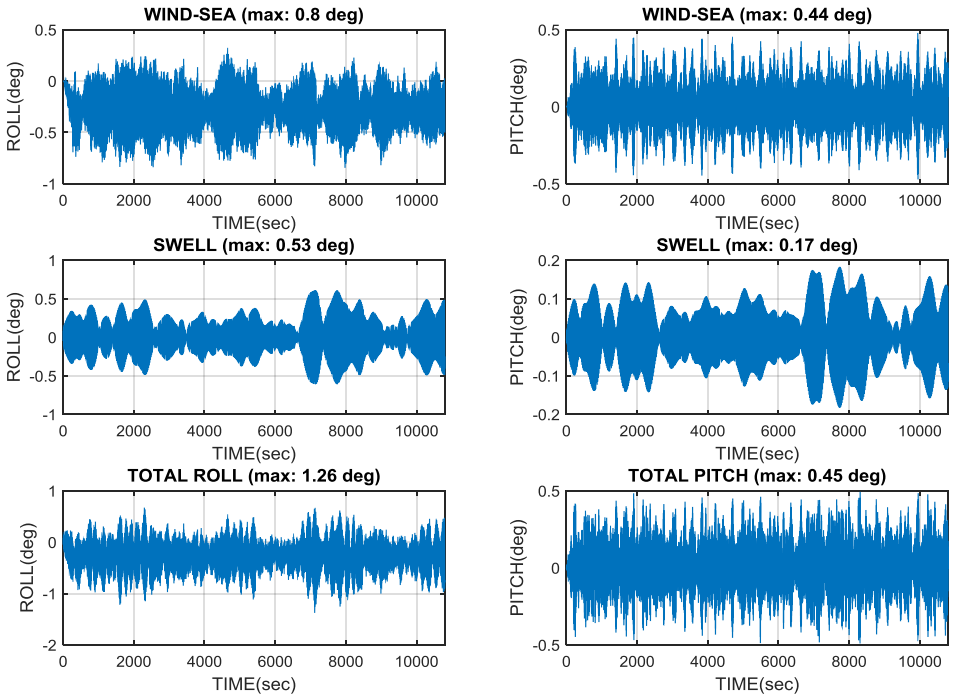

Figure 32. Test result: ZCG=4m under 1-year extreme condition (Part 1+ Part 2)

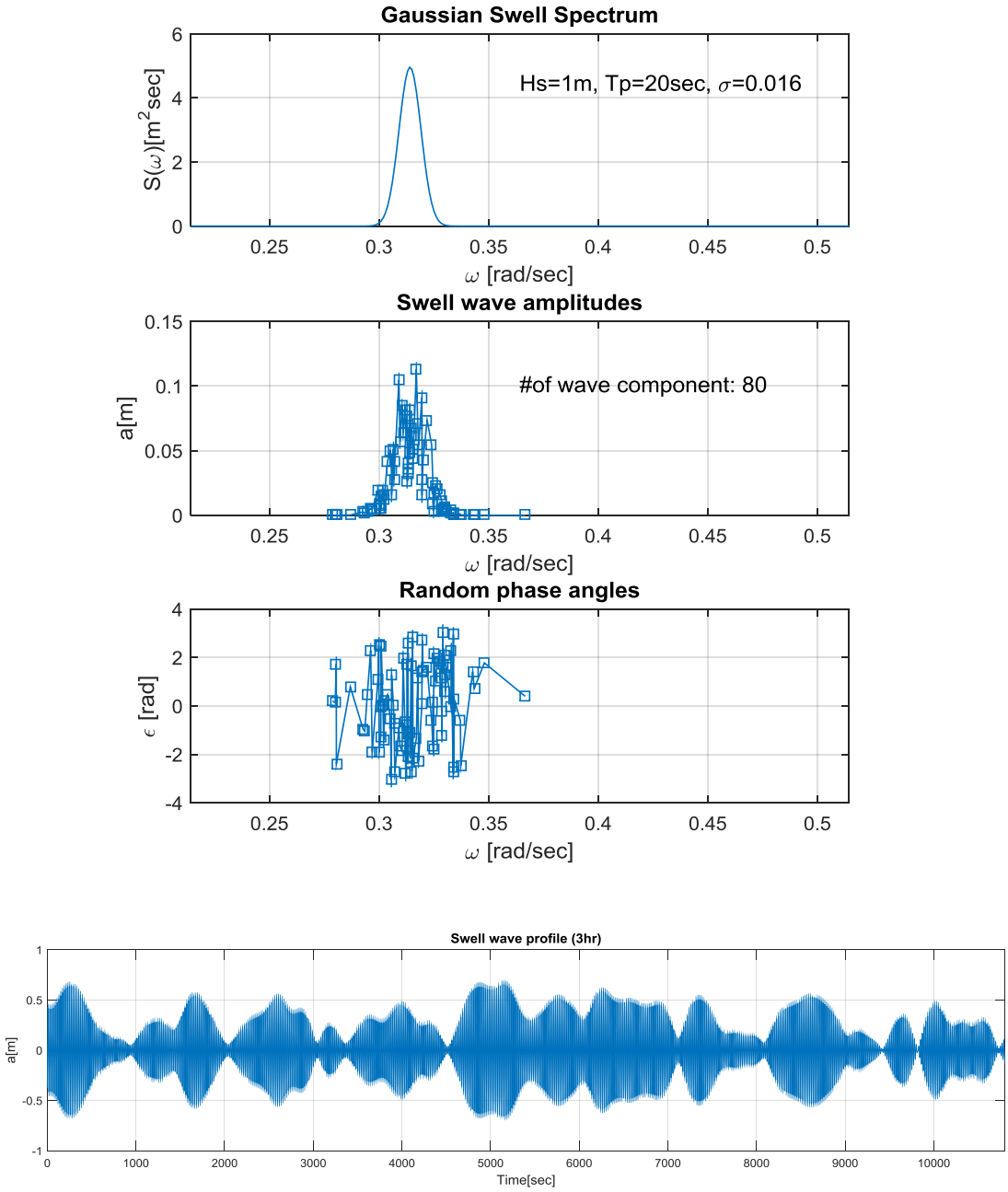

Figure 33. Random swell-wave generation (Hs=1m, Tp=20sec) for the test case of ZCG=4m under 10-year extreme condition

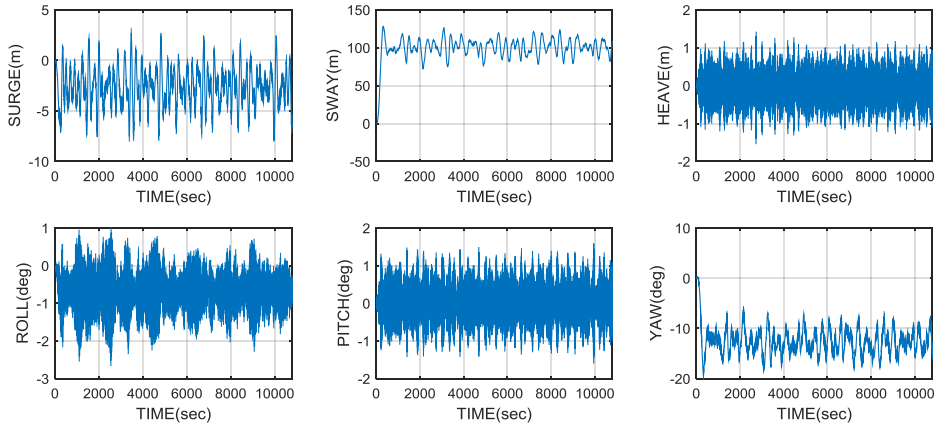

Figure 34. Test result: ZCG=4m under 10-year extreme condition (Part 1)

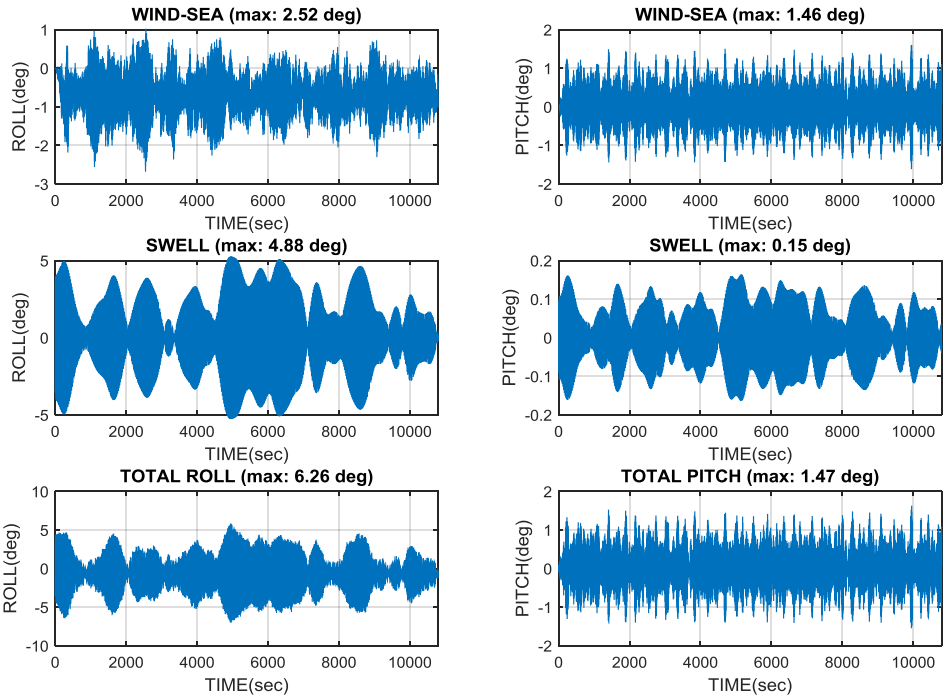

Figure 35. Test result: ZCG=4m under 10-year extreme condition (Part 1+ Part 2)

The same results in the first part (motions under sea-wave, wind, and current) are superposed with the swell-induced motion in a different direction, 10° deviated more on the beam side (BETA=250) as shown in Figure 36. The superposed test result of ZCG=4m case in this heading configuration is presented in Figure 37; and the results of the other FLNG models (ZCG=5~11m) are accessible in Appendix 3.

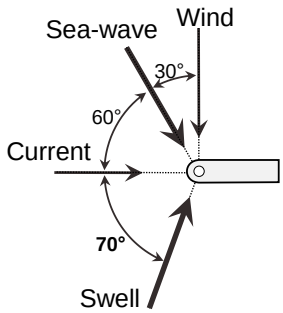

Figure 36. Heading configuration (#2) of the environmental forces considered in the following model tests under extreme conditions

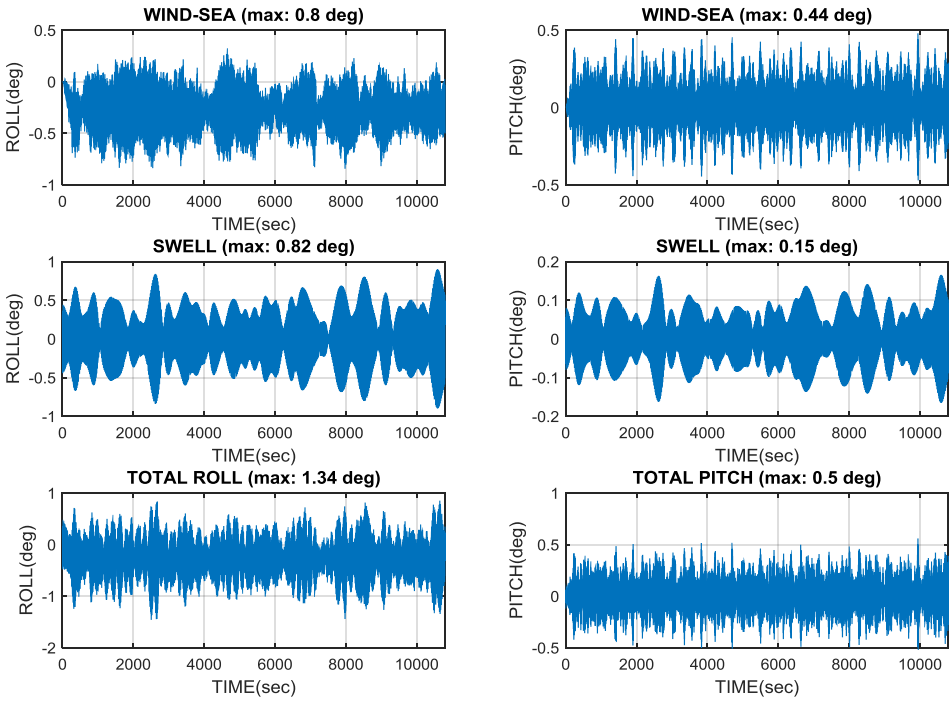

Figure 37. Test result: ZCG=4m under 1-year extreme condition (Swell BETA=250)

The maximum absolute roll and pitch angles of the FLNG models varied by the ZCGs are collected from the model tests in 4 combined-environmental conditions of heading configurations and return periods.

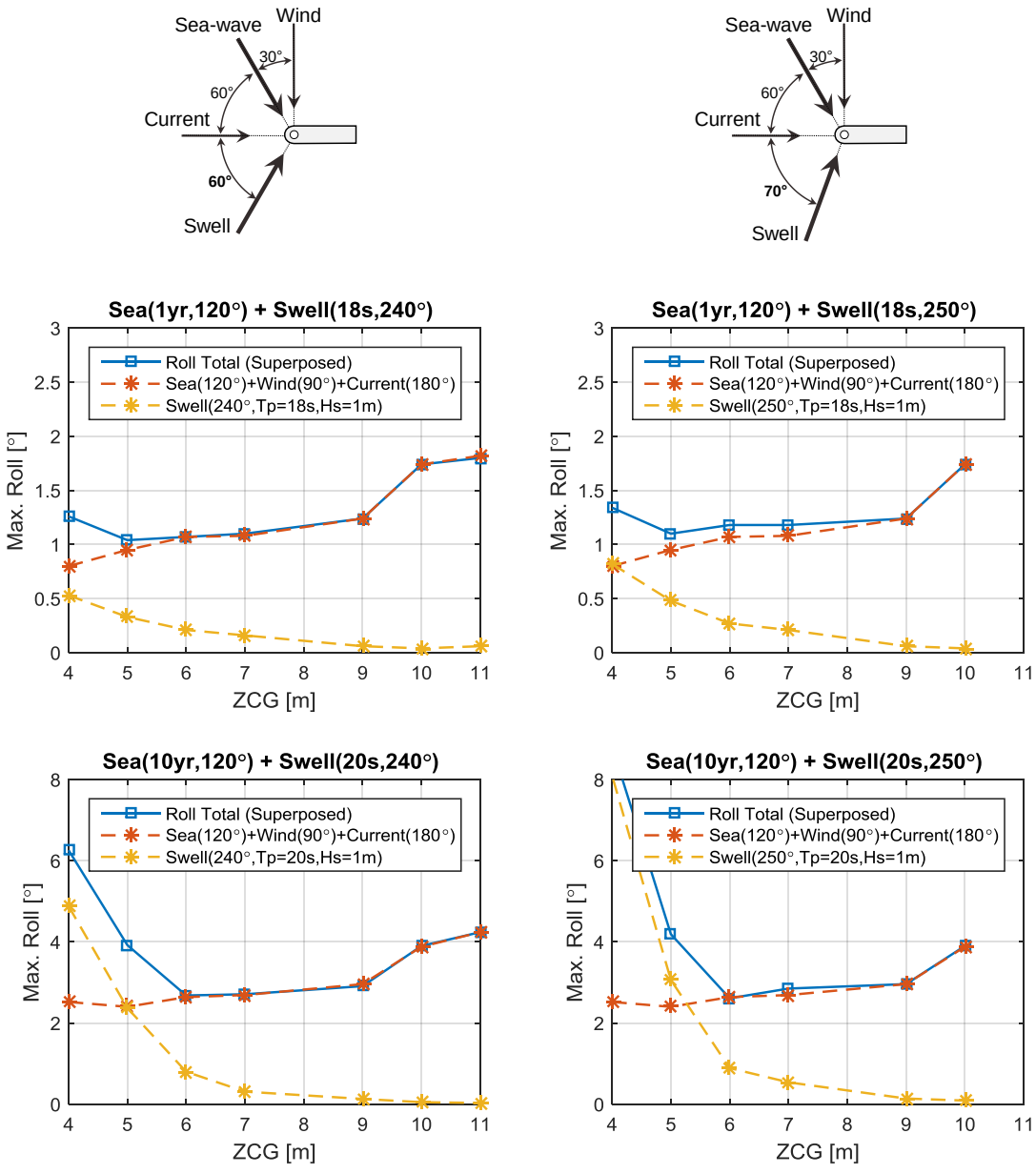

Figure 38. The maximum roll angles of the FLNG models collected from the tests

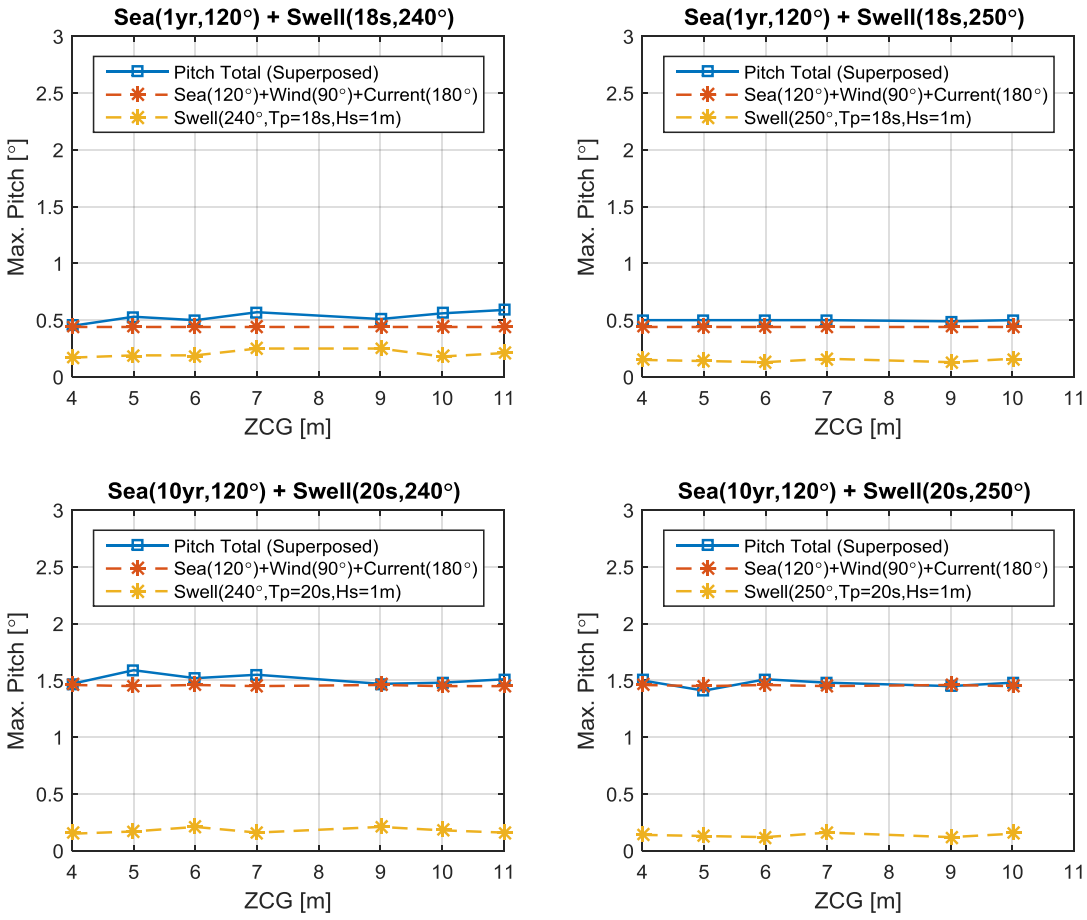

Figure 39. The maximum pitch angles of the FLNG models collected from the tests

The overall trends of the results shown in Figure 38 and Figure 39 are corresponding with the previously made expectation based on the roll/pitch RAOs. First, the roll motion shows different correlation with ZCGs based on the characteristics of the environmental forces. Wind-sea-induced roll motion increases as ZCG increases, while swell-induced roll motion increases as ZCG decreases.

In addition, the severity of the environmental forces is not the only factor that demonstrates that the roll motion is sensitive, but also the roll motion is very sensitive to

the directions of the environmental forces. From the characteristics based on the four cases of the tests, the FLNG models with ZCGs between 6m and 9m are observed to be the most stable models, which implies the natural periods would be better in the range of the models' in regard to minimizing the tilting motions. Below, the main properties of interest for the FLNG models with ZCG=4~11m, particularly in regard to roll motions, are summarized in Table 19.

Table 19. Main properties related to roll motions for the varied FLNG models

ZCG	*Roll natural period* [sec]	*Roll restoring coefficient (K_{44}, Hydrostatic stiffness)*	*Roll radius of gyration (R_{xx})* [m]
4m	20.070	7.050E+10	29.394
5m	20.980	6.420E+10	29.460
6m	22.050	5.780E+10	29.527
7m	23.260	5.150E+10	29.594
8m	24.720	4.520E+10	29.660
9m	26.500	3.890E+10	29.726
10m	28.860	3.260E+10	29.792
11m	31.811	2.630E+10	29.858

From the FLNG models with different vertical distributions of mass, the model with the center of gravity at 6m above the mean sea level (ZCG=6m) is selected for further comparative study. The selected model, which is considered to have practically acceptable design, will provide a reference to the other FLNG models under hypothetical scenarios in the next chapter.

CHAPTER IV

DOWNTIME IN HYPOTHETICAL SCENARIOS

4.1. Introduction

In this chapter, hypothetical scenarios are made in order to investigate how a practical change of weight distribution can contribute to weather-downtime under sea-swell combined conditions.

The reference model selected from the FLNGs of varied ZCGs is modified based on two hypothetical scenarios that reflect practical assumptions of a design modification and an operation stage. Therefore, this chapter includes all of the steps previously presented up to this point, beginning with the numerical modeling, and extends to further procedures of downtime analysis.

4.1.1. Scenario 1: Reduced Topside Weight (Lean FLNG Design Concept)

A conceptual design revised from the original FLNG has been suggested (Pek, 2013), which is for leaner gas fields while the current design is targeting rich gas fields. According to the conceptual design, although some of the topside utilities had to be relocated to its substructure, eventually the topside weight is reduced while the other structures are replicated. Assuming that the original FLNG model from the previous chapter is subject to a conversion stage of its design, the effects by lighter topside weight on the performance of the FLNG are examined. The original FLNG and its lean concept are shown in Figure 40.

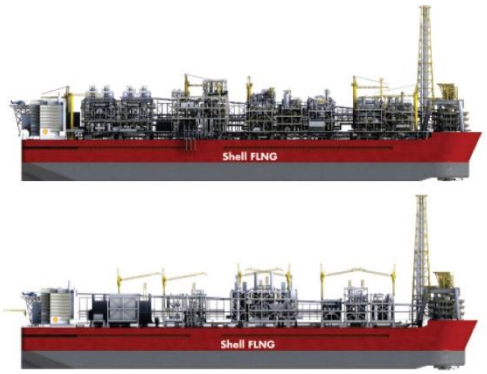

Figure 40. FLNG Original vs. Lean concept (courtesy of Shell)

A new model is built by simply removing 30% of the topside weight from the previous model with ZCG=6m, then the total weight, the draft, mass matrix, and the drag plates are modified based on the change (wind areas are roughly reduced by 10%). Finally, downtimes during a specific year from a hind-cast data are compared in practice.

4.1.2. Scenario 2: Reduced Hull Weight (FLNG in Operation)

The other scenario comes up from a question what if the same amount of the weight change happens in the hull, not in the topside. Thus, this scenario implies a condition of storage weight change (less product loading) during an operation stage.

Based on the second scenario, another new model is built by subtracting exactly the same weight (30% of the original topside weight) from the hull of the original model. Then, the total weight, draft, and drag plates are the same as in the first scenario, but the mass matrix and wind areas are re-calculated. Downtimes are analyzed and compared in the same way at the end.

4.2. Numerical Models for The Two Scenarios

The two scenarios are intended to have the same total weight not only to remove the effect of weight difference but also to take advantage for numerical modeling. A uniform draft can be used for the both scenarios. The assumptions and the plans for the modifications regarding these two scenarios are summarized in Table 20.

Table 20. Plans of model modifications for the hypothetical scenarios

Scenario	***#1. Reduced Topside Weight*** *(design modification)*	***#2. Reduced Hull Weight*** *(less laden condition)*
Assumption	30% of the original topside weight is removed	30% of the original topside weight is removed from the Hull
Revision for the numerical model	▪ Draft, Wetted surface, Mass matrix ▪ Drag plates and Wind area ▪ Viscous damping (from free-decay simulations) ▪ Hydrostatic stiffness (from WAMIT)	▪ Mass matrix, Wind area ▪ Viscous damping (from free-decay simulations) ▪ Hydrostatic stiffness (from WAMIT) ▪ The others are replicated from the scenario 1.

30% of the original topside weight (87,907 *0.3 = 26,372 metric tons) is subtracted from the original topside (in equal rate for both front and back parts) for the scenario 1, and the same weight is subtracted from the hull (in equal rate for both upper and lower parts) for the scenario 2.

The new draft can be obtained by repeating measurements of the displaced volume while shifting up the 3D surface model. The draft length that corresponds with the new displacement was found to be 0.77m shorter than the original model's. Consequently, the body-fixed coordinate system was re-defined as the body was repositioned to the 0.77m

higher position. Then, the geometric data of the wetted surface was also updated by relocating and trimming out the upper 0.77m height of the panels as in Figure 41.

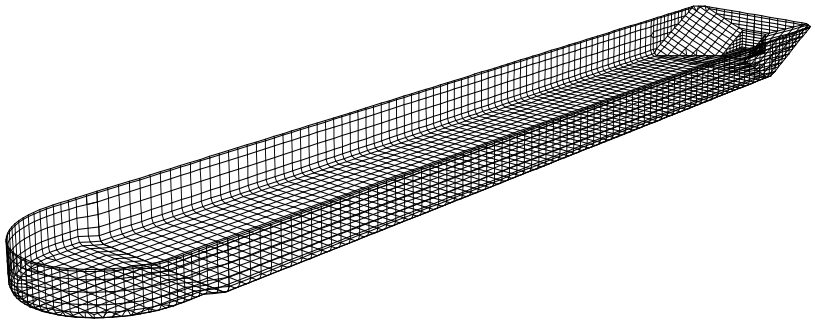

Figure 41. The wetted surface discretized into 3,100 panels for the modified FLNGs (draft: 18.23m, in the both scenario 1 and 2)

The relocation of the body also lets the volume product moments of the each body component updated. The total weight of the topside (front and back portions), and the total weight of the hull (upper and lower parts) are given by the previous assumptions; thus, the vertical mass distributions for the two scenarios are already determined but the weights between the upper/lower hulls, or between the front/back topsides are equally distributed as proportional to the original weight of each part.

Following the process described above, the volume product moments, or the products of inertia for unit mass (1kg for each body component), are calculated as follows by using the 3D modeling software, Rhino. The products of inertia for the two modified models are obtained by multiplying the corresponding density to each part's volume moments. The calculation and the resulting mass matrices are following after the table of volume moments. (Table 21~Table 23)

Table 21. Discretized volume properties of modified model (Draft=18.23m)

		Upper Hull	*Lower Hull*	*Topside Front*	*Topside Back*	*Turret*	*Total*
Volume Centroid	***X***	1.170	-4.542	89.770	-126.613	211.000	
	Y	0.000	0.000	0.000	0.000	0.000	
	Z	12.713	-8.531	44.770	44.770	16.020	
Volume [m3]		8.0680E+05	6.1782E+05	5.5801E+05	6.6271E+05	3.7781E+04	2.6831E+06
Volume product moments	$I'^{B}_{XX,i}$	1.5131E+10	1.0157E+10	5.9957E+09	1.3135E+10	1.6837E+09	
	$I'^{B}_{YY,i}$	3.6851E+08	2.7704E+08	2.5464E+08	3.0241E+08	1.6582E+06	
	$I'^{B}_{ZZ,i}$	1.6962E+08	6.3192E+07	1.2005E+09	1.4257E+09	2.4469E+07	
	$I'^{B}_{XY,i}$	-1.2159E+01	-9.8608E+00	1.1960E-03	-3.7299E-02	0.0000E+00	
	$I'^{B}_{YZ,i}$	-9.2088E-01	5.0000E-01	6.3740E-03	1.7383E-02	0.0000E+00	
	$I'^{B}_{ZX,i}$	8.9983E+07	1.9887E+07	2.2426E+09	-3.7565E+09	1.2771E+08	

Table 22. Mass distribution for Scenario 1 (Lighter Topside)

		Upper Hull	*Lower Hull*	*Topside Front*	*Topside Back*	*Turret*	*Total*
Center of Gravity	***XCG***	1.170	-4.542	89.770	-126.613	211.000	**-0.663697**
	YCG	0.000	0.000	0.000	0.000	0.000	**0.000000**
	ZCG	12.713	-8.531	44.770	44.770	16.020	**5.104029**
Fixed weight %		84.60%		14.00%		1.41%	100.00%
weight %		36.83%	51.48%	5.14%	5.09%	1.46%	100.00%
mass [kg]		2.2707E+08	3.1741E+08	3.1664E+07	3.1409E+07	9.0104E+06	6.1657E+08
mass/volume		281.449	513.767	56.744	47.395	238.492	229.796
Mass Products of Inertia	I^{B}_{XX}	4.2587E+12	5.2182E+12	3.4022E+11	6.2252E+11	4.0155E+11	**1.0841E+13**
	I^{B}_{YY}	1.0372E+11	1.4233E+11	1.4449E+10	1.4333E+10	3.9547E+08	**2.7523E+11**
	I^{B}_{ZZ}	4.7740E+10	3.2466E+10	6.8120E+10	6.7572E+10	5.8357E+09	**2.2173E+11**
	I^{B}_{XY}	-3.4220E+03	-5.0662E+03	6.7866E-02	-1.7678E+00	0.0000E+00	**-8.4899E+03**
	I^{B}_{YZ}	-2.5918E+02	2.5688E+02	3.6169E-01	8.2387E-01	0.0000E+00	**-1.1122E+00**
	I^{B}_{ZX}	2.5325E+10	1.0217E+10	1.2726E+11	-1.7804E+11	3.0457E+10	**1.5215E+10**

Table 23. Mass distribution for Scenario 2 (Lighter Hull)

		Upper Hull	*Lower Hull*	*Topside Front*	*Topside Back*	*Turret*	*Total*
Center of Gravity	***XCG***	1.170	-4.542	89.770	-126.613	211	**-0.663697**
	YCG	0.000	0.000	0.000	0.000	0	**0.000000**
	ZCG	12.713	-8.531	44.770	44.770	16.02	**7.052404**
Fixed weight %		84.60%		14.00%		1.41%	100.00%
weight %		35.00%	48.92%	7.66%	6.96%	1.46%	100.00%
mass [kg]		2.1580E+08	3.0166E+08	4.7211E+07	4.2893E+07	9.0104E+06	6.1657E+08
mass/volume		267.476	488.261	84.606	64.725	238.492	229.796
Mass Products of Inertia	I_{XX}^{B}	4.0472E+12	4.9592E+12	5.0728E+11	8.5013E+11	4.0155E+11	**1.0765E+13**
	I_{YY}^{B}	9.8568E+10	1.3527E+11	2.1544E+10	1.9574E+10	3.9547E+08	**2.7535E+11**
	I_{ZZ}^{B}	4.5370E+10	3.0854E+10	1.0157E+11	9.2279E+10	5.8357E+09	**2.7591E+11**
	I_{XY}^{B}	-3.2521E+03	-4.8147E+03	1.0119E-01	-2.4142E+00	0.0000E+00	**-8.0691E+03**
	I_{YZ}^{B}	-2.4631E+02	2.4413E+02	5.3928E-01	1.1251E+00	0.0000E+00	**-5.1927E-01**
	I_{ZX}^{B}	2.4068E+10	9.7099E+09	1.8974E+11	-2.4314E+11	3.0457E+10	**1.0837E+10**

Mass matrix for the scenario 1 (Lean FLNG concept, Lighter topside weight):

$$M = \begin{bmatrix} 6.166E+08 & 0 & 0 & 0 & 3.147E+09 & 0 \\ 0 & 6.166E+08 & 0 & -3.147E+09 & 0 & -4.092E+08 \\ 0 & 0 & 6.166E+08 & 0 & 4.092E+08 & 0 \\ 0 & -3.147E+09 & 0 & 4.970E+11 & 8.490E+03 & -1.522E+10 \\ 3.147E+09 & 0 & 4.092E+08 & 8.490E+03 & 1.106E+13 & 1.112E+00 \\ 0 & -4.092E+08 & 0 & -1.522E+10 & 1.112E+00 & 1.112E+13 \end{bmatrix}$$

Mass matrix for the scenario 2 (FLNG in Operation, Lighter hull weight):

$$M = \begin{bmatrix} 6.166E+08 & 0 & 0 & 0 & 4.348E+09 & 0 \\ 0 & 6.166E+08 & 0 & -4.348E+09 & 0 & -4.092E+08 \\ 0 & 0 & 6.166E+08 & 0 & 4.092E+08 & 0 \\ 0 & -4.348E+09 & 0 & 5.513E+11 & 8.069E+03 & -1.084E+10 \\ 4.348E+09 & 0 & 4.092E+08 & 8.069E+03 & 1.104E+13 & 5.193E-01 \\ 0 & -4.092E+08 & 0 & -1.084E+10 & 5.193E-01 & 1.104E+13 \end{bmatrix}$$

Table 24. Main particulars of the modified FLNGs for comparison

Designation	*Symbol*	*Unit*	***Original*** *(ZCG=6m)*	***Scenario1*** *(Lighter Topside)*	***Scenario2*** *(Lighter Hull)*
Overall Length		m	488.00	488.00	488.00
Length between perpendiculars	L	m	472.00	472.00	472.00
Breadth	B	m	74.00	74.00	74.00
Depth of Hull	D	m	43.00	43.00	43.00
z-coordinate of CG	ZCG	m	**6.00**	**5.10**	**7.05**
Draft	T	m	**19.00**	**18.23**	**18.23**
Displacement	V	m^3	**627,904.00**	**601,532.03**	**601,532.03**
Center of Buoyancy above Base	FB	m	**9.71**	**10.09**	**10.09**
Center of Gravity above Base	KG	m	**25.00**	**24.10**	**26.05**
Water Plane Area	A	m^2	**34,332.75**	**34,318.29**	**34,318.29**
Length/Beam Ratio	L/B		6.38	6.38	6.38
Draft/Length Ratio	T/L		0.04	0.04	0.04
Beam/Draft Ratio	B/T		**3.89**	**4.06**	**4.06**
Beam/Depth Ratio	B/D		1.72	1.72	1.72
Block Coefficient	Cb		**0.95**	**0.94**	**0.94**
Water Plane Coefficient	Cw		0.98	0.98	0.98
Roll Radius of Gyration	Rx	m	**29.53**	**28.39**	**29.90**
Pitch Radius of Gyration	Ry	m	**133.74**	**133.95**	**133.82**
Yaw Radius of Gyration	Rz	m	**133.82**	**134.27**	**133.82**

The main particulars of the two modified FLNGs are compared with their original model's in Table 24.

While the mooring stiffness for the modified models are replicated from the original FLNG's, the hydrostatic stiffness, K matrix, is separately calculated from WAMIT for each modified model in advance of free-decay simulations. Like what has been learned in the Chapter 3, the uncoupled roll stiffness (K44) is the only component of the restoring coefficients that shows visible differences between the two FLNG models. The K matrices obtained from WAMIT are presented below.

Hydrostatic stiffness for the scenario 1 (Lighter Topside):

$$K = \begin{bmatrix} 0 & 0 & 0 & 0 & 0 & 0 \\ 0 & 0 & 0 & 0 & 0 & 0 \\ 0 & 0 & 0.345E+09 & -0.826E+04 & 0.130E+10 & 0 \\ 0 & 0 & -0.826E+04 & \mathbf{0.694E+11} & -0.241E+06 & 0.238E+09 \\ 0 & 0 & 0.130E+10 & -0.241E+06 & 0.611E+13 & -0.226E+06 \\ 0 & 0 & 0 & 0 & 0 & 0 \end{bmatrix}$$

Hydrostatic stiffness for the scenario 2 (Lighter Hull):

$$K = \begin{bmatrix} 0 & 0 & 0 & 0 & 0 & 0 \\ 0 & 0 & 0 & 0 & 0 & 0 \\ 0 & 0 & 0.345E+09 & -0.826E+04 & 0.130E+10 & 0 \\ 0 & 0 & -0.826E+04 & \mathbf{0.576E+11} & -0.241E+06 & 0.238E+09 \\ 0 & 0 & 0.130E+10 & -0.241E+06 & 0.610E+13 & -0.226E+06 \\ 0 & 0 & 0 & 0 & 0 & 0 \end{bmatrix}$$

Free-decay simulations are conducted for the FLNG models in the hypothetical scenarios. As a result, plots of the body displacement with their logarithmic decrements for heave, roll, and pitch modes are presented below in Figure 42 and Figure 43, respectively for the scenario 1 and 2. Then, the calculation tables and the external damping matrices follow after the plots. (Table 25~Table 27)

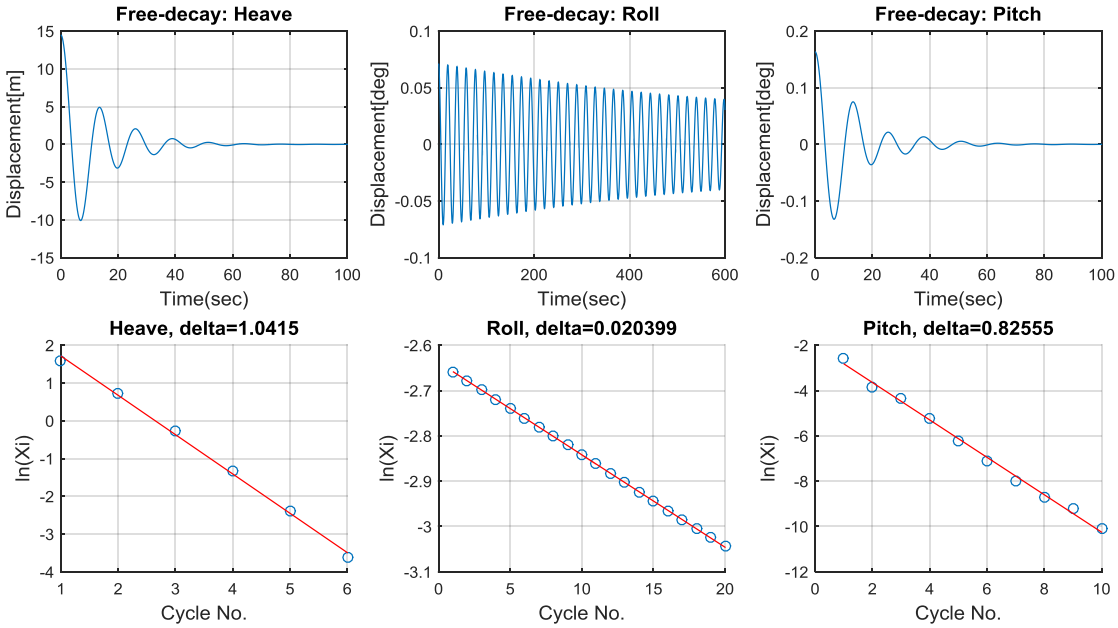

Figure 42. Free-decay simulations for the Scenario #1. Lighter Topside

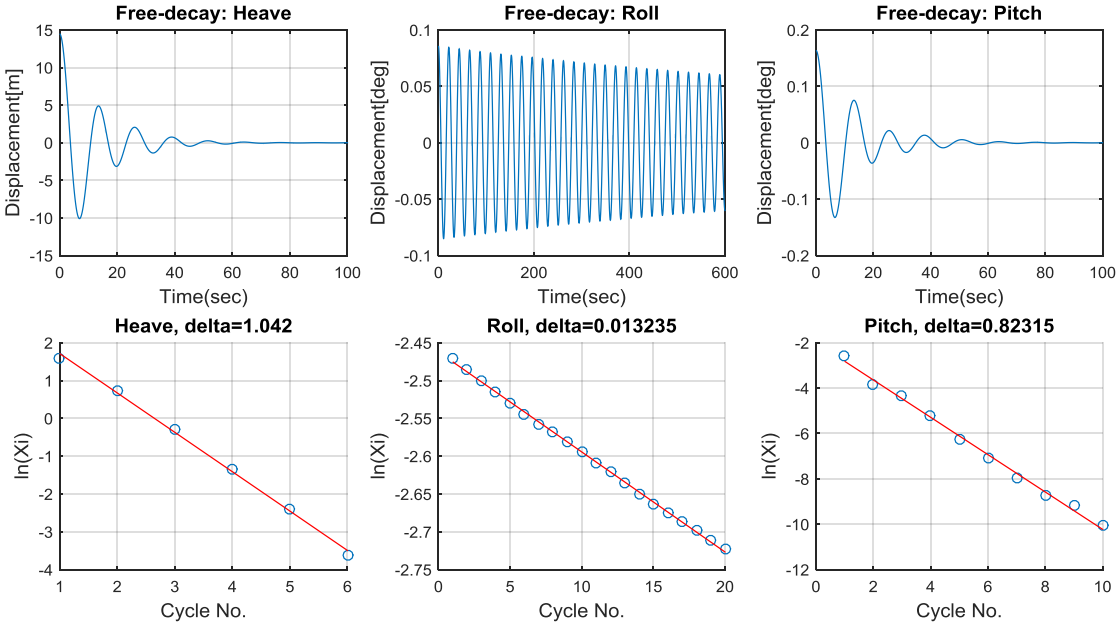

Figure 43. Free-decay simulations for the Scenario #2. Lighter Hull

Table 25. Heave free-decay simulation results for the scenarios (# of cycles=6)

Scenario	T_D	ω_D	δ	ζ	ω_n	T_n	k	b_r	b
Original	12.867	0.488	1.010	15.87%	0.495	12.704	3.450E+08	1.395E+09	2.214E+08
#1	12.733	0.493	1.041	16.35%	0.500	12.562	3.450E+08	1.380E+09	2.256E+08
#2	12.733	0.493	1.042	16.36%	0.500	12.562	3.450E+08	1.379E+09	2.257E+08

Table 26. Roll free-decay simulation results for the scenarios (# of cycles=20)

Scenario	T_D	ω_D	δ	ζ	ω_n	T_n	k	b_r	b
Original	22.050	0.285	0.012	0.19%	0.285	22.050	5.780E+10	4.057E+11	7.904E+08
#1	19.290	0.326	0.020	0.32%	0.326	19.290	6.940E+10	4.261E+11	1.383E+09
#2	21.820	0.288	0.013	0.21%	0.288	21.820	5.760E+10	4.001E+11	8.427E+08

Table 27. Pitch free-decay simulation results for the scenarios (# of cycles=10)

Scenario	T_D	ω_D	δ	ζ	ω_n	T_n	k	b_r	b
Original	12.780	0.492	0.815	12.86%	0.496	12.674	6.110E+12	2.465E+13	3.171E+12
#1	12.660	0.496	0.826	13.03%	0.501	12.552	6.110E+12	2.441E+13	3.180E+12
#2	12.680	0.496	0.823	12.99%	0.500	12.573	6.100E+12	2.441E+13	3.171E+12

External damping for the scenario 1 (Lighter Topside):

$$EXDAMP = \begin{bmatrix} 0 & & & & & \\ & 0 & & & & \\ & & 2.256e8 & & & \\ & & & 1.383e9 & & \\ & & & & 3.180e12 & \\ & & & & & 0 \end{bmatrix}$$

External damping for the scenario 2 (Lighter Hull):

$$EXDAMP = \begin{bmatrix} 0 & & & & & \\ & 0 & & & & \\ & & 2.257e8 & & & \\ & & & 8.427e8 & & \\ & & & & 3.171e12 & \\ & & & & & 0 \end{bmatrix}$$

4.3. RAO Comparison

Taking the mooring stiffness and the viscous damping as external stiffness and damping matrices back into WAMIT, the results from the frequency-domain analyses on the FLNGs of different scenarios are presented by the comparison of RAOs about several directions as follows:

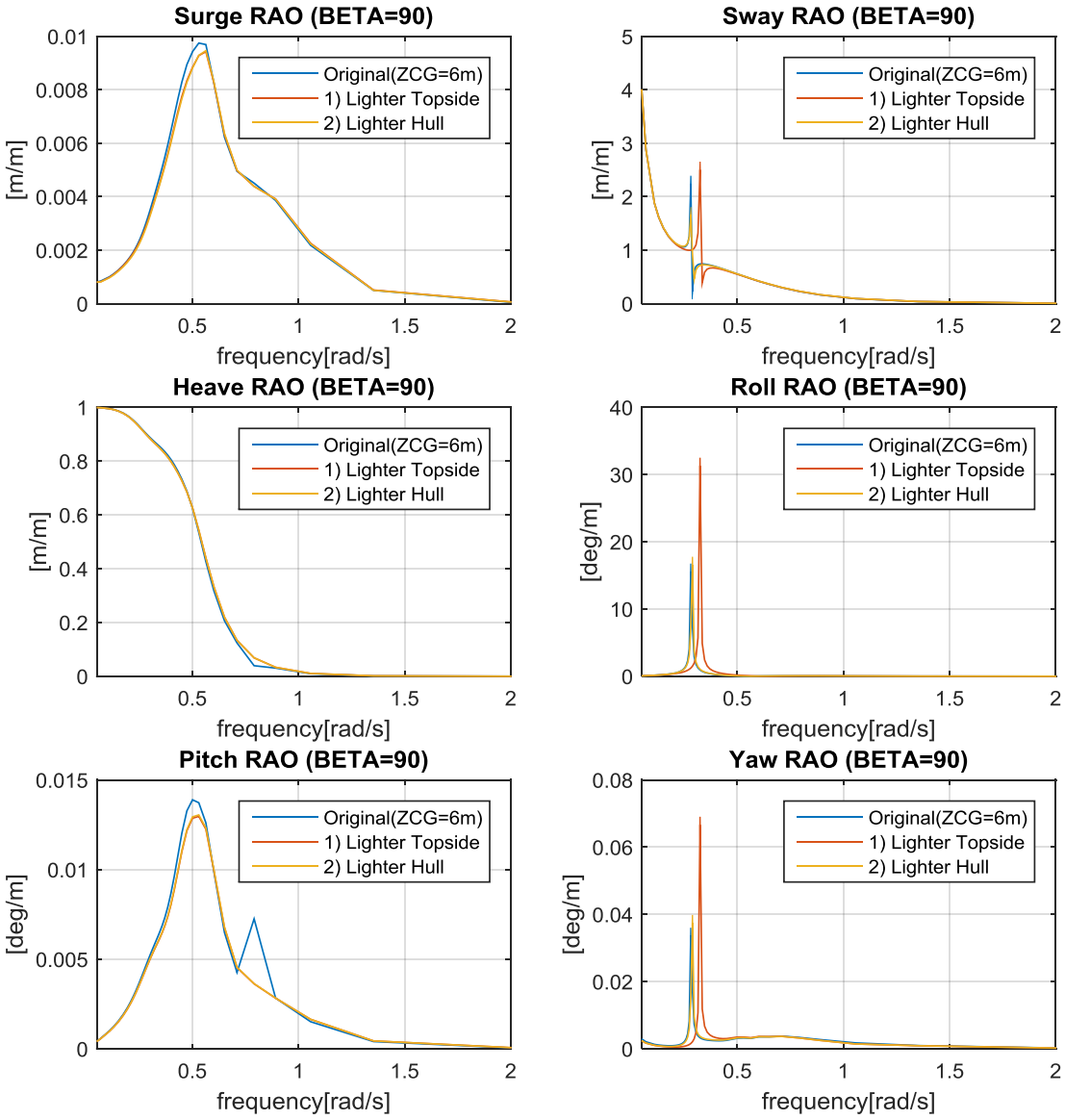

Figure 44. Comparison of RAOs for the FLNGs in the scenarios (BETA=90)

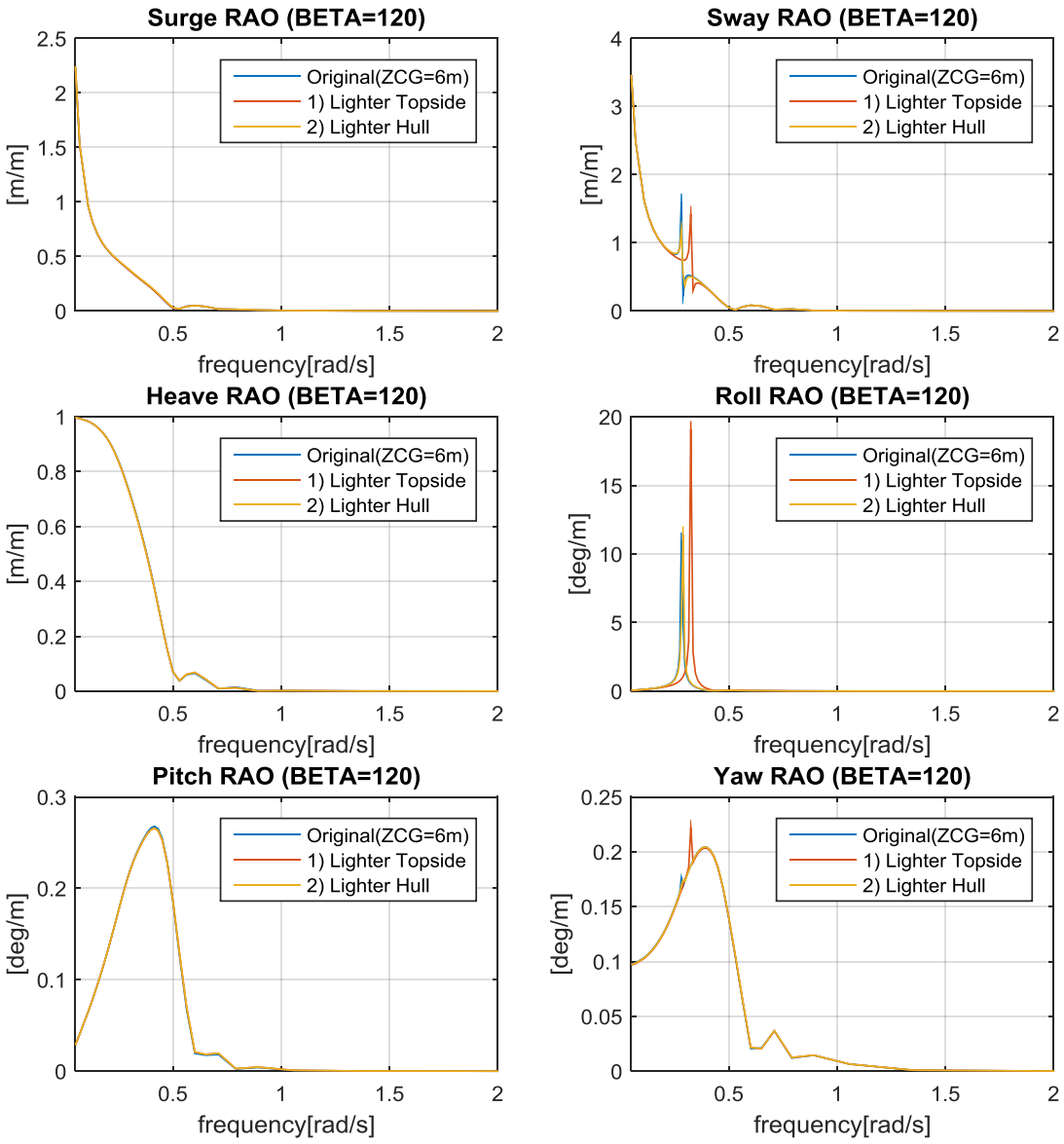

Figure 45. Comparison of RAOs for the FLNGs in the scenarios (BETA=120)

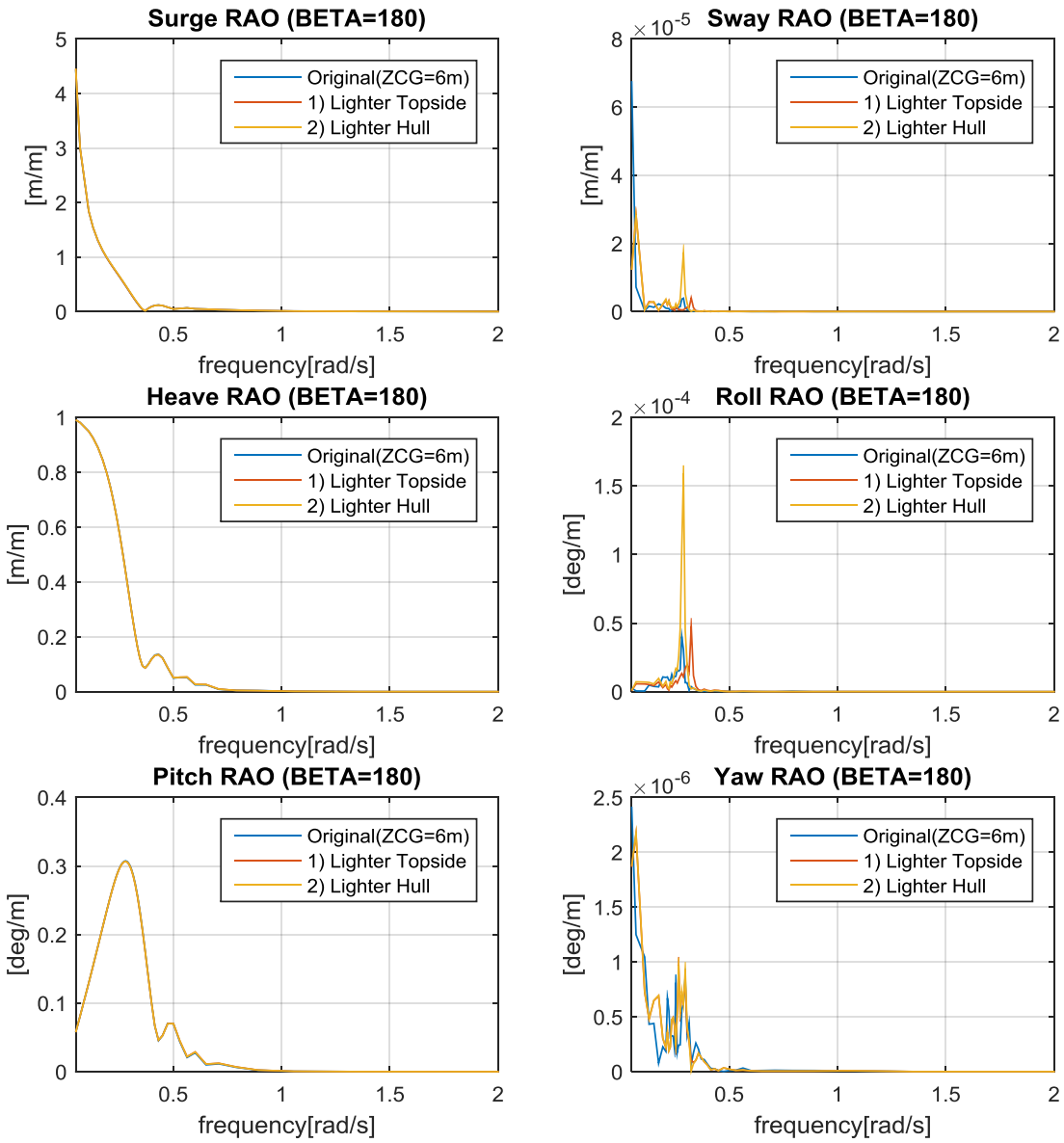

Figure 46. Comparison of RAOs for the FLNGs in the scenarios (BETA=180)

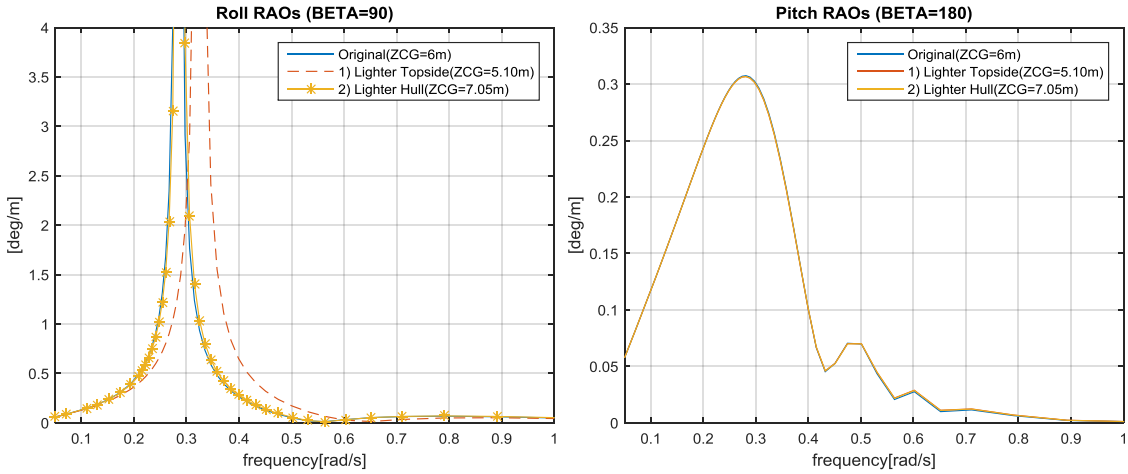

Figure 47. Roll (left) and Pitch (right) RAOs of the FLNGs in the scenarios

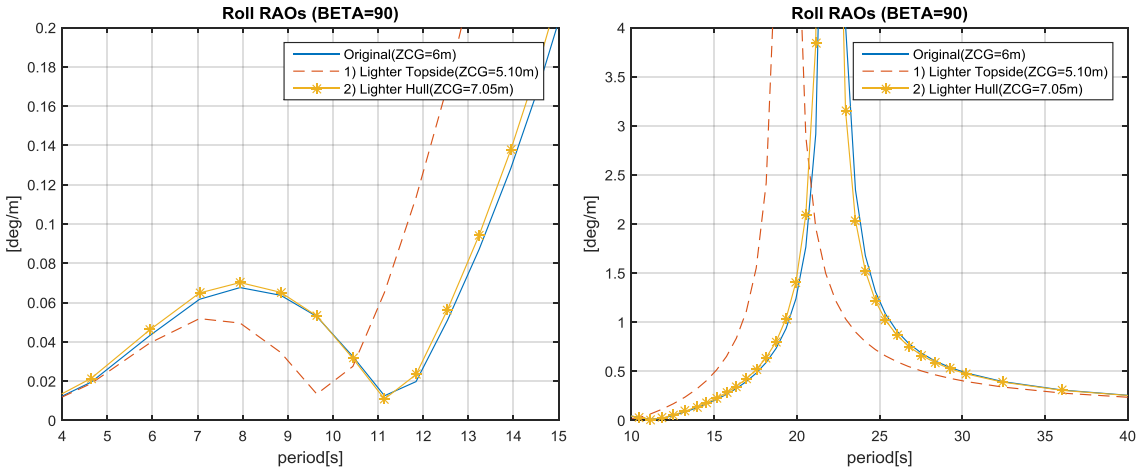

Figure 48. Closer view of the Roll RAOs about short (left) / long (right) periods

Again, the roll and pitch RAOs are shown in Figure 47; as it was found in the previous chapter, pitch RAOs are almost identical regardless of the modifications in the scenarios. On the other hand, the roll RAOs from the two hypothetical scenarios show distinct differences. Figure 48 shows a closer view of the roll RAOs about short / long

period zones. What can be estimated from the above comparisons is that the governing parameter for the roll responses in frequency domain is closely related to the roll natural periods.

In the scenario 1, the vertical location of the center of gravity is 5.1m above the mean sea level, which is the lowest position compared to the other models in this chapter, so the restoring coefficients are relatively bigger than the others. However, reducing a part of the topside weight derives a significant impact on the roll natural period of the floating system. Having differences in natural periods means the responses will be different in regard to the incident wave periods. Therefore, it would be reasonable to expect that the roll responses of the FLNG models will show large differences due to long-period waves, particularly when the peak periods of the waves are bigger than 15 seconds.

The minor difference observed from the second scenario's roll RAO can be interpreted as complementation between the effects from the reduced total weight and the relocated CG. As it was shown in the earlier chapter, the roll natural period increases if the CG is shifted to higher positions, which makes the roll natural period of this model (scenario 2) supposed to be enlarged. But the resulting roll natural period is slightly even smaller than the original one because of the shortened draft due to the total weight change. This compensation is practically quite meaningful because it implies that the roll natural period may not change significantly but rather stay in similar values to what was already tuned even if the floater is under diverse loading conditions during its operation.

4.4. Environmental Condition

The available weather data consists of significant wave height, wave peak period, wave direction, wind speed, and wind direction in 3-hour time step for a year. Even though 3D spectral data set of multi-directional wave trains should be obtained for more accurate downtime estimation, a manipulated sample data set of wind-sea and swell from the available information is utilized in practice for this chapter, as a comparative study. A 1-year data set is selected; Figure 49 shows its scatter diagrams.

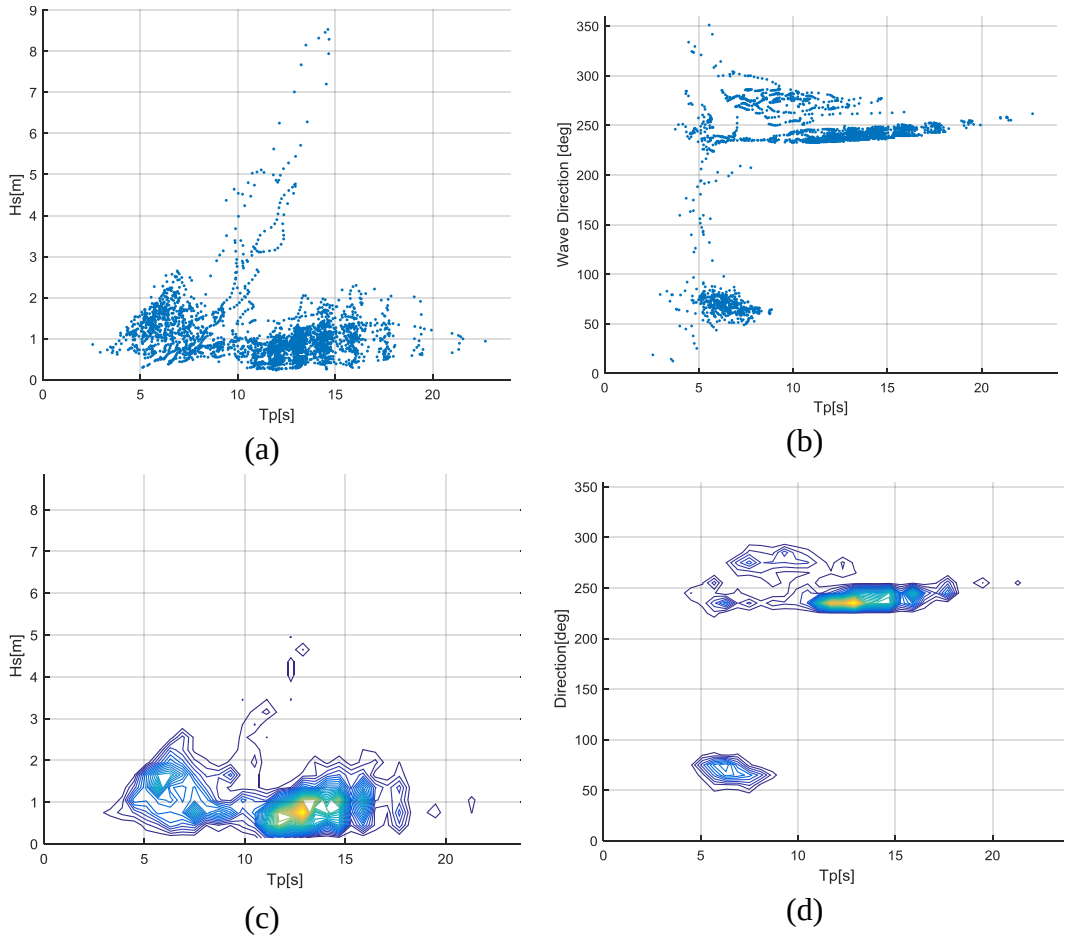

Figure 49. Wave scatter diagrams of occurrence during 1 year (August 2011 – July 2012): (a) Tp vs. Hs scattered data; (b) Tp vs. Direction scattered data; (c) Tp vs. Hs contour; (d) Tp vs. Direction contour

In order to make a sample data of two distinct wave systems (wind-sea and swell), an equation is adopted. The equation, in terms of wave age and wave-wind relative direction with a calibration factor, identifies whether a spectrum is wind-sea or swell. This method is originally intended to be used for partitioned 2D spectrum or spectral grid points in practice, it can still provide a physically acceptable basis-data in regard to the research purposes. The following is the equation, introduced by Portilla et al. (2008) based on the theory from Komen and Hasselmann's (1984), which defines wind-sea systems.

$$\beta \frac{U_z}{C_p} cos(\theta_{wave} - \theta_{wind}) > 1 \qquad \textbf{(20)}$$

where

β : calibration factor *($\beta \leq 1.3$ for pure wind-sea; $1.3 < \beta \leq 2.0$ for old wind-sea)*

U_z : wind speed at height z

C_p : phase speed

From the equation, limits of wind-induced sea-waves (or so-called wind-sea) and swell-waves can be presented by curves in a plane of peak period vs. wave-wind relative direction, based on a constant wind speed.

A calibration factor was selected so that the above equation identifies the waves with extreme Hs as wind-seas, which makes the result to be separated into sea-waves with extreme wave heights and swell-waves with large wave-periods. Examples of the limiting curves varied by wind speeds are shown in Figure 50, and the result of the sea-swell separation is presented by the contours as follows (Figure 51).

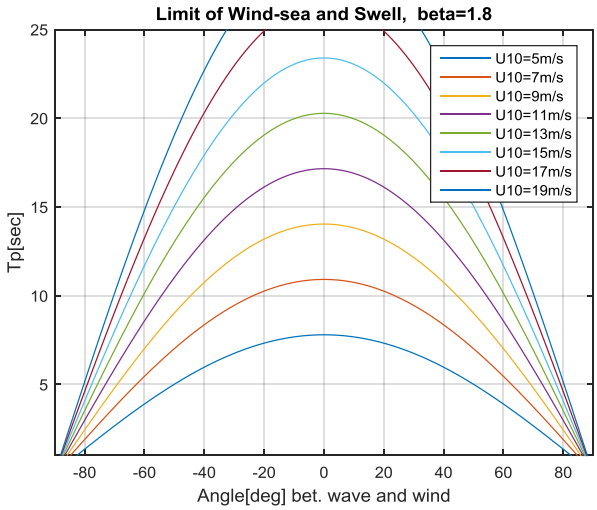

Figure 50. Limit of wind-sea and swell varied by wind speed (U10), from the equation of Portilla et al. (2008).

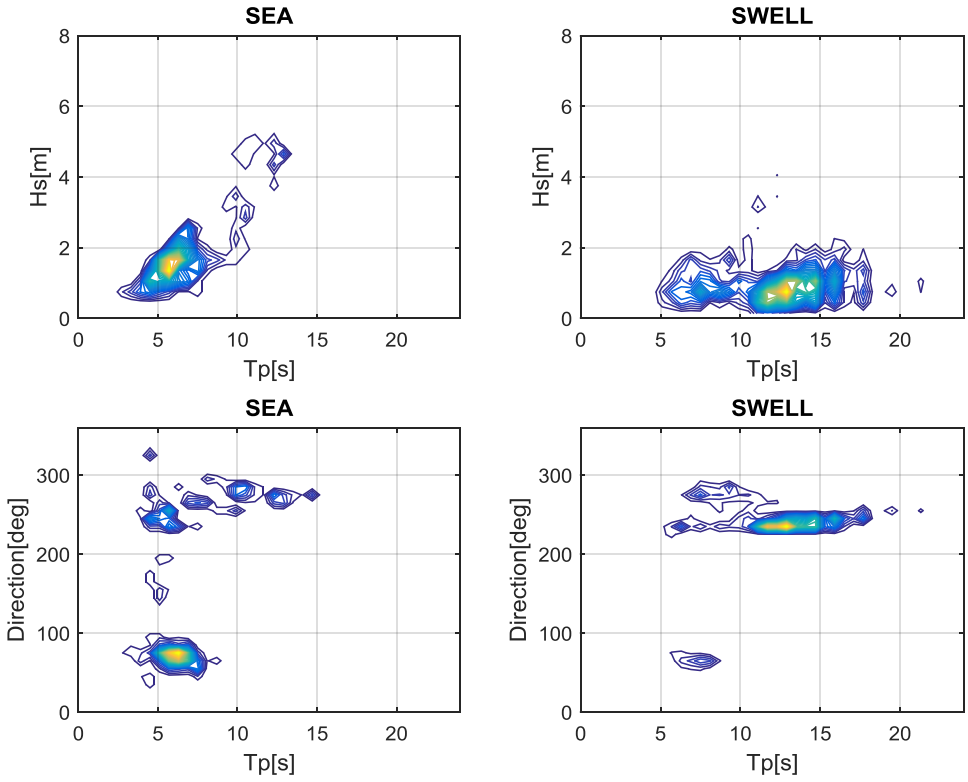

Figure 51. Sea/Swell separation presented about Tp vs. Hs, and Tp vs. wave direction

The areas below the limiting curves, in Figure 50, define the joint-conditions of the three variables (wind speed, peak period of wave, wave-wind relative direction) for sea-waves while the upper areas define the conditions for swell-waves.

In Figure 52, the five metocean properties (significant wave height, peak period, wave direction, wind direction, and wind speed) for each data point that represents 3 hours are individually scattered along a 1-year axis in different colors for sea-waves and swell-waves, forming a set of the annual diagrams. In the diagrams, the directions of wave and wind follow the meteorological convention, which means the direction that the wind or wave propagates from, counting clockwise from the North (0°).

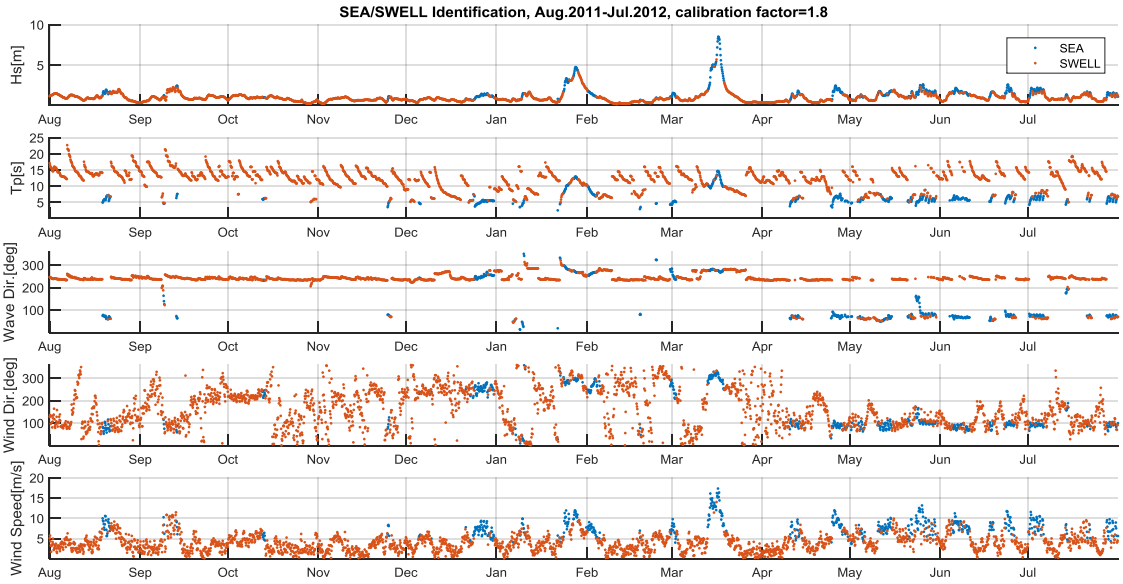

Figure 52. Annual diagrams of wave/wind properties after sea/swell identification

The seasonal characteristics (wet season from December to March and dry season from April to November, according to the EIS) are clearly observed from the annual

diagrams of wave/wind properties. In order to take advantages of the seasonality, the wave scatter diagrams of occurrence are separated again into two seasons, winter swell-season (from April to November) and summer cyclone-season (from December to March) as in Figure 53.

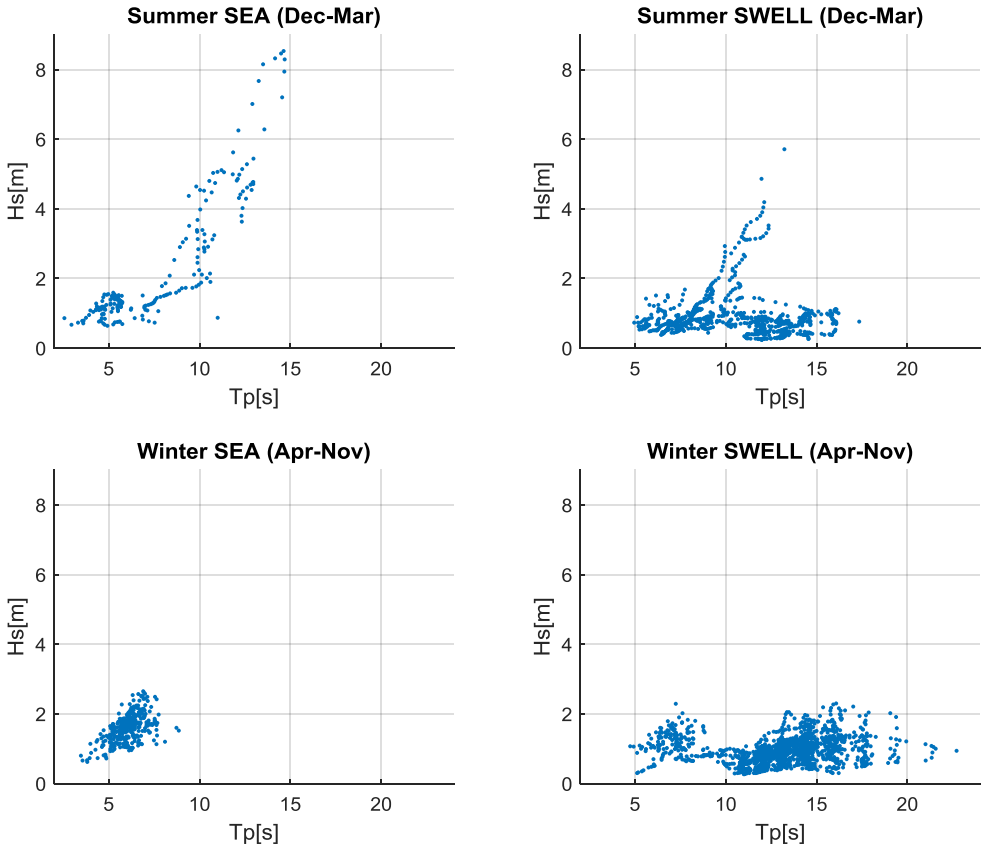

Figure 53. Separation by seasons after sea/swell separation

Then, for downtime estimation, the wave scatter diagram of a dominant wave system for each season provides Hs-Tp joint conditions while the minor wave system is considered a constant set of Hs and Tp. This approach can be valid because the wind-sea during dry season and the swell during wet season are relatively very mild. Finally,

downtime regions can be found from the wave scatter diagram (joint occurrence table) of swell during dry season (labeled ‘winter swell’), and from that of wind-sea during wet season (labeled ‘summer sea’). The variable data points (interesting areas) are highlighted in Figure 54.

- ‘wet’ season (December – March): Wind-sea wave scatter diagram + constant Swell
- ‘dry’ season (April – November): Swell wave scatter diagram + constant Wind-sea

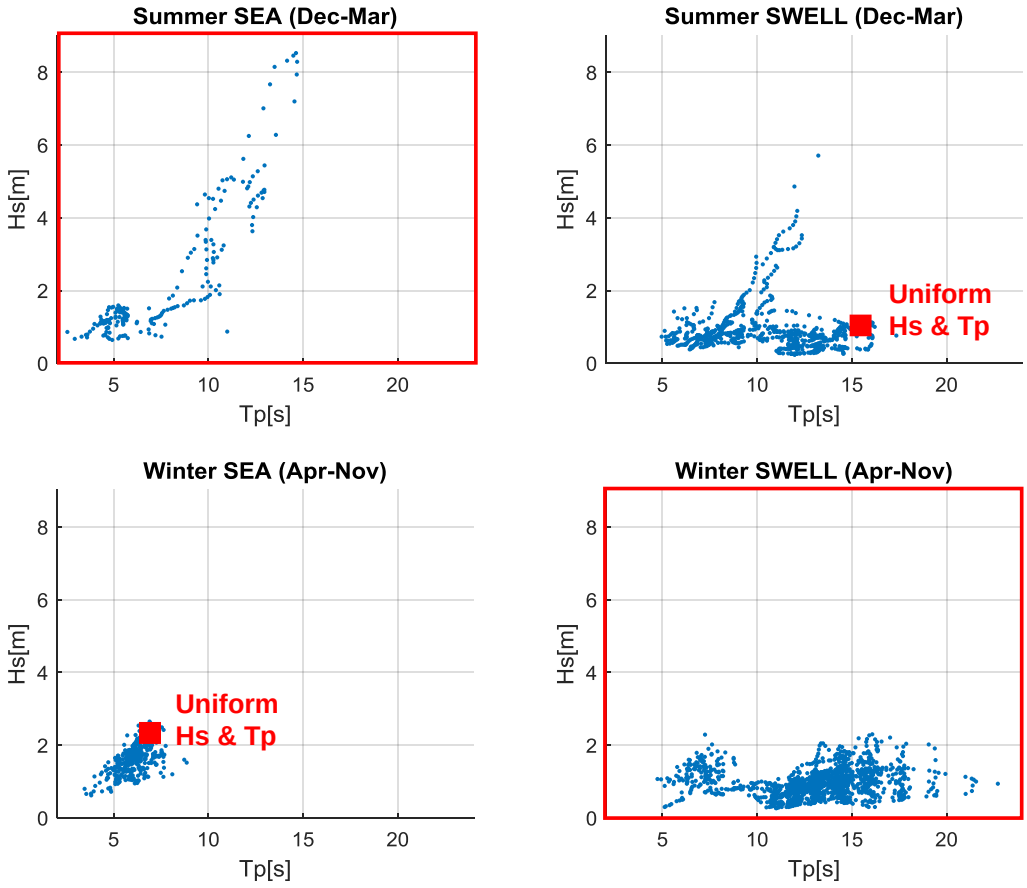

Figure 54. Wave scatter diagrams of summer-sea/swell and winter-sea/swell; the highlighted sections will provide the variables of environmental conditions for the downtime analysis.

Discretizing the significant wave heights by 0.5m and the peak periods by 0.5sec in the wave scatter diagrams presented above, the joint occurrence tables are obtained and provide simplified wave conditions for downtime analysis as follows (Table 28~Table 31).

Table 28. Summer Wind-sea Hs-Tp joint occurrence
(The region of summer downtime conditions will be determined in this plane)

Hs\Tp	min	2.0	2.5	3.0	3.5	4.0	4.5	5.0	5.5	6.0	6.5	7.0	7.5	8.0	8.5	9.0	9.5	10.0	10.5	11.0	11.5	12.0	12.5	13.0	13.5	14.0	14.5	15.0
min	max	2.5	3.0	3.5	4.0	4.5	5.0	5.5	6.0	6.5	7.0	7.5	8.0	8.5	9.0	9.5	10.0	10.5	11.0	11.5	12.0	12.5	13.0	13.5	14.0	14.5	15.0	15.5
0.0	0.5																											
0.5	1.0		2	1	5	1	10	3	3	1	2	1	1							1								
1.0	1.5				1	10	12	15	21	2	2	7	5															
1.5	2.0						3	7	2		1		1	5	2	2	3	1	1									
2.0	2.5													1			3	2	1									
2.5	3.0														2		2	4										
3.0	3.5															2	3	3	2									
3.5	4.0															1	1	1				2						
4.0	4.5															1		1	1			3	1					
4.5	5.0																1	2	2		1	4	6					
5.0	5.5																		2	2		1	2					
5.5	6.0																				1							
6.0	6.5																					1			1			
6.5	7.0																											
7.0	7.5																						1				1	
7.5	8.0																							1			1	
8.0	8.5																								1	2	1	
8.5	9.0																										1	
9.0	9.5																											

Table 29. Summer Swell Hs-Tp joint occurrence (The median Hs & Tp combination in the highlighted region is set as the constant swell condition during summer)

Hs\Tp	min	4.0	4.5	5.0	5.5	6.0	6.5	7.0	7.5	8.0	8.5	9.0	9.5	10.0	10.5	11.0	11.5	12.0	12.5	13.0	13.5	14.0	14.5	15.0	15.5	16.0	16.5	17.0	17.5	18.0	18.5	19.0	19.5	20.0	20.5	21.0	21.5	22.0	22.5	23.0	23.5
min	max	4.5	5.0	5.5	6.0	6.5	7.0	7.5	8.0	8.5	9.0	9.5	10.0	10.5	11.0	11.5	12.0	12.5	13.0	13.5	14.0	14.5	15.0	15.5	16.0	16.5	17.0	17.5	18.0	18.5	19.0	19.5	20.0	20.5	21.0	21.5	22.0	22.5	23.0	23.5	24.0
0.0	0.5				2	2	8	5	1			1				13	30	27	13	29	3	11	12	2	5	1															
0.5	1.0		1	10	20	19	24	34	33	19	25	24	7	11	15	14	27	26	24	31	11	23	14	2	**11**	**5**		1													
1.0	1.5				2	5	7	2	5	13	9	6	9	5	7	1	4	2	2	1		4	4	1	**3**	**6**															
1.5	2.0					1	1		2		2	18		4	5																									
2.0	2.5											4	3	4																										
2.5	3.0											3	1	3	1																									
3.0	3.5													5	4	2	3																							
3.5	4.0														2	2	2																								
4.0	4.5																2																								
4.5	5.0																1																								
5.0	5.5																																							
5.5	6.0																			1																				

Table 30. Winter Wind-sea Hs-Tp joint occurrence (median Hs & Tp combination in the box is set as the constant wind-sea condition during winter)

Hs\Tp	min	2.0	2.5	3.0	3.5	4.0	4.5	5.0	5.5	6.0	6.5	7.0	7.5	8.0	8.5	9.0	9.5	10.0	10.5	11.0	11.5	12.0	12.5	13.0	13.5	14.0	14.5	15.0
min	max	2.5	3.0	3.5	4.0	4.5	5.0	5.5	6.0	6.5	7.0	7.5	8.0	8.5	9.0	9.5	10.0	10.5	11.0	11.5	12.0	12.5	13.0	13.5	14.0	14.5	15.0	15.5
0.0	0.5																											
0.5	1.0			1	4	3	4	4		2																		
1.0	1.5				1	2	10	28	33	17	9	3	2	1														
1.5	2.0						1	17	45	53	20	12	9		2													
2.0	2.5								2	16	17	7	2															
2.5	3.0									1	6	1																
3.0	3.5																											

Table 31. Winter Swell Hs-Tp joint occurrence
(The region of winter downtime conditions will be determined in this plane)

Hs\Tp	min	4.0	4.5	5.0	5.5	6.0	6.5	7.0	7.5	8.0	8.5	9.0	9.5	10.0	10.5	11.0	11.5	12.0	12.5	13.0	13.5	14.0	14.5	15.0	15.5	16.0	16.5	17.0	17.5	18.0	18.5	19.0	19.5	20.0	20.5	21.0	21.5	22.0	22.5	23.0	23.5
min	max	4.5	5.0	5.5	6.0	6.5	7.0	7.5	8.0	8.5	9.0	9.5	10.0	10.5	11.0	11.5	12.0	12.5	13.0	13.5	14.0	14.5	15.0	15.5	16.0	16.5	17.0	17.5	18.0	18.5	19.0	19.5	20.0	20.5	21.0	21.5	22.0	22.5	23.0	23.5	24.0
0.0	0.5			4	2									3	18	20	33	18	10	9	2	2	11	2	9	6		1	1												
0.5	1.0			1	2	9	6	7	11	7	8	5	18	9	40	24	83	104	78	134	35	79	48	11	26	18	4	8	27	2	1	7	1			3			1		
1.0	1.5		2	3	5	15	11	22	17	5	2			1		1	13	19	33	73	34	64	66	17	44	24	7	9	18	1		4	2			3	1				
1.5	2.0					3	5	9	5	2	3									10	4	18	16	8	15	10		2	6			2									
2.0	2.5							1	1											2				1	3	3	1	1	1			1									
2.5	3.0																																								

Moreover, the other environmental conditions can be further simplified as constant values or as a function of Hs or Tp. These simplifications are necessary if we are going to define the downtime zones in a 2-dimensional plane of Hs-Tp joint conditions. In the present study, the wind speeds are defined as a function of Hs by taking the trend (2D poly-fit) from the Hs (sea-wave) vs. wind-speed correlation as presented in Figure 55. Also, a uniform current speed is assumed to be the same as in the previous model tests'.

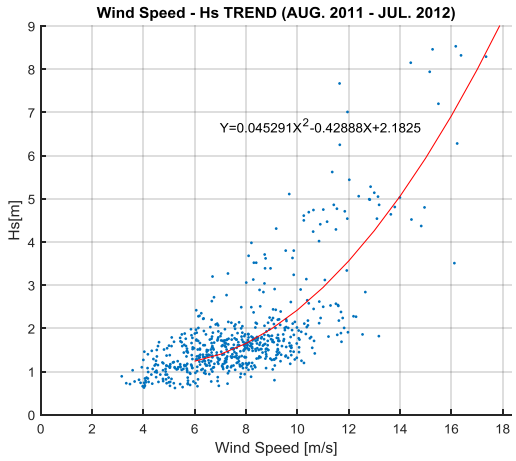

Figure 55. Correlation function to set simplified wind speeds based on significant wave heights obtained from wind-sea data for 1 year

4.5. Downtime Estimation

4.5.1. Overall Plan

The maximum magnitudes and the mean angles of the roll or pitch displacements in the superposed time-series are compared to the operation limits (max. 2° and mean 1°).

First, from the summer conditions, time-series of motions under sea/wind/current loadings can be obtained by using CHARM3D. Meanwhile, the linear wave-induced motion under the constant summer-swell condition with random frequencies and random phase angles can be linearly superposed with the time-series from CHARM3D. Finally, the maximum roll/pitch displacement during 3-hour time-series is compared with the threshold, 2 degrees, so that the joint environmental condition in the summer-sea table can be defined as whether operable condition or downtime condition. For the winter season, the zone of downtime conditions can be defined in the winter-swell table by following the same procedure described above.

Lastly, considering that recovery-hours must follow every shutdown event, chronological aspect helps estimate more practical downtime-period. The recovery time would be even more necessary for an FLNG which has temperature-sensitive facilities, and it can be varied by the previous period of downtime event. The recovery time is roughly assumed to be 3~24 hours for this study.

The downtime estimations described above are conducted based on two different heading assumptions. The FLNG is assumed to be heading always toward (1) wind-sea direction, or (2) swell direction for an entire year. Since the directional spreading of the waves cannot be considered through the analysis because of limited information, the

FLNG headings are set as 10 degree-deviated angles to the front waves. The heading configuration set in this chapter is shown in Figure 56 and Table 32.

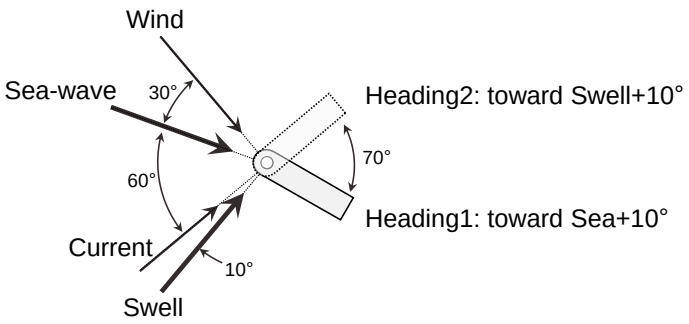

Figure 56. Directional configuration of environmental forces and FLNG headings for downtime estimations

Table 32. Directions of environmental forces

Heading case	*BETA(°)*			
	Sea	*Wind*	*Swell*	*Current*
#1. Toward Sea+10°	190	160	260	250
#2. Toward Swell+10°	120	90	190	180

4.5.2. Downtime during Winter Swell-Season (April – November)

The joint-occurrence table of "winter-swell" consists of the combinations of Hs and Tp discretized by 0.5m and 0.5 second, respectively. Linear wave-induced motions under the joint-conditions in two heading scenarios are superposed with the time-series of motions under the constant wind-sea condition from CHARM3D for every 0.2 second during 3 hours. As a result, excessive mean angles were not found throughout the entire cases, and the maximum roll/pitch for the three FLNG models are presented as follows (Table 33 ~ Table 45).

Table 33. Input environmental conditions for winter swell-season

Part	*by CHARM3D*							*by RAOs*		
Heading case	Sea wave			Current		Wind		Swell		
	BETA	Hs	Tp	BETA	speed	BETA	speed	BETA	Hs	Tp
#1	190	2.5 m	7 sec	250	0.6 m/s	160	11 m/s	260	varied	varied
#2	120	2.5 m	7 sec	180	0.6 m/s	90	11 m/s	190	varied	varied

Table 34. Maximum Roll (°) of the original FLNG, Winter, Heading #1 (toward Sea)

Hs \ Tp	4.25	4.75	5.25	5.75	6.25	6.75	7.25	7.75	8.25	8.75	9.25	9.75	10.25	10.75	11.25	11.75	12.25	12.75	13.25	13.75	14.25	14.75	15.25	15.75	16.25	16.75	17.25	17.75	18.25	18.75	19.25	19.75	20.25	20.75	21.25	21.75	22.25	22.75	23.25	23.75
0.25	0.1	0.1	0.1	0.1	0.1	0.1	0.1	0.1	0.1	0.1	0.1	0.1	0.1	0.1	0.1	0.1	0.1	0.1	0.1	0.1	0.1	0.2	0.1	0.2	0.1	0.2	0.2	0.2	0.2	0.2	0.3	0.3	0.3	0.5	0.9	1.9	2.0	1.9	0.9	0.5
0.75	0.1	0.1	0.1	0.1	0.1	0.1	0.1	0.1	0.1	0.1	0.2	0.1	0.1	0.1	0.1	0.1	0.1	0.1	0.1	0.2	0.2	0.2	0.2	0.2	0.2	0.2	0.3	0.3	0.4	0.4	0.5	0.8	0.8	1.3	2.4	4.2	4.8	4.2	2.6	1.1
1.25	0.1	0.1	0.1	0.1	0.1	0.1	0.1	0.1	0.1	0.2	0.1	0.2	0.2	0.2	0.1	0.1	0.1	0.2	0.2	0.2	0.2	0.2	0.3	0.3	0.4	0.4	0.5	0.5	0.6	0.8	0.7	0.9	1.4	2.6	4.4	10.3	12.7	8.2	3.7	2.1
1.75	0.1	0.1	0.1	0.1	0.1	0.1	0.1	0.2	0.1	0.2	0.2	0.2	0.2	0.2	0.1	0.2	0.2	0.2	0.2	0.2	0.2	0.3	0.4	0.4	0.5	0.5	0.5	0.7	0.7	1.0	1.2	1.3	1.9	3.1	5.6	9.1	15.7	10.5	5.0	3.8
2.25	0.1	0.1	0.1	0.1	0.1	0.1	0.1	0.1	0.2	0.2	0.2	0.2	0.2	0.2	0.2	0.2	0.2	0.2	0.2	0.2	0.3	0.3	0.4	0.5	0.5	0.6	0.7	0.8	1.1	1.3	1.9	1.5	2.6	3.8	7.5	12.7	21.9	11.3	7.3	3.2
2.75	0.1	0.1	0.1	0.1	0.1	0.1	0.1	0.2	0.2	0.2	0.2	0.2	0.2	0.2	0.2	0.2	0.2	0.2	0.2	0.3	0.3	0.4	0.4	0.6	0.6	0.8	0.9	1.2	1.4	1.6	1.7	1.8	3.2	4.9	7.8	18.2	24.9	15.2	8.6	4.7

Table 35. Maximum Pitch (°) of the original FLNG, Winter, Heading #1 (toward Sea)

Hs \ Tp	4.25	4.75	5.25	5.75	6.25	6.75	7.25	7.75	8.25	8.75	9.25	9.75	10.25	10.75	11.25	11.75	12.25	12.75	13.25	13.75	14.25	14.75	15.25	15.75	16.25	16.75	17.25	17.75	18.25	18.75	19.25	19.75	20.25	20.75	21.25	21.75	22.25	22.75	23.25	23.75
0.25	0.0	0.0	0.0	0.0	0.0	0.0	0.0	0.0	0.0	0.0	0.0	0.0	0.0	0.0	0.0	0.0	0.0	0.0	0.0	0.0	0.0	0.0	0.0	0.0	0.0	0.0	0.0	0.0	0.0	0.0	0.0	0.0	0.0	0.0	0.0	0.0	0.0	0.0	0.0	0.0
0.75	0.0	0.0	0.0	0.0	0.0	0.0	0.0	0.0	0.0	0.0	0.0	0.1	0.1	0.1	0.1	0.1	0.1	0.1	0.1	0.1	0.1	0.1	0.1	0.1	0.1	0.1	0.1	0.1	0.1	0.1	0.1	0.0	0.0	0.0	0.0	0.0	0.0	0.0	0.0	0.0
1.25	0.0	0.0	0.0	0.0	0.0	0.0	0.0	0.0	0.0	0.0	0.1	0.1	0.1	0.2	0.1	0.2	0.1	0.2	0.1	0.2	0.2	0.2	0.1	0.1	0.1	0.1	0.1	0.1	0.1	0.1	0.1	0.1	0.1	0.1	0.1	0.1	0.1	0.1	0.1	0.1
1.75	0.0	0.0	0.0	0.0	0.0	0.0	0.0	0.0	0.0	0.1	0.1	0.1	0.1	0.2	0.2	0.2	0.2	0.2	0.2	0.2	0.2	0.2	0.2	0.2	0.2	0.1	0.1	0.2	0.1	0.1	0.1	0.1	0.1	0.1	0.1	0.1	0.1	0.1	0.1	0.1
2.25	0.0	0.0	0.0	0.0	0.0	0.0	0.0	0.0	0.1	0.1	0.1	0.2	0.2	0.3	0.2	0.3	0.2	0.3	0.3	0.3	0.2	0.2	0.3	0.2	0.2	0.2	0.2	0.2	0.2	0.2	0.2	0.1	0.2	0.1	0.1	0.2	0.1	0.1	0.1	0.1
2.75	0.0	0.0	0.0	0.0	0.0	0.0	0.0	0.0	0.1	0.1	0.1	0.2	0.2	0.3	0.3	0.3	0.3	0.4	0.3	0.3	0.3	0.3	0.3	0.3	0.2	0.3	0.2	0.2	0.2	0.2	0.2	0.2	0.2	0.2	0.2	0.2	0.2	0.2	0.1	0.2

Table 36. Maximum Roll (°) of the original FLNG, Winter, Heading #2 (toward Swell)

Hs \ Tp	4.25	4.75	5.25	5.75	6.25	6.75	7.25	7.75	8.25	8.75	9.25	9.75	10.25	10.75	11.25	11.75	12.25	12.75	13.25	13.75	14.25	14.75	15.25	15.75	16.25	16.75	17.25	17.75	18.25	18.75	19.25	19.75	20.25	20.75	21.25	21.75	22.25	22.75	23.25	23.75
0.25	0.5	0.5	0.5	0.5	0.5	0.5	0.5	0.5	0.5	0.5	0.5	0.5	0.5	0.5	0.5	0.5	0.5	0.5	0.5	0.5	0.5	0.5	0.5	0.5	0.5	0.5	0.5	0.5	0.5	0.5	0.5	0.5	0.5	0.5	0.5	0.5	0.5	0.5	0.5	0.5
0.75	0.5	0.5	0.5	0.5	0.5	0.5	0.5	0.5	0.5	0.5	0.5	0.5	0.5	0.5	0.5	0.5	0.5	0.5	0.5	0.5	0.5	0.5	0.5	0.5	0.5	0.5	0.5	0.5	0.5	0.5	0.5	0.5	0.5	0.5	0.5	0.6	0.7	0.7	0.5	0.6
1.25	0.5	0.5	0.5	0.5	0.5	0.5	0.5	0.5	0.5	0.5	0.5	0.5	0.5	0.5	0.5	0.5	0.5	0.5	0.5	0.5	0.5	0.5	0.5	0.5	0.5	0.5	0.5	0.5	0.5	0.5	0.5	0.5	0.5	0.5	0.5	0.7	0.9	0.8	0.7	0.5
1.75	0.5	0.5	0.5	0.5	0.5	0.5	0.5	0.5	0.5	0.5	0.5	0.5	0.5	0.5	0.5	0.5	0.5	0.5	0.5	0.5	0.5	0.5	0.5	0.5	0.5	0.5	0.5	0.5	0.5	0.5	0.5	0.5	0.5	0.5	0.6	1.0	1.2	1.2	0.8	0.7
2.25	0.5	0.5	0.5	0.5	0.5	0.5	0.5	0.5	0.5	0.5	0.5	0.5	0.5	0.5	0.5	0.5	0.5	0.5	0.5	0.5	0.5	0.5	0.5	0.5	0.5	0.5	0.5	0.5	0.5	0.5	0.5	0.5	0.5	0.5	0.7	1.1	1.4	1.1	0.8	0.7
2.75	0.5	0.5	0.5	0.5	0.5	0.5	0.5	0.5	0.5	0.5	0.5	0.5	0.5	0.5	0.5	0.5	0.5	0.5	0.5	0.5	0.5	0.5	0.5	0.5	0.5	0.5	0.5	0.5	0.5	0.5	0.5	0.6	0.5	0.6	0.9	1.4	1.7	1.4	0.9	0.8

Table 37. Maximum Pitch (°) of the original FLNG, Winter, Heading #2 (toward Swell)

Hs \ Tp	4.25	4.75	5.25	5.75	6.25	6.75	7.25	7.75	8.25	8.75	9.25	9.75	10.25	10.75	11.25	11.75	12.25	12.75	13.25	13.75	14.25	14.75	15.25	15.75	16.25	16.75	17.25	17.75	18.25	18.75	19.25	19.75	20.25	20.75	21.25	21.75	22.25	22.75	23.25	23.75
0.25	0.0	0.0	0.0	0.0	0.0	0.0	0.0	0.0	0.0	0.0	0.0	0.0	0.0	0.0	0.0	0.0	0.0	0.0	0.0	0.0	0.0	0.0	0.0	0.0	0.0	0.0	0.0	0.0	0.1	0.1	0.1	0.1	0.1	0.1	0.1	0.1	0.1	0.1	0.1	0.1
0.75	0.0	0.0	0.0	0.0	0.0	0.0	0.0	0.0	0.0	0.0	0.0	0.0	0.0	0.0	0.0	0.0	0.1	0.1	0.1	0.0	0.0	0.0	0.1	0.1	0.1	0.1	0.1	0.1	0.1	0.2	0.2	0.2	0.2	0.2	0.2	0.2	0.2	0.2	0.2	0.2
1.25	0.0	0.0	0.0	0.0	0.0	0.0	0.0	0.0	0.0	0.0	0.0	0.0	0.0	0.0	0.0	0.0	0.1	0.1	0.1	0.1	0.1	0.1	0.1	0.1	0.2	0.2	0.2	0.2	0.2	0.2	0.2	0.3	0.3	0.3	0.3	0.3	0.3	0.3	0.3	0.3
1.75	0.0	0.0	0.0	0.0	0.0	0.0	0.0	0.0	0.0	0.0	0.0	0.0	0.0	0.0	0.0	0.1	0.1	0.1	0.1	0.1	0.1	0.1	0.1	0.2	0.2	0.2	0.3	0.3	0.3	0.5	0.3	0.4	0.4	0.4	0.4	0.4	0.4	0.4	0.6	0.4
2.25	0.0	0.0	0.0	0.0	0.0	0.0	0.0	0.0	0.0	0.0	0.0	0.0	0.0	0.1	0.0	0.1	0.1	0.1	0.1	0.1	0.1	0.1	0.2	0.2	0.4	0.3	0.5	0.4	0.5	0.5	0.4	0.5	0.6	0.5	0.5	0.6	0.6	0.5	0.5	
2.75	0.0	0.0	0.0	0.0	0.0	0.0	0.0	0.0	0.0	0.0	0.0	0.0	0.1	0.1	0.1	0.1	0.1	0.1	0.2	0.1	0.1	0.1	0.2	0.2	0.3	0.4	0.4	0.5	0.5	0.6	0.7	0.6	0.6	0.6	0.6	0.7	0.7	0.6	0.6	0.6

Table 38. Maximum Roll (°) for FLNG #1 (Lighter Topside), Winter, Heading #1

Hs \ Tp	4.25	4.75	5.25	5.75	6.25	6.75	7.25	7.75	8.25	8.75	9.25	9.75	10.25	10.75	11.25	11.75	12.25	12.75	13.25	13.75	14.25	14.75	15.25	15.75	16.25	16.75	17.25	17.75	18.25	18.75	19.25	19.75	20.25	20.75	21.25	21.75	22.25	22.75	23.25	23.75
0.25	0.1	0.1	0.1	0.1	0.1	0.1	0.1	0.1	0.1	0.1	0.1	0.1	0.1	0.1	0.1	0.1	0.1	0.1	0.1	0.1	0.2	0.1	0.2	0.2	0.2	0.3	0.3	0.4	0.8	2.4	4.2	2.9	1.0	0.5	0.4	0.4	0.3	0.3	0.3	0.2
0.75	0.1	0.1	0.1	0.1	0.1	0.1	0.1	0.1	0.1	0.1	0.1	0.1	0.1	0.1	0.1	0.1	0.2	0.2	0.2	0.3	0.3	0.4	0.4	0.5	0.5	0.5	0.9	1.2	2.0	5.7	14.5	9.3	3.8	1.6	1.4	1.0	0.8	0.6	0.7	0.7
1.25	0.1	0.1	0.1	0.1	0.1	0.1	0.1	0.1	0.1	0.1	0.1	0.1	0.1	0.1	0.1	0.2	0.2	0.2	0.3	0.3	0.4	0.5	0.5	0.7	0.7	0.9	1.1	2.0	3.1	9.5	16.3	14.7	5.1	2.6	2.3	1.7	1.4	1.3	1.0	0.7
1.75	0.1	0.1	0.1	0.1	0.1	0.1	0.1	0.1	0.2	0.2	0.2	0.2	0.1	0.1	0.1	0.2	0.2	0.3	0.3	0.4	0.5	0.6	0.7	0.8	1.0	1.3	1.8	2.3	6.3	16.8	34.4	24.0	8.9	3.3	3.0	1.7	1.8	1.5	1.1	1.3
2.25	0.1	0.1	0.1	0.1	0.1	0.1	0.1	0.1	0.2	0.2	0.2	0.1	0.2	0.1	0.2	0.2	0.3	0.3	0.4	0.5	0.6	0.7	0.9	1.1	1.3	1.6	2.2	2.5	7.5	20.5	31.4	23.2	11.0	5.0	3.6	2.6	2.2	1.8	1.8	1.3
2.75	0.1	0.1	0.1	0.1	0.1	0.1	0.1	0.2	0.2	0.2	0.2	0.2	0.1	0.2	0.2	0.2	0.3	0.4	0.5	0.7	0.7	0.9	1.3	1.6	2.0	2.0	2.4	3.2	9.9	23.8	41.7	27.7	12.5	6.4	3.8	3.1	3.0	2.3	1.5	1.8

Table 39. Maximum Pitch (°) for FLNG #1 (Lighter Topside), Winter, Heading #1

Hs \ Tp	4.25	4.75	5.25	5.75	6.25	6.75	7.25	7.75	8.25	8.75	9.25	9.75	10.25	10.75	11.25	11.75	12.25	12.75	13.25	13.75	14.25	14.75	15.25	15.75	16.25	16.75	17.25	17.75	18.25	18.75	19.25	19.75	20.25	20.75	21.25	21.75	22.25	22.75	23.25	23.75
0.25	0.0	0.0	0.0	0.0	0.0	0.0	0.0	0.0	0.0	0.0	0.0	0.0	0.0	0.0	0.0	0.0	0.0	0.0	0.0	0.0	0.0	0.0	0.0	0.0	0.0	0.0	0.0	0.0	0.0	0.0	0.0	0.0	0.0	0.0	0.0	0.0	0.0	0.0	0.0	0.0
0.75	0.0	0.0	0.0	0.0	0.0	0.0	0.0	0.0	0.0	0.0	0.0	0.1	0.1	0.1	0.1	0.1	0.1	0.1	0.1	0.1	0.1	0.1	0.1	0.1	0.1	0.1	0.1	0.1	0.1	0.1	0.1	0.1	0.1	0.0	0.1	0.1	0.0	0.0	0.1	0.0
1.25	0.0	0.0	0.0	0.0	0.0	0.0	0.0	0.0	0.0	0.1	0.1	0.1	0.1	0.1	0.1	0.2	0.2	0.1	0.2	0.1	0.1	0.2	0.1	0.1	0.1	0.1	0.1	0.1	0.1	0.1	0.1	0.1	0.1	0.1	0.1	0.1	0.1	0.1	0.1	0.1
1.75	0.0	0.0	0.0	0.0	0.0	0.0	0.0	0.0	0.0	0.1	0.1	0.1	0.1	0.2	0.2	0.2	0.2	0.2	0.2	0.2	0.2	0.2	0.2	0.2	0.2	0.2	0.2	0.1	0.1	0.1	0.2	0.1	0.1	0.1	0.1	0.1	0.1	0.1	0.1	0.1
2.25	0.0	0.0	0.0	0.0	0.0	0.0	0.0	0.0	0.1	0.1	0.1	0.1	0.2	0.3	0.3	0.2	0.4	0.3	0.3	0.3	0.2	0.2	0.2	0.2	0.2	0.2	0.2	0.1	0.2	0.2	0.2	0.1	0.1	0.2	0.2	0.1	0.1	0.1	0.1	0.1
2.75	0.0	0.0	0.0	0.0	0.0	0.0	0.0	0.0	0.1	0.1	0.1	0.2	0.2	0.3	0.3	0.3	0.4	0.4	0.3	0.4	0.3	0.3	0.3	0.3	0.3	0.2	0.2	0.2	0.3	0.2	0.2	0.2	0.2	0.2	0.2	0.2	0.2	0.2	0.1	0.1

Table 40. Maximum Roll (°) for FLNG #1 (Lighter Topside), Winter, Heading #2

Hs \ Tp	4.25	4.75	5.25	5.75	6.25	6.75	7.25	7.75	8.25	8.75	9.25	9.75	10.25	10.75	11.25	11.75	12.25	12.75	13.25	13.75	14.25	14.75	15.25	15.75	16.25	16.75	17.25	17.75	18.25	18.75	19.25	19.75	20.25	20.75	21.25	21.75	22.25	22.75	23.25	23.75
0.25	0.4	0.4	0.4	0.4	0.4	0.4	0.4	0.4	0.4	0.4	0.4	0.4	0.4	0.4	0.4	0.4	0.4	0.4	0.4	0.4	0.4	0.4	0.4	0.4	0.4	0.4	0.4	0.4	0.4	0.4	0.4	0.4	0.4	0.4	0.4	0.4	0.4	0.4	0.4	0.4
0.75	0.4	0.4	0.4	0.4	0.4	0.4	0.4	0.4	0.4	0.4	0.4	0.4	0.4	0.4	0.4	0.4	0.4	0.4	0.4	0.4	0.4	0.4	0.4	0.4	0.4	0.4	0.4	0.4	0.4	0.4	0.5	0.5	0.4	0.4	0.4	0.4	0.4	0.4	0.4	0.4
1.25	0.4	0.4	0.4	0.4	0.4	0.4	0.4	0.4	0.4	0.4	0.4	0.4	0.4	0.4	0.4	0.4	0.4	0.4	0.4	0.4	0.4	0.4	0.4	0.4	0.4	0.4	0.4	0.4	0.4	0.5	0.6	0.5	0.4	0.4	0.4	0.4	0.4	0.4	0.4	0.4
1.75	0.4	0.4	0.4	0.4	0.4	0.4	0.4	0.4	0.4	0.4	0.4	0.4	0.4	0.4	0.4	0.4	0.4	0.4	0.4	0.4	0.4	0.4	0.4	0.4	0.4	0.4	0.4	0.4	0.4	0.5	0.7	0.8	0.5	0.5	0.4	0.4	0.4	0.4	0.4	0.4
2.25	0.4	0.4	0.4	0.4	0.4	0.4	0.4	0.4	0.4	0.4	0.4	0.4	0.4	0.4	0.4	0.4	0.4	0.4	0.4	0.4	0.4	0.4	0.4	0.4	0.4	0.4	0.4	0.4	0.4	0.6	0.8	0.9	0.5	0.4	0.4	0.4	0.4	0.4	0.4	0.4
2.75	0.4	0.4	0.4	0.4	0.4	0.4	0.4	0.4	0.4	0.4	0.4	0.4	0.4	0.4	0.4	0.4	0.4	0.4	0.4	0.4	0.4	0.4	0.4	0.4	0.4	0.4	0.4	0.4	0.4	0.5	1.2	0.9	0.6	0.4	0.6	0.4	0.4	0.5	0.5	0.4

Table 41. Maximum Pitch (°) for FLNG #1 (Lighter Topside), Winter, Heading #2

Hs \ Tp	4.25	4.75	5.25	5.75	6.25	6.75	7.25	7.75	8.25	8.75	9.25	9.75	10.25	10.75	11.25	11.75	12.25	12.75	13.25	13.75	14.25	14.75	15.25	15.75	16.25	16.75	17.25	17.75	18.25	18.75	19.25	19.75	20.25	20.75	21.25	21.75	22.25	22.75	23.25	23.75
0.25	0.0	0.0	0.0	0.0	0.0	0.0	0.0	0.0	0.0	0.0	0.0	0.0	0.0	0.0	0.0	0.0	0.0	0.0	0.0	0.0	0.0	0.0	0.0	0.0	0.0	0.0	0.0	0.0	0.1	0.1	0.1	0.1	0.1	0.1	0.1	0.1	0.1	0.1	0.1	0.1
0.75	0.0	0.0	0.0	0.0	0.0	0.0	0.0	0.0	0.0	0.0	0.0	0.0	0.0	0.0	0.0	0.0	0.0	0.1	0.0	0.0	0.0	0.0	0.1	0.1	0.1	0.1	0.1	0.1	0.2	0.2	0.2	0.2	0.2	0.2	0.2	0.2	0.2	0.2	0.1	0.2
1.25	0.0	0.0	0.0	0.0	0.0	0.0	0.0	0.0	0.0	0.0	0.0	0.0	0.0	0.0	0.0	0.1	0.1	0.1	0.1	0.1	0.1	0.1	0.1	0.1	0.1	0.2	0.2	0.2	0.3	0.3	0.3	0.2	0.4	0.3	0.3	0.3	0.4	0.3	0.3	0.3
1.75	0.0	0.0	0.0	0.0	0.0	0.0	0.0	0.0	0.0	0.0	0.0	0.0	0.0	0.0	0.0	0.1	0.1	0.1	0.1	0.1	0.1	0.1	0.1	0.1	0.2	0.2	0.3	0.3	0.4	0.3	0.3	0.5	0.3	0.4	0.4	0.4	0.4	0.4	0.4	0.6
2.25	0.0	0.0	0.0	0.0	0.0	0.0	0.0	0.0	0.0	0.0	0.0	0.0	0.1	0.1	0.1	0.1	0.1	0.1	0.1	0.1	0.1	0.1	0.2	0.3	0.3	0.3	0.4	0.4	0.5	0.5	0.5	0.6	0.6	0.4	0.4	0.5	0.5	0.5	0.5	0.5
2.75	0.0	0.0	0.0	0.0	0.0	0.0	0.0	0.0	0.0	0.0	0.0	0.0	0.1	0.1	0.1	0.1	0.1	0.2	0.1	0.1	0.1	0.1	0.2	0.3	0.3	0.3	0.4	0.5	0.5	0.5	0.5	0.5	0.7	0.5	0.7	0.6	0.7	0.6	0.6	0.6

Table 42. Maximum Roll (°) for FLNG #2 (Lighter Hull), Winter, Heading #1

Hs \ Tp	4.25	4.75	5.25	5.75	6.25	6.75	7.25	7.75	8.25	8.75	9.25	9.75	10.25	10.75	11.25	11.75	12.25	12.75	13.25	13.75	14.25	14.75	15.25	15.75	16.25	16.75	17.25	17.75	18.25	18.75	19.25	19.75	20.25	20.75	21.25	21.75	22.25	22.75	23.25	23.75
0.25	0.2	0.2	0.2	0.2	0.2	0.2	0.2	0.2	0.2	0.2	0.2	0.2	0.2	0.2	0.2	0.2	0.2	0.2	0.2	0.2	0.2	0.2	0.2	0.2	0.2	0.2	0.2	0.2	0.2	0.3	0.3	0.3	0.4	0.8	1.6	2.2	1.4	1.2	0.6	0.3
0.75	0.2	0.2	0.2	0.2	0.2	0.2	0.2	0.2	0.2	0.2	0.2	0.2	0.2	0.2	0.2	0.2	0.2	0.2	0.2	0.2	0.2	0.2	0.2	0.2	0.3	0.3	0.3	0.3	0.4	0.5	0.5	0.7	0.8	1.5	2.1	4.4	4.9	4.8	2.9	1.8	1.5
1.25	0.2	0.2	0.2	0.2	0.2	0.2	0.2	0.2	0.2	0.2	0.2	0.2	0.2	0.2	0.2	0.2	0.2	0.2	0.2	0.2	0.2	0.2	0.2	0.3	0.3	0.5	0.4	0.5	0.6	0.7	0.8	1.0	1.4	2.2	3.1	8.0	11.7	9.9	4.9	2.7	1.6
1.75	0.2	0.2	0.2	0.2	0.2	0.2	0.2	0.2	0.2	0.2	0.2	0.2	0.2	0.2	0.2	0.2	0.2	0.2	0.2	0.2	0.2	0.2	0.3	0.4	0.4	0.7	0.6	0.7	0.8	1.2	1.3	1.6	1.7	2.9	4.2	11.0	15.0	13.4	7.2	3.4	2.5
2.25	0.2	0.2	0.2	0.2	0.2	0.2	0.2	0.2	0.2	0.2	0.2	0.2	0.2	0.2	0.2	0.2	0.2	0.2	0.2	0.3	0.3	0.3	0.4	0.6	0.5	0.7	1.0	1.1	1.0	1.8	1.9	2.4	3.5	6.1	17.8	20.1	15.0	8.9	4.1	2.9
2.75	0.2	0.2	0.2	0.2	0.2	0.2	0.2	0.2	0.2	0.2	0.3	0.2	0.2	0.2	0.2	0.2	0.2	0.2	0.3	0.3	0.4	0.4	0.6	0.5	0.7	0.8	0.9	1.3	1.5	1.5	1.9	3.4	3.5	7.3	14.8	23.9	19.8	10.2	6.0	4.6

Table 43. Maximum Pitch (°) for FLNG #2 (Lighter Hull), Winter, Heading #1

Hs \ Tp	4.25	4.75	5.25	5.75	6.25	6.75	7.25	7.75	8.25	8.75	9.25	9.75	10.25	10.75	11.25	11.75	12.25	12.75	13.25	13.75	14.25	14.75	15.25	15.75	16.25	16.75	17.25	17.75	18.25	18.75	19.25	19.75	20.25	20.75	21.25	21.75	22.25	22.75	23.25	23.75
0.25	0.0	0.0	0.0	0.0	0.0	0.0	0.0	0.0	0.0	0.0	0.0	0.0	0.0	0.0	0.0	0.0	0.0	0.0	0.0	0.0	0.0	0.0	0.0	0.0	0.0	0.0	0.0	0.0	0.0	0.0	0.0	0.0	0.0	0.0	0.0	0.0	0.0	0.0	0.0	0.0	0.0
0.75	0.0	0.0	0.0	0.0	0.0	0.0	0.0	0.0	0.0	0.0	0.0	0.1	0.1	0.1	0.1	0.1	0.1	0.1	0.1	0.1	0.1	0.1	0.1	0.1	0.1	0.1	0.1	0.1	0.1	0.1	0.1	0.1	0.1	0.1	0.0	0.0	0.0	0.0	0.1	0.1
1.25	0.0	0.0	0.0	0.0	0.0	0.0	0.0	0.0	0.0	0.0	0.1	0.1	0.1	0.1	0.1	0.1	0.2	0.2	0.2	0.1	0.1	0.1	0.1	0.1	0.2	0.1	0.1	0.1	0.1	0.1	0.1	0.1	0.1	0.1	0.1	0.1	0.1	0.1	0.1	0.1
1.75	0.0	0.0	0.0	0.0	0.0	0.0	0.0	0.0	0.1	0.1	0.1	0.1	0.2	0.2	0.2	0.2	0.2	0.2	0.2	0.2	0.2	0.2	0.2	0.2	0.2	0.2	0.1	0.1	0.2	0.1	0.1	0.1	0.1	0.1	0.1	0.1	0.1	0.1	0.1	0.1
2.25	0.0	0.0	0.0	0.0	0.0	0.0	0.0	0.0	0.1	0.1	0.2	0.1	0.2	0.2	0.2	0.3	0.3	0.3	0.3	0.3	0.2	0.2	0.2	0.2	0.2	0.2	0.2	0.2	0.1	0.2	0.2	0.2	0.2	0.1	0.1	0.1	0.1	0.1	0.1	0.1
2.75	0.0	0.0	0.0	0.0	0.0	0.0	0.0	0.1	0.1	0.1	0.2	0.2	0.2	0.3	0.3	0.3	0.3	0.3	0.4	0.3	0.3	0.3	0.3	0.2	0.2	0.2	0.2	0.2	0.2	0.2	0.2	0.2	0.2	0.2	0.1	0.1	0.2	0.1	0.1	0.2

Table 44. Maximum Roll (°) for FLNG #2 (Lighter Hull), Winter, Heading #2

Hs \ Tp	4.25	4.75	5.25	5.75	6.25	6.75	7.25	7.75	8.25	8.75	9.25	9.75	10.25	10.75	11.25	11.75	12.25	12.75	13.25	13.75	14.25	14.75	15.25	15.75	16.25	16.75	17.25	17.75	18.25	18.75	19.25	19.75	20.25	20.75	21.25	21.75	22.25	22.75	23.25	23.75
0.25	0.5	0.5	0.5	0.5	0.5	0.5	0.5	0.5	0.5	0.5	0.5	0.5	0.5	0.5	0.5	0.5	0.5	0.5	0.5	0.5	0.5	0.5	0.5	0.5	0.5	0.5	0.5	0.5	0.5	0.5	0.5	0.5	0.5	0.5	0.5	0.5	0.6	0.5	0.5	0.5
0.75	0.5	0.5	0.5	0.5	0.5	0.5	0.5	0.5	0.5	0.5	0.5	0.5	0.5	0.5	0.5	0.5	0.5	0.5	0.5	0.5	0.5	0.5	0.5	0.5	0.5	0.5	0.5	0.5	0.5	0.5	0.5	0.5	0.5	0.5	0.6	0.7	0.7	0.6	0.5	0.5
1.25	0.5	0.5	0.5	0.5	0.5	0.5	0.5	0.5	0.5	0.5	0.5	0.5	0.5	0.5	0.5	0.5	0.5	0.5	0.5	0.5	0.5	0.5	0.5	0.5	0.5	0.5	0.5	0.5	0.5	0.5	0.5	0.5	0.5	0.6	0.8	0.8	0.7	0.7	0.6	0.6
1.75	0.5	0.5	0.5	0.5	0.5	0.5	0.5	0.5	0.5	0.5	0.5	0.5	0.5	0.5	0.5	0.5	0.5	0.5	0.5	0.5	0.5	0.5	0.5	0.5	0.5	0.5	0.5	0.5	0.5	0.5	0.5	0.5	0.5	0.6	1.3	1.1	1.0	0.8	0.8	0.6
2.25	0.5	0.5	0.5	0.5	0.5	0.5	0.5	0.5	0.5	0.5	0.5	0.5	0.5	0.5	0.5	0.5	0.5	0.5	0.5	0.5	0.5	0.5	0.5	0.5	0.5	0.5	0.5	0.5	0.5	0.5	0.5	0.5	0.6	0.6	1.0	1.7	1.2	0.8	0.8	0.6
2.75	0.5	0.5	0.5	0.5	0.5	0.5	0.5	0.5	0.5	0.5	0.5	0.5	0.5	0.5	0.5	0.5	0.5	0.5	0.5	0.5	0.5	0.5	0.5	0.5	0.5	0.5	0.5	0.5	0.5	0.5	0.5	0.5	0.6	0.7	1.2	1.9	1.5	1.0	0.7	0.7

Table 45. Maximum Pitch (°) for FLNG #2 (Lighter Hull), Winter, Heading #2

Hs \ Tp	4.25	4.75	5.25	5.75	6.25	6.75	7.25	7.75	8.25	8.75	9.25	9.75	10.25	10.75	11.25	11.75	12.25	12.75	13.25	13.75	14.25	14.75	15.25	15.75	16.25	16.75	17.25	17.75	18.25	18.75	19.25	19.75	20.25	20.75	21.25	21.75	22.25	22.75	23.25	23.75
0.25	0.0	0.0	0.0	0.0	0.0	0.0	0.0	0.0	0.0	0.0	0.0	0.0	0.0	0.0	0.0	0.0	0.0	0.0	0.0	0.0	0.0	0.0	0.0	0.0	0.0	0.0	0.0	0.1	0.1	0.1	0.1	0.1	0.1	0.1	0.1	0.1	0.1	0.1	0.1	0.1
0.75	0.0	0.0	0.0	0.0	0.0	0.0	0.0	0.0	0.0	0.0	0.0	0.0	0.0	0.0	0.0	0.0	0.0	0.0	0.0	0.0	0.0	0.0	0.1	0.1	0.1	0.1	0.1	0.1	0.1	0.2	0.2	0.2	0.2	0.1	0.2	0.1	0.2	0.2	0.2	0.2
1.25	0.0	0.0	0.0	0.0	0.0	0.0	0.0	0.0	0.0	0.0	0.0	0.0	0.0	0.0	0.0	0.0	0.1	0.1	0.1	0.1	0.1	0.1	0.1	0.1	0.2	0.2	0.2	0.3	0.3	0.2	0.3	0.3	0.3	0.3	0.3	0.3	0.3	0.3	0.3	0.2
1.75	0.0	0.0	0.0	0.0	0.0	0.0	0.0	0.0	0.0	0.0	0.0	0.0	0.0	0.0	0.0	0.1	0.1	0.1	0.1	0.1	0.1	0.1	0.1	0.2	0.2	0.2	0.3	0.2	0.3	0.3	0.3	0.4	0.4	0.4	0.6	0.3	0.4	0.4	0.4	0.4
2.25	0.0	0.0	0.0	0.0	0.0	0.0	0.0	0.0	0.0	0.0	0.0	0.0	0.1	0.1	0.1	0.1	0.1	0.1	0.1	0.1	0.1	0.1	0.2	0.2	0.3	0.3	0.4	0.4	0.5	0.4	0.4	0.4	0.5	0.5	0.5	0.6	0.5	0.6	0.5	0.5
2.75	0.0	0.0	0.0	0.0	0.0	0.0	0.0	0.0	0.0	0.0	0.0	0.0	0.1	0.1	0.1	0.1	0.1	0.2	0.2	0.1	0.1	0.1	0.2	0.2	0.3	0.3	0.4	0.5	0.4	0.6	0.5	0.7	0.6	0.6	0.6	0.6	0.7	0.6	0.6	0.6

The downtime conditions (max. roll or pitch > 2° or the mean >1°) are not observed when the FLNG heading was toward swell (heading case #2) during winter season. Meanwhile, the roll motions, particularly due to long-period waves near the natural roll periods of the FLNGs, are found to be the main causes of the downtime events.

The resulting downtime conditions (zones in the joint-occurrence tables), for the three FLNG models during winter season, are highlighted in the joint-occurrence tables as shown in Table 46~Table 48.

Table 46. Downtime zone of the original FLNG, Winter, Heading #1

Hs \ Tp	4.25	4.75	5.25	5.75	6.25	6.75	7.25	7.75	8.25	8.75	9.25	9.75	10.25	10.75	11.25	11.75	12.25	12.75	13.25	13.75	14.25	14.75	15.25	15.75	16.25	16.75	17.25	17.75	18.25	18.75	19.25	19.75	20.25	20.75	21.25	21.75	22.25	22.75	23.25	23.75
0.25			4	2									3	18	20	33	18	10	9	2	2	11	2	9	6		1	1												
0.75			1	2	9	6	7	11	7	8	5	18	9	40	24	83	104	78	134	35	79	48	11	26	18	4	8	27	2	1	7	1			3			1		
1.25		2	3	5	15	11	22	17	5	2			1		1	13	19	33	73	34	64	66	17	44	24	7	9	18	1		4	2			3	1				
1.75					3	5	9	5	2	3									10	4	18	16	8	15	10		2	6			2									
2.25							1	1											2				1	3	3	1	1	1			1									
2.75																																								

Table 47. Downtime zone of the FLNG #1 (Lighter Topside), Winter, Heading #1

Hs \ Tp	4.25	4.75	5.25	5.75	6.25	6.75	7.25	7.75	8.25	8.75	9.25	9.75	10.25	10.75	11.25	11.75	12.25	12.75	13.25	13.75	14.25	14.75	15.25	15.75	16.25	16.75	17.25	17.75	18.25	18.75	19.25	19.75	20.25	20.75	21.25	21.75	22.25	22.75	23.25	23.75
0.25			4	2									3	18	20	33	18	10	9	2	2	11	2	9	6		1	1												
0.75			1	2	9	6	7	11	7	8	5	18	9	40	24	83	104	78	134	35	79	48	11	26	18	4	8	27	2	1	7	1			3			1		
1.25		2	3	5	15	11	22	17	5	2			1		1	13	19	33	73	34	64	66	17	44	24	7	9	18	1		4	2			3	1				
1.75					3	5	9	5	2	3									10	4	18	16	8	15	10		2	6			2									
2.25							1	1											2				1	3	3	1	1	1			1									
2.75																																								

Table 48. Downtime zone of the FLNG #2 (Lighter Hull), Winter, Heading #1

Hs \ Tp	4.25	4.75	5.25	5.75	6.25	6.75	7.25	7.75	8.25	8.75	9.25	9.75	10.25	10.75	11.25	11.75	12.25	12.75	13.25	13.75	14.25	14.75	15.25	15.75	16.25	16.75	17.25	17.75	18.25	18.75	19.25	19.75	20.25	20.75	21.25	21.75	22.25	22.75	23.25	23.75
0.25			4	2									3	18	20	33	18	10	9	2	2	11	2	9	6		1	1												
0.75			1	2	9	6	7	11	7	8	5	18	9	40	24	83	104	78	134	35	79	48	11	26	18	4	8	27	2	1	7	1			3			1		
1.25		2	3	5	15	11	22	17	5	2			1		1	13	19	33	73	34	64	66	17	44	24	7	9	18	1		4	2			3	1				
1.75					3	5	9	5	2	3									10	4	18	16	8	15	10		2	6			2									
2.25							1	1											2				1	3	3	1	1	1			1									
2.75																																								

4.5.3. Downtime during Summer Cyclone-Season (December – March)

Taking the same procedure, downtime conditions for the three models during 4 months of summer season have been evaluated under the two FLNG heading cases. As a result, however, the 3-hour responses of the three models from the most extreme conditions in the heading case #1 (when the FLNG's heading is toward sea-waves) do not exceed the operation limits; thus, the downtime zones are only observed in the heading case #2 (toward swell).

CHARM3D time-simulation is conducted under wind-sea, wind, and current forces. Then, the time-series of motion is linearly superposed with another time-series of swell-induced motion, which is generated separately for every wind-sea case by using RAOs but has a constant Hs and Tp. (constant summer swell: Hs=1m, Tp=16s)

Table 49. Input environmental conditions for summer cyclone-season

Part	***by CHARM3D***							***by RAOs***		
Heading case	Sea wave			Current		Wind		Swell		
	BETA	Hs	Tp	BETA	speed	BETA	speed	BETA	Hs	Tp
#1	190	9m	15sec	250	0.6m/s	160	18m/s	260	1m	16sec
#2	120	varied		180	0.6m/s	90	varied	190	1m	16sec

For specific harsh case (Heading case #2, Hs=8.25m, Tp=14.25s, U_{10}=18m/s, V_C=0.6m/s), the maximum wave, wind, and current forces (roll moment) are 1.59E+09 N·m, 5.04E+08 N·m, and 2.73E+08 N·m, respectively.

The estimated downtime zones are presented in the following joint-occurrence tables, surrounded by thick border lines (Table 50~Table 52). The cells filled with green

outside the downtime zones are verified to be operable conditions. The maximum mean angle during 3-hour simulations in the all cases was 0.53°, so the mean-angle limits did not contribute to the downtime estimation.

Table 50. Downtime zone of the original FLNG in summer (Dec-Mar, heading#2)

Hs\Tp	min	2.0	2.5	3.0	3.5	4.0	4.5	5.0	5.5	6.0	6.5	7.0	7.5	8.0	8.5	9.0	9.5	10.0	10.5	11.0	11.5	12.0	12.5	13.0	13.5	14.0	14.5
min	max	2.5	3.0	3.5	4.0	4.5	5.0	5.5	6.0	6.5	7.0	7.5	8.0	8.5	9.0	9.5	10.0	10.5	11.0	11.5	12.0	12.5	13.0	13.5	14.0	14.5	15.0
0.0	0.5																										
0.5	1.0		2	1	5	1	10	3	3	1	2	1	1							1							
1.0	1.5				1	10	12	15	21	2	2	7	5														
1.5	2.0						3	7	2		1		1	5	2	2	3	1	1								
2.0	2.5													1			3	2	1								
2.5	3.0														2		2	4									
3.0	3.5															2	3	3	2								
3.5	4.0															1	1	1				2					
4.0	4.5															1		1	1			3	1				
4.5	5.0																1	2	2		1	4	6				
5.0	5.5																		2	2		1	2				
5.5	6.0																				1						
6.0	6.5																					1			1		
6.5	7.0																										
7.0	7.5																						1				1
7.5	8.0																							1			1
8.0	8.5																								1	2	1
8.5	9.0																										1

Table 51. Downtime zone for the scenario#1 (Lighter Topside, Dec-Mar, heading#2)

Hs\Tp	min	2.0	2.5	3.0	3.5	4.0	4.5	5.0	5.5	6.0	6.5	7.0	7.5	8.0	8.5	9.0	9.5	10.0	10.5	11.0	11.5	12.0	12.5	13.0	13.5	14.0	14.5
min	max	2.5	3.0	3.5	4.0	4.5	5.0	5.5	6.0	6.5	7.0	7.5	8.0	8.5	9.0	9.5	10.0	10.5	11.0	11.5	12.0	12.5	13.0	13.5	14.0	14.5	15.0
0.0	0.5																										
0.5	1.0		2	1	5	1	10	3	3	1	2	1	1							1							
1.0	1.5				1	10	12	15	21	2	2	7	5														
1.5	2.0						3	7	2		1		1	5	2	2	3	1	1								
2.0	2.5													1			3	2	1								
2.5	3.0														2		2	4									
3.0	3.5															2	3	3	2								
3.5	4.0															1	1	1				2					
4.0	4.5															1		1	1			3	1				
4.5	5.0																1	2	2		1	4	6				
5.0	5.5																		2	2		1	2				
5.5	6.0																				1						
6.0	6.5																					1			1		
6.5	7.0																										
7.0	7.5																						1				1
7.5	8.0																							1			1
8.0	8.5																								1	2	1
8.5	9.0																										1

Table 52. Downtime zone for the scenario#2 (Lighter Hull, Dec-Mar, heading#2)

Hs\Tp	min	2.0	2.5	3.0	3.5	4.0	4.5	5.0	5.5	6.0	6.5	7.0	7.5	8.0	8.5	9.0	9.5	10.0	10.5	11.0	11.5	12.0	12.5	13.0	13.5	14.0	14.5
min	max	2.5	3.0	3.5	4.0	4.5	5.0	5.5	6.0	6.5	7.0	7.5	8.0	8.5	9.0	9.5	10.0	10.5	11.0	11.5	12.0	12.5	13.0	13.5	14.0	14.5	15.0
0.0	0.5																										
0.5	1.0		2	1	5	1	10	3	3	1	2	1	1							1							
1.0	1.5				1	10	12	15	21	2	2	7	5														
1.5	2.0						3	7	2		1		1	5	2	2	3	1	1								
2.0	2.5													1			3	2	1								
2.5	3.0														2		2	4									
3.0	3.5															2	3	3	2								
3.5	4.0															1	1	1				2					
4.0	4.5															1		1	1			3	1				
4.5	5.0																1	2	2		1	4	6				
5.0	5.5																		2	2		1	2				
5.5	6.0																				1						
6.0	6.5																					1			1		
6.5	7.0																										
7.0	7.5																						1				1
7.5	8.0																							1			1
8.0	8.5																								1	2	1
8.5	9.0																										1

4.5.4. Estimation of Total Downtime Period for a Year

Once topside facilities are shut down due to harsh weather conditions, it takes additional time from the end of the weather event until the facilities re-start the operation; the total downtime should be longer than the time span that the downtime-generating weather condition continues for. Topside facilities of any production platforms require extra-time to recover the system from a downtime event, and even more time would be required for the topside facilities that have temperature-sensitive processes as mentioned earlier. In this study, the recovery time for every continuous shutdown event (under excessive weather conditions) is assumed to be 3 hours for the minimum, and 24 hours for the maximum.

The post process to obtain the total downtime period including the recovery hours should be done by taking a chronological view. Each of the original weather data sets for every 3 hours can be defined as operable conditions or downtime conditions by the pre-

determined Hs-Tp combinations of the downtime zones. Then, the recovery time follows for 3 or 24 hours unless another downtime condition interrupts during the recovery periods. From the procedure presented up to here, the complete weather data sets during downtime periods can be listed up in the order of time.

In Table 53~Table 64, the downtime lists are collected from the original weather data sets based on the FLNG models (3 models including the original FLNG model as a reference), the heading cases (2 assumptions), and the minimum/maximum recovery time assumptions (3 hours or 24 hours). Indices are introduced to define each data set as "downtime weather condition" or "additional downtime for recovery". The descriptions for the index 1 and 2 are presented below Table 53.

Table 53. Downtime list of the FLNG Original (Heading #1, Recovery time: 3 hours)

- Model: FLNG Original (ZCG=6m)
- Heading: #1. Toward Sea+10deg.
- Data: 1 year (Aug.2011 – Jul.2012)
- Recovery time: 3 hours/event
- # of total downtime event: 2
- Total downtime: hours 30 = 1.25 days

No.	Month	day	year	hour	Hs(m)	Tp(s)	WaveDir	WindS	WindDir	index1*	index2**
1	8	7	2011	0	0.94	22.71	261.67	4.66	84.09	1	1
2	8	7	2011	3	1	21.56	255.17	6.28	79.73	1	2
3	8	7	2011	6	1.05	21.44	255.05	4.67	105.14	1	2
4	8	7	2011	9	1.08	21.33	257.66	3.40	103.10	1	2
5	8	7	2011	12	1.13	21	258.07	3.50	79.97	1	2
6	8	7	2011	15	1.21	19.94	250.31	4.57	80.17	0	1
7	9	9	2011	12	0.89	21.38	257.59	1.75	60.50	1	1
8	9	9	2011	15	0.74	21.34	258.50	3.03	125.74	1	2
9	9	9	2011	18	0.66	21.01	257.13	2.52	96.62	1	2
10	9	9	2011	21	0.74	19.51	254.33	6.72	104.93	0	1

* index1=1 for shutdown (excessive weather condition), and 0 for recovery hours

** when (index1, index2)=(1,1), a new downtime event begins,
and if (index1, index2)=(0,1), the downtime event closes.

Table 54. Downtime list of the FLNG Original (Heading #2, Recovery time: 3 hours)

- Model: FLNG Original (ZCG=6m)
- Heading: #2. Toward Swell+10deg.
- Data: 1 year (Aug.2011 – Jul.2012)
- Recovery time: 3 hours/event
- # of total downtime event: 1
- Total downtime: 24 hours = 1 days

No.	Month	day	year	hour	Hs(m)	Tp(s)	WaveDir	WindS	WindDir	index1*	index2**
1	3	16	2012	15	7.2	14.55	276.77	15.50	325.54	1	1
2	3	16	2012	18	7.94	14.67	277.13	15.16	324.42	1	2
3	3	16	2012	21	8.29	14.69	277.19	17.35	324.17	1	2
4	3	17	2012	0	8.53	14.63	276.21	16.17	317.05	1	2
5	3	17	2012	3	8.46	14.49	274.52	15.27	304.14	1	2
6	3	17	2012	6	8.32	14.16	272.87	16.38	301.88	1	2
7	3	17	2012	9	8.15	13.5	272.02	14.42	298.86	1	2
8	3	17	2012	12	7.67	13.26	269.64	11.65	298.46	0	1

Table 55. Downtime list of the FLNG Original (Heading #1, Recovery time: 24 hours)

- Model: FLNG Original (ZCG=6m)
- Heading: #1. Toward Sea+10deg.
- Data: 1 year (Aug.2011 – Jul.2012)
- Recovery time: 24 hours/event
- # of total downtime event: 2
- Total downtime: 72 hours = 3 days

No.	Month	day	year	hour	Hs(m)	Tp(s)	WaveDir	WindS	WindDir	index1*	index2**
1	8	7	2011	0	0.94	22.71	261.67	4.66	84.09	1	1
2	8	7	2011	3	1	21.56	255.17	6.28	79.73	1	2
3	8	7	2011	6	1.05	21.44	255.05	4.67	105.14	1	3
4	8	7	2011	9	1.08	21.33	257.66	3.40	103.10	1	4
5	8	7	2011	12	1.13	21	258.07	3.50	79.97	1	5
6	8	7	2011	15	1.21	19.94	250.31	4.57	80.17	0	5
7	8	7	2011	18	1.24	19.58	250.99	3.87	75.03	0	5
8	8	7	2011	21	1.27	19.38	252.99	3.39	87.63	0	5
9	8	8	2011	0	1.3	19.09	253.27	3.63	97.28	0	5
10	8	8	2011	3	1.34	18.26	246.68	4.77	92.04	0	4
11	8	8	2011	6	1.36	17.79	247.5	3.77127	96.0883	0	3
12	8	8	2011	9	1.34	17.6	248.57	2.62945	104.987	0	2
13	8	8	2011	12	1.33	17.4	248.82	2.09239	182.74	0	1
14	9	9	2011	12	0.89	21.38	257.59	1.74642	60.4991	1	1
15	9	9	2011	15	0.74	21.34	258.5	3.03059	125.735	1	2
16	9	9	2011	18	0.66	21.01	257.13	2.51676	96.6165	1	3
17	9	9	2011	21	0.74	19.51	254.33	6.71662	104.926	0	3
18	9	10	2011	0	1.11	19.42	253.78	10.8228	99.9495	0	3
19	9	10	2011	3	1.59	19.42	254.7	10.841	90.7926	0	3
20	9	10	2011	6	1.91	19.38	253.63	8.19525	83.9762	0	3
21	9	10	2011	9	2.02	19.06	253.72	6.89701	67.6739	0	3
22	9	10	2011	12	2.04	17.87	249.93	5.52254	76.0642	0	3
23	9	10	2011	15	1.96	17.72	250.26	5.04026	81.9019	0	2
24	9	10	2011	18	1.81	17.7	249.51	6.54047	93.2428	0	1

Table 56. Downtime list of the FLNG Original (Heading #2, Recovery time: 24 hours)

- Model: FLNG Original (ZCG=6m)
- Heading: #2. Toward Swell+10deg.
- Data: 1 year (Aug.2011 – Jul.2012)
- Recovery time: 24 hours/event
- # of total downtime event: 1
- Total downtime: 45 hours = 1.875 days

No.	Month	day	year	hour	Hs(m)	Tp(s)	WaveDir	WindS	WindDir	index1*	index2**
1	3	16	2012	15	7.2	14.55	276.77	15.4997	325.541	1	1
2	3	16	2012	18	7.94	14.67	277.13	15.1599	324.423	1	2
3	3	16	2012	21	8.29	14.69	277.19	17.3548	324.167	1	3
4	3	17	2012	0	8.53	14.63	276.21	16.1749	317.054	1	4
5	3	17	2012	3	8.46	14.49	274.52	15.2714	304.138	1	5
6	3	17	2012	6	8.32	14.16	272.87	16.3802	301.876	1	6
7	3	17	2012	9	8.15	13.5	272.02	14.4208	298.858	1	7
8	3	17	2012	12	7.67	13.26	269.64	11.6473	298.457	0	7
9	3	17	2012	15	7.01	12.91	268.13	11.9558	290.618	0	7
10	3	17	2012	18	6.25	12.14	268.36	11.6561	291.701	0	6
11	3	17	2012	21	5.62	11.85	270.24	11.3612	290.668	0	5
12	3	18	2012	0	5.11	11.21	269.87	9.68654	286.864	0	4
13	3	18	2012	3	4.74	10.86	272.44	10.6291	286.901	0	3
14	3	18	2012	6	4.47	10.67	274.57	11.1615	284.211	0	2
15	3	18	2012	9	4.24	10.36	271.41	10.6182	284.063	0	1

Table 57. Downtime list of Scenario#1: Lighter Topside (Heading #1, Recovery: 3 hr)

- Model: Lighter Topside (Scenario #1)
- Heading: #1. Toward Sea+10deg.
- Data: 1 year (Aug.2011 – Jul.2012)
- Recovery time: 3 hours/event
- # of total downtime event: 14
- Total downtime: 192 hours = 8 days

No.	Month	day	year	hour	Hs(m)	Tp(s)	WaveDir	WindS	WindDir	index1*	index2**
1	8	7	2011	6	1.05	21.44	255.05	4.67	105.14	1	1
2	8	7	2011	9	1.08	21.33	257.66	3.40	103.10	1	2
3	8	7	2011	12	1.13	21	258.07	3.50	79.97	1	2
4	8	7	2011	15	1.21	19.94	250.31	4.57	80.17	1	2
5	8	7	2011	18	1.24	19.58	250.99	3.87	75.03	1	2
6	8	7	2011	21	1.27	19.38	252.99	3.39	87.63	1	2
7	8	8	2011	0	1.3	19.09	253.27	3.63	97.28	1	2
8	8	8	2011	3	1.34	18.26	246.68	4.77	92.04	1	2
9	8	8	2011	6	1.36	17.79	247.50	3.77	96.09	1	2
10	8	8	2011	9	1.34	17.6	248.57	2.63	104.99	1	2
11	8	8	2011	12	1.33	17.4	248.82	2.09239	182.74	0	1
12	8	22	2011	0	1.55	17.56	247.92	7.20924	112.51	1	1
:	:	:	:	:	:	:	:	:	:	:	:

(The full list is presented in the appendix)

Table 58. Downtime list of Scenario#1: Lighter Topside (Heading #2, Recovery: 3 hr)

- Model: Lighter Topside (Scenario #1)
- Heading: #2. Toward Swell+10deg.
- Data: 1 year (Aug.2011 – Jul.2012)
- Recovery time: 3 hours/event
- # of total downtime event: 1
- Total downtime: 30 hours = 1.25 days

No.	Month	day	year	hour	Hs(m)	Tp(s)	WaveDir	WindS	WindDir	index1*	index2**
1	3	16	2012	12	6.28	13.57	277.49	16.2306	331.919	1	1
2	3	16	2012	15	7.2	14.55	276.77	15.4997	325.541	1	2
3	3	16	2012	18	7.94	14.67	277.13	15.1599	324.423	1	2
4	3	16	2012	21	8.29	14.69	277.19	17.3548	324.167	1	2
5	3	17	2012	0	8.53	14.63	276.21	16.1749	317.054	1	2
6	3	17	2012	3	8.46	14.49	274.52	15.2714	304.138	1	2
7	3	17	2012	6	8.32	14.16	272.87	16.3802	301.876	1	2
8	3	17	2012	9	8.15	13.5	272.02	14.4208	298.858	1	2
9	3	17	2012	12	7.67	13.26	269.64	11.6473	298.457	1	2
10	3	17	2012	15	7.01	12.91	268.13	11.9558	290.618	0	1

Table 59. Downtime list of Scenario#1: Lighter Topside (Heading #1, Recovery: 24 hr)

- Model: Lighter Topside (Scenario #1)
- Heading: #1. Toward Sea+10deg.
- Data: 1 year (Aug.2011 – Jul.2012)
- Recovery time: 24 hours/event
- # of total downtime event: 14
- Total downtime: 480 hours = 20 days

No.	Month	day	year	hour	Hs(m)	Tp(s)	WaveDir	WindS	WindDir	index1*	index2**
1	8	7	2011	6	1.05	21.44	255.05	4.67	105.14	1	1
2	8	7	2011	9	1.08	21.33	257.66	3.40	103.10	1	2
3	8	7	2011	12	1.13	21	258.07	3.50	79.97	1	3
4	8	7	2011	15	1.21	19.94	250.31	4.57	80.17	1	4
5	8	7	2011	18	1.24	19.58	250.99	3.87	75.03	1	5
6	8	7	2011	21	1.27	19.38	252.99	3.39	87.63	1	6
7	8	8	2011	0	1.3	19.09	253.27	3.63	97.28	1	7
8	8	8	2011	3	1.34	18.26	246.68	4.77	92.04	1	8
9	8	8	2011	6	1.36	17.79	247.50	3.77	96.09	1	9
10	8	8	2011	9	1.34	17.6	248.57	2.63	104.99	1	9
11	8	8	2011	12	1.33	17.4	248.82	2.09239	182.74	0	8
12	8	8	2011	15	1.33	17.05	249.53	1.72699	157.89	0	7
13	8	8	2011	18	1.34	16.47	244.62	2.20166	137.761	0	6
14	8	8	2011	21	1.33	16.23	245.38	1.94833	144.188	0	5
15	8	9	2011	0	1.3	16.08	245.58	2.64622	149.073	0	4
:	:	:	:	:	:	:	:	:	:	:	:

(The full list is presented in the appendix)

Table 60. Downtime list of Scenario#1: Lighter Topside (Heading #2, Recovery: 24 hr)

- Model: Lighter Topside (Scenario #1)
- Heading: #2. Toward Swell+10deg.
- Data: 1 year (Aug.2011 – Jul.2012)
- Recovery time: 3 hours/event
- # of total downtime event: 1
- Total downtime: 51 hours = 2.125 days

No.	Month	day	year	hour	Hs(m)	Tp(s)	WaveDir	WindS	WindDir	index1*	index2**
1	3	16	2012	12	6.28	13.57	277.49	16.2306	331.919	1	1
2	3	16	2012	15	7.2	14.55	276.77	15.4997	325.541	1	2
3	3	16	2012	18	7.94	14.67	277.13	15.1599	324.423	1	3
4	3	16	2012	21	8.29	14.69	277.19	17.3548	324.167	1	4
5	3	17	2012	0	8.53	14.63	276.21	16.1749	317.054	1	5
6	3	17	2012	3	8.46	14.49	274.52	15.2714	304.138	1	6
7	3	17	2012	6	8.32	14.16	272.87	16.3802	301.876	1	7
8	3	17	2012	9	8.15	13.5	272.02	14.4208	298.858	1	8
9	3	17	2012	12	7.67	13.26	269.64	11.6473	298.457	1	9
10	3	17	2012	15	7.01	12.91	268.13	11.9558	290.618	0	8
11	3	17	2012	18	6.25	12.14	268.36	11.6561	291.701	0	7
12	3	17	2012	21	5.62	11.85	270.24	11.3612	290.668	0	6
13	3	18	2012	0	5.11	11.21	269.87	9.68654	286.864	0	5
14	3	18	2012	3	4.74	10.86	272.44	10.6291	286.901	0	4
15	3	18	2012	6	4.47	10.67	274.57	11.1615	284.211	0	3
16	3	18	2012	9	4.24	10.36	271.41	10.6182	284.063	0	2
17	3	18	2012	12	3.98	10.04	274.78	8.21231	292.631	0	1

Table 61. Downtime list of Scenario#2: Lighter Hull (Heading #1, Recovery: 3 hr)

- Model: Lighter Hull (Scenario #2)
- Heading: #1. Toward Sea+10deg.
- Data: 1 year (Aug.2011 – Jul.2012)
- Recovery time: 3 hours/event
- # of total downtime event: 2
- Total downtime: 30 hours = 1.25 days

No.	Month	day	year	hour	Hs(m)	Tp(s)	WaveDir	WindS	WindDir	index1*	index2**
1	8	7	2011	0	0.94	22.71	261.67	4.66	84.09	1	1
2	8	7	2011	3	1	21.56	255.17	6.28	79.73	1	2
3	8	7	2011	6	1.05	21.44	255.05	4.67	105.14	1	2
4	8	7	2011	9	1.08	21.33	257.66	3.40	103.10	1	2
5	8	7	2011	12	1.13	21	258.07	3.50	79.97	1	2
6	8	7	2011	15	1.21	19.94	250.31	4.57	80.17	0	1
7	9	9	2011	12	0.89	21.38	257.59	1.75	60.50	1	1
8	9	9	2011	15	0.74	21.34	258.50	3.03	125.74	1	2
9	9	9	2011	18	0.66	21.01	257.13	2.52	96.62	1	2
10	9	9	2011	21	0.74	19.51	254.33	6.72	104.93	0	1

Table 62. Downtime list of Scenario#2: Lighter Hull (Heading #2, Recovery: 3 hr)

- Model: Lighter Hull (Scenario #2)
- Heading: #2. Toward Swell+10deg.
- Data: 1 year (Aug.2011 – Jul.2012)
- Recovery time: 3 hours/event
- # of total downtime event: 1
- Total downtime: 24 hours = 1 day

No.	Month	day	year	hour	Hs(m)	Tp(s)	WaveDir	WindS	WindDir	index1*	index2**
1	3	16	2012	15	7.2	14.55	276.77	15.4997	325.541	1	1
2	3	16	2012	18	7.94	14.67	277.13	15.1599	324.423	1	2
3	3	16	2012	21	8.29	14.69	277.19	17.3548	324.167	1	2
4	3	17	2012	0	8.53	14.63	276.21	16.1749	317.054	1	2
5	3	17	2012	3	8.46	14.49	274.52	15.2714	304.138	1	2
6	3	17	2012	6	8.32	14.16	272.87	16.3802	301.876	1	2
7	3	17	2012	9	8.15	13.5	272.02	14.4208	298.858	1	2
8	3	17	2012	12	7.67	13.26	269.64	11.6473	298.457	0	1

Table 63. Downtime list of Scenario#2: Lighter Hull (Heading #1, Recovery: 24 hr)

- Model: Lighter Hull (Scenario #2)
- Heading: #1. Toward Sea+10deg.
- Data: 1 year (Aug.2011 – Jul.2012)
- Recovery time: 24 hours/event
- # of total downtime event: 2
- Total downtime: 72 hours = 3 days

No.	Month	day	year	hour	Hs(m)	Tp(s)	WaveDir	WindS	WindDir	index1*	index2**
1	8	7	2011	0	0.94	22.71	261.67	4.66	84.09	1	1
2	8	7	2011	3	1	21.56	255.17	6.28	79.73	1	2
3	8	7	2011	6	1.05	21.44	255.05	4.67	105.14	1	3
4	8	7	2011	9	1.08	21.33	257.66	3.40	103.10	1	4
5	8	7	2011	12	1.13	21	258.07	3.50	79.97	1	5
6	8	7	2011	15	1.21	19.94	250.31	4.57	80.17	0	5
7	8	7	2011	18	1.24	19.58	250.99	3.87	75.03	0	5
8	8	7	2011	21	1.27	19.38	252.99	3.39	87.63	0	5
9	8	8	2011	0	1.3	19.09	253.27	3.63	97.28	0	5
10	8	8	2011	3	1.34	18.26	246.68	4.77	92.04	0	4
11	8	8	2011	6	1.36	17.79	247.5	3.77127	96.0883	0	3
12	8	8	2011	9	1.34	17.6	248.57	2.62945	104.987	0	2
13	8	8	2011	12	1.33	17.4	248.82	2.09239	182.74	0	1
14	9	9	2011	12	0.89	21.38	257.59	1.74642	60.4991	1	1
15	9	9	2011	15	0.74	21.34	258.5	3.03059	125.735	1	2
16	9	9	2011	18	0.66	21.01	257.13	2.51676	96.6165	1	3
17	9	9	2011	21	0.74	19.51	254.33	6.71662	104.926	0	3
18	9	10	2011	0	1.11	19.42	253.78	10.8228	99.9495	0	3
19	9	10	2011	3	1.59	19.42	254.7	10.841	90.7926	0	3
20	9	10	2011	6	1.91	19.38	253.63	8.19525	83.9762	0	3
21	9	10	2011	9	2.02	19.06	253.72	6.89701	67.6739	0	3
22	9	10	2011	12	2.04	17.87	249.93	5.52254	76.0642	0	3
23	9	10	2011	15	1.96	17.72	250.26	5.04026	81.9019	0	2
24	9	10	2011	18	1.81	17.7	249.51	6.54047	93.2428	0	1

Table 64. Downtime list of Scenario#2: Lighter Hull (Heading #2, Recovery: 24 hr)

- Model: Lighter Hull (Scenario #2)
- Heading: #2. Toward Swell+10deg.
- Data: 1 year (Aug.2011 – Jul.2012)
- Recovery time: 24 hours/event
- # of total downtime event: 1
- Total downtime: 45 hours = 1.875 day

No.	Month	day	year	hour	Hs(m)	Tp(s)	WaveDir	WindS	WindDir	index1*	index2**
1	3	16	2012	15	7.2	14.55	276.77	15.4997	325.541	1	1
2	3	16	2012	18	7.94	14.67	277.13	15.1599	324.423	1	2
3	3	16	2012	21	8.29	14.69	277.19	17.3548	324.167	1	3
4	3	17	2012	0	8.53	14.63	276.21	16.1749	317.054	1	4
5	3	17	2012	3	8.46	14.49	274.52	15.2714	304.138	1	5
6	3	17	2012	6	8.32	14.16	272.87	16.3802	301.876	1	6
7	3	17	2012	9	8.15	13.5	272.02	14.4208	298.858	1	7
8	3	17	2012	12	7.67	13.26	269.64	11.6473	298.457	0	7
9	3	17	2012	15	7.01	12.91	268.13	11.9558	290.618	0	7
10	3	17	2012	18	6.25	12.14	268.36	11.6561	291.701	0	6
11	3	17	2012	21	5.62	11.85	270.24	11.3612	290.668	0	5
12	3	18	2012	0	5.11	11.21	269.87	9.68654	286.864	0	4
13	3	18	2012	3	4.74	10.86	272.44	10.6291	286.901	0	3
14	3	18	2012	6	4.47	10.67	274.57	11.1615	284.211	0	2
15	3	18	2012	9	4.24	10.36	271.41	10.6182	284.063	0	1

The “index 1” given in the downtime lists, which define each 3-hour time period as downtime-weather conditions or additional downtime for recovery, is presented along the horizontal axis of 1 year in Figure 57and Figure 58. The excessive weather conditions that lead the FLNGs to downtime (when index 1 = 1) are labeled “Shutdown”, while the extra hours for recovery-time (when index 1 = 0) are labeled “Recovery” on the vertical axis of the bar-charts.

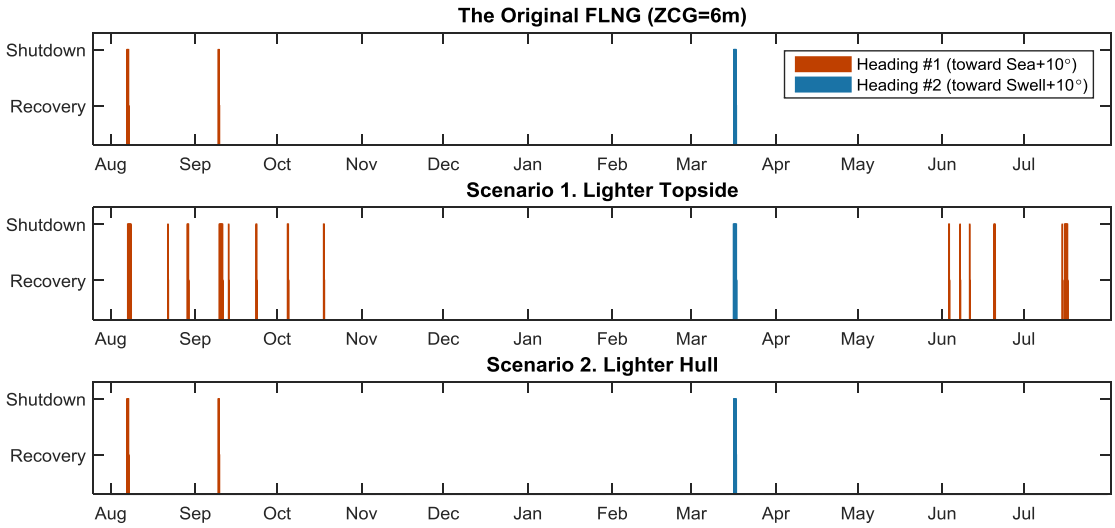

Figure 57. The minimum downtime event logs for the FLNG models in the two heading scenarios for a year (August 2011~ July 2012), assuming 3-hour of the minimum recovery time is required for every continuous downtime event.

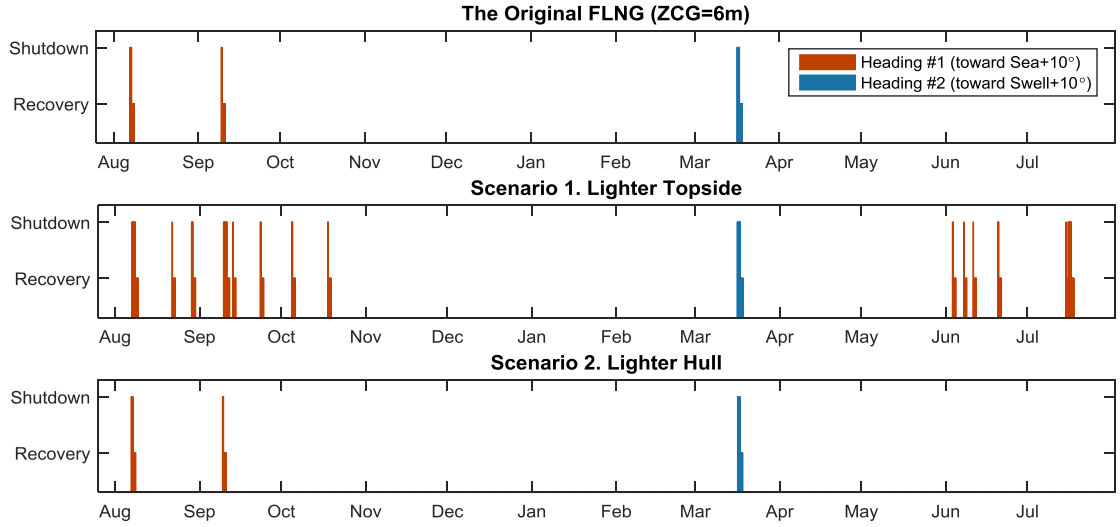

Figure 58. The maximum downtime event logs for the FLNG models in the two heading scenarios for a year (August 2011~ July 2012), assuming 24-hour of the maximum recovery time is required for every continuous downtime event.

The total downtimes estimated for the three FLNG models, based on two different heading strategies for a year, are summarized in Table 65.

Table 65. Total downtime periods under min/max recovery-time assumptions

Heading / *Model*	*Case #1. toward Wind-Sea for an entire year (sea+10°)*	*Case #2. toward Swell for an entire year (swell+10°)*
The original FLNG	30~72 hours (1.25~3 days)	24~45 hours (1~1.875 days)
Scenario1. Lighter Topside	192~480 hours (8~20 days)	30~51 hours (1.25~2.125 days)
Scenario2. Lighter Hull	30~72 hours (1.25~3 days)	24~45 hours (1~1.875 days)

While the "scenario 1" shows larger downtime periods for both heading cases, the original FLNG model and the model with lighter hull in the second scenario have the identical downtime periods under both of the heading strategies. Because the downtime zones of the two models were slightly different for the winter swell-season, the results would be a little different if another year's weather data was selected for the analysis even though the variance will be minor.

CHAPTER V

SUMMARY AND CONCLUSION

The numerical modeling of a particular FLNG facility is done for two purposes. One is the design philosophy that considers field-specific metocean conditions, and the other is a comparative study about the change of downtime due to design modifications.

Evaluating the performances of ZCG-varied FLNG models finally delivered a proper range of the natural periods, for the given environmental conditions. The result shows that the roll-motion characteristics of the different models of the FLNG are distinct by the ZCGs and the incident wave periods. This means the design of the FLNG must be tuned for the specific environmental conditions in the project location.

The test results also provided a reference model for further comparative studies under more practical assumptions of different vertical mass distributions. One scenario assumes a design modification with less mass in the topside facilities, while the other scenario assumes an operational condition by reducing the hull weight reflecting less stored weight of the products.

When comparing the consequences from the different weight distributions of the FLNGs, in the topside design or the storage weight, the operability of the FLNG was more sensitive to the variation of topside weights as shown by the downtime estimations in the last chapter. The natural roll period of the FLNG in the scenario 1, lighter-topside assumption, was relatively much smaller than the other models', which results in larger roll motions compared to other cases.

The lesson learned from the results can be even more emphasized for an FLNG with a single-point mooring system under swell-dominant environmental conditions. Because this type of floaters may weathervane toward wind or wind-sea in general, they are frequently exposed to directional swells. Thus, to minimize downtime, the target-natural periods should be properly designed for such weather conditions.

The two hypothetical scenarios of hull or topside conversion have the shorter draft and the smaller total weight than the original FLNG. The draft change for the second scenario is intended to reflect an operational loading condition, which is represented by the weight change in the hull part. The downtime estimated for this model shows that the FLNG would keep its motional characteristics quite similarly even if the hull weight is changed, which may allow flexible control range of its storage capacity.

On the other hand, when the topside weight was reduced, the impact on its downtime was significant. The main reason must be that the position of the topside units are normally far from the rotational axis, so the changes of topside weight have greater impact on its inertia, which also affects natural periods of the floating system. In this regard, the topside design or the arrangement should be optimized together with the hull storage capacity to achieve target-natural periods for given environment. Likewise, any modification of topside facilities that includes nontrivial weight changes requires very careful dynamic-performance study prior to its application.

The environmental conditions and the numerical models of the FLNG were built on several assumptions for simplification. Although it provided probable base-conditions

for comparative studies, model tests and detailed analysis on the environmental conditions would enhance the accuracy of performance evaluation and downtime estimation.

REFERENCES

Ewans, K., Valk, C. van de, Shaw, C., Haan, J. den, Tromans, P., and Vanderschuren, L., 2003. Oceanographic and Motion Response Statistics for The Operation of a Weathervaning LNG FPSO. Proceedings of OMAE 2003, 22nd International Conference on Offshore Mechanics and Arctic Engineering, June 8-13, 2003, Cancun, Mexico.

Ewans, K. C., Vanderschuren, L., and Tromans, P. S., 2006. FPSO Conference-Estimating Wind-Sea and Swell for FPSO Operability. Journal of Offshore Mechanics and Arctic Engineering, Vol. 128, November 2006.

Faltinsen, O., 1990. Sea Loads on Ships and Offshore Structures. Publication, Cambridge University Press.

Ha, T.P., 2011. Frequency and Time Domain Motion and Mooring Analyses for a FPSO Operating in Deep Water. A Thesis for PhD, Newcastle University.

Khaw T., Rawstron P. and Lagstrom K., 2005. A New Approach to the Design of Monohull FPSOs. OMAE 67033, Halkidiki, Greece.

Kim, H.J., Kwak, H.U., Lee, J., Kim, S.E., and Seo, J.S., 2012. Offloading Operability with Heading Control of Side-By-Side Moored FLNG and LNGC. Proceedings of the ASME 2012 31st International Conference on Ocean, Offshore and Arctic Engineering, OMAE 2012, Rio de Janeiro, Brazil.

Lee, J.H., Kim, Y.S., and Kim, D., 2010. Development of Roll Suppression Device for LNG FPSO Application. Proceedings of Offshore Technology Conference, Houston, U.S.A.

McDonald, L., 2013. Floating LNG: Contracting and Project Structuring Considerations, Seoul, Korea. Presentation. 7th Annual FLNG Conference, Seoul, Korea.

Mercier, R., 2014. OCEN 676: Dynamics of Offshore Structures. Course Material, Texas A&M University, College Station, TX.

MIT Opencourse, 2011. 2.019: Design of Ocean Systems, Lecture 14: Mooring Dynamics (III).

Pek, B., 2011. Floating LNG Grows up. Presentation. 25th Annual Gastech Conference, Amsterdam, Netherlands, March 23rd, 2011.

Pek, B. and Velder, H. van der, 2013. A High Capacity Floating LNG Design. LNG 17, Houston, U.S.A.

Portilla J., Ocampo-Torres, F. J., and Monbaliu, J., 2009. Spectral Partitioning and Identification of Wind Sea and Swell. In The Journal of Atmospheric and Oceanic Technology, vol.26, 107-122.

Ran, Z., 2000. Coupled dynamic analysis of floating structures in waves and currents. Ph.D. Dissertation, Civil Engineering Department, Texas A&M University, College Station, TX.

Rice, C. L., 1985. Effects of Motion on Design of Process Facilities for Floating Production Systems. Offshore Technology Conference, OTC 5034, Houston, USA.

Shell Development (Australia) Proprietary Limited, 2009. Prelude Floating LNG Project Draft Environmental Impact Statement, Chapter 1 and 5.

Wichers, I.J., 2013. Guide to Single Point Moorings. Publication, WMooring Inc.

Wilde, J.J. de, Dijik, A. W. van, Berg, J. van den, and Dekker, J., 2009. Direct Time Domain Downtime Assessment for LNG Operations using Computer Cluster. Proceedings of the 19th International Offshore Polar Engineering Conference, Osaka, Japan, June 21-26, 2009.

Xia, J., 2012. FPSO Design to Minimize Operational Downtime due to Adverse Metocean Conditions off North West Australia. Deep Offshore Technology, 27-29 November 2012, Perth, Australia.

Vestbostad, T.M., Andersen, O.J., Haver, S., and Albert, A., 2002. Prediction of Extreme Roll Motion on an FPSO using Long Term Statistics. Proceedings of OMAE, June 23-28, 2002, Oslo, Norway.

APPENDIX 1

Table 66. Downtime list of Scenario#1: Lighter Topside (Heading #1, Recovery: 3 hr)

- Model: Lighter Topside (Scenario #1)
- Heading: #1. Toward Sea+10deg.
- Data: 1 year (Aug.2011 – Jul.2012)
- Recovery time: 3 hours/event
- # of total downtime event: 14
- Total downtime: 192 hours = 8 days

No.	Month	day	year	hour	Hs(m)	Tp(s)	WaveDir	WindS	WindDir	index1*	index2**
1	8	7	2011	6	1.05	21.44	255.05	4.67	105.14	1	1
2	8	7	2011	9	1.08	21.33	257.66	3.40	103.10	1	2
3	8	7	2011	12	1.13	21	258.07	3.50	79.97	1	2
4	8	7	2011	15	1.21	19.94	250.31	4.57	80.17	1	2
5	8	7	2011	18	1.24	19.58	250.99	3.87	75.03	1	2
6	8	7	2011	21	1.27	19.38	252.99	3.39	87.63	1	2
7	8	8	2011	0	1.3	19.09	253.27	3.63	97.28	1	2
8	8	8	2011	3	1.34	18.26	246.68	4.77	92.04	1	2
9	8	8	2011	6	1.36	17.79	247.50	3.77	96.09	1	2
10	8	8	2011	9	1.34	17.6	248.57	2.63	104.99	1	2
11	8	8	2011	12	1.33	17.4	248.82	2.09239	182.74	0	1
12	8	22	2011	0	1.55	17.56	247.92	7.20924	112.51	1	1
13	8	22	2011	3	1.47	17.07	247.84	8.75918	99.4621	0	1
14	8	29	2011	3	0.61	19.46	252.95	5.65799	123.465	1	1
15	8	29	2011	6	0.65	19.45	253.36	4.25027	131.566	1	2
16	8	29	2011	9	0.62	19.35	254.88	1.67287	101.377	1	2
17	8	29	2011	12	0.59	18.94	254.52	1.52712	23.5434	1	2
18	8	29	2011	15	0.57	17.99	245.08	0.657343	76.8092	0	1
19	9	9	2011	21	0.74	19.51	254.33	6.71662	104.926	1	1
20	9	10	2011	0	1.11	19.42	253.78	10.8228	99.9495	1	2
21	9	10	2011	3	1.59	19.42	254.7	10.841	90.7926	1	2
22	9	10	2011	6	1.91	19.38	253.63	8.19525	83.9762	1	2
23	9	10	2011	9	2.02	19.06	253.72	6.89701	67.6739	1	2
24	9	10	2011	12	2.04	17.87	249.93	5.52254	76.0642	1	2
25	9	10	2011	15	1.96	17.72	250.26	5.04026	81.9019	1	2
26	9	10	2011	18	1.81	17.7	249.51	6.54047	93.2428	1	2
27	9	10	2011	21	1.7	17.7	249.45	10.2192	116.063	1	2
28	9	11	2011	0	1.75	17.65	249.23	9.67512	102.657	1	2
29	9	11	2011	3	1.94	17.37	250.07	10.5326	93.756	0	1
30	9	13	2011	6	2.21	17.02	251.63	11.4719	84.0457	1	1
31	9	13	2011	9	2.39	6.37	73.38	9.35183	69.8597	0	1
32	9	23	2011	9	0.79	19.19	247.44	1.73612	189.951	1	1
33	9	23	2011	12	0.84	18.07	243.51	2.67081	202.917	1	2
34	9	23	2011	15	0.91	17.68	243.45	1.66208	211.969	0	1
35	10	4	2011	21	1.37	17.97	243.44	3.71442	212.578	1	1
36	10	5	2011	0	1.38	17.75	242.7	4.06503	196.875	1	2

- Model: Lighter Topside (Scenario #1)
- Heading: #1. Toward Sea+10deg.
- Data: 1 year (Aug.2011 – Jul.2012)
- Recovery time: 3 hours/event
- # of total downtime event: 14
- Total downtime: 192 hours = 8 days

No.	Month	day	year	hour	Hs(m)	Tp(s)	WaveDir	WindS	WindDir	index1*	index2**
37	10	5	2011	3	1.38	17.51	243.4	3.3754	196.878	1	2
38	10	5	2011	6	1.38	17.16	244.55	3.09627	212.202	0	1
39	10	18	2011	3	1.07	17.77	244.15	4.17969	123.88	1	1
40	10	18	2011	6	1.03	17.52	243.23	1.89992	123.188	1	2
41	10	18	2011	9	0.99	17.36	243.27	1.60078	268.21	0	1
42	6	3	2012	12	1.22	17.77	242.76	6.07119	75.2082	1	1
43	6	3	2012	15	1.26	17.59	242.71	6.13705	80.338	1	2
44	6	3	2012	18	1.32	16.58	239.66	7.10927	81.9951	0	1
45	6	7	2012	15	1.56	17.53	250.32	7.6893	75.078	1	1
46	6	7	2012	18	1.61	17.43	250.95	8.63296	82.5455	0	1
47	6	11	2012	3	1.44	17.77	251.51	6.7743	86.2757	1	1
48	6	11	2012	6	1.38	17.49	252.04	5.3051	85.6756	0	1
49	6	20	2012	3	1.27	17.67	250.87	5.4159	118.931	1	1
50	6	20	2012	6	1.25	17.64	251.25	4.95556	81.4119	1	2
51	6	20	2012	9	1.23	17.56	252.09	4.5124	63.2644	1	2
52	6	20	2012	12	1.22	17.33	252.42	3.05408	52.7172	0	1
53	7	15	2012	3	0.8	18.03	243.81	4.14673	64.7325	1	1
54	7	15	2012	6	0.7	17.85	245.79	5.0711	61.1099	0	1
55	7	16	2012	0	0.72	19.05	253.17	6.53471	124.273	1	1
56	7	16	2012	3	0.84	19.29	252.85	7.41659	98.7636	1	2
57	7	16	2012	6	0.95	19.31	250.91	5.93507	82.9347	1	2
58	7	16	2012	9	1	19.07	249.74	4.36835	58.3838	1	2
59	7	16	2012	12	1.07	17.98	247.88	3.79084	54.3392	1	2
60	7	16	2012	15	1.13	17.81	247.23	3.91261	68.0897	1	2
61	7	16	2012	18	1.14	17.76	246.27	4.05346	85.3301	1	2
62	7	16	2012	21	1.11	17.7	245.81	4.4419	91.6769	1	2
63	7	17	2012	0	1.06	17.56	245.51	5.43089	104.829	1	2
64	7	17	2012	3	1.01	17.33	245.52	6.17029	131.518	0	1

Table 67. Downtime list of Scenario#1: Lighter Topside (Heading #1, Recovery: 24 hr)

- Model: Lighter Topside (Scenario #1)
- Heading: #1. Toward Sea+10deg.
- Data: 1 year (Aug.2011 – Jul.2012)
- Recovery time: 24 hours/event
- # of total downtime event: 14
- Total downtime: 480 hours = 20 days

No.	Month	day	year	hour	Hs(m)	Tp(s)	WaveDir	WindS	WindDir	index1*	index2**
1	8	7	2011	6	1.05	21.44	255.05	4.67	105.14	1	1
2	8	7	2011	9	1.08	21.33	257.66	3.40	103.10	1	2
3	8	7	2011	12	1.13	21	258.07	3.50	79.97	1	3
4	8	7	2011	15	1.21	19.94	250.31	4.57	80.17	1	4
5	8	7	2011	18	1.24	19.58	250.99	3.87	75.03	1	5
6	8	7	2011	21	1.27	19.38	252.99	3.39	87.63	1	6
7	8	8	2011	0	1.3	19.09	253.27	3.63	97.28	1	7
8	8	8	2011	3	1.34	18.26	246.68	4.77	92.04	1	8
9	8	8	2011	6	1.36	17.79	247.50	3.77	96.09	1	9
10	8	8	2011	9	1.34	17.6	248.57	2.63	104.99	1	9
11	8	8	2011	12	1.33	17.4	248.82	2.09239	182.74	0	8
12	8	8	2011	15	1.33	17.05	249.53	1.72699	157.89	0	7
13	8	8	2011	18	1.34	16.47	244.62	2.20166	137.761	0	6
14	8	8	2011	21	1.33	16.23	245.38	1.94833	144.188	0	5
15	8	9	2011	0	1.3	16.08	245.58	2.64622	149.073	0	4
16	8	9	2011	3	1.28	15.95	246.1	3.76416	165.853	0	3
17	8	9	2011	6	1.26	15.82	246.21	4.12685	186.54	0	2
18	8	9	2011	9	1.23	15.67	246.69	3.82188	204.42	0	1
19	8	22	2011	0	1.55	17.56	247.92	7.20924	112.51	1	1
20	8	22	2011	3	1.47	17.07	247.84	8.75918	99.4621	0	1
21	8	22	2011	6	1.53	16.3	242.48	8.00626	86.3476	0	1
22	8	22	2011	9	1.57	16.14	243.7	7.49104	66.8916	0	1
23	8	22	2011	12	1.64	16.04	245.09	7.57312	67.5662	0	1
24	8	22	2011	15	1.76	15.96	245.95	7.41875	71.3695	0	1
25	8	22	2011	18	1.83	15.88	245.81	6.91788	87.2656	0	1
26	8	22	2011	21	1.78	15.77	245.58	7.59471	119.501	0	1
27	8	23	2011	0	1.67	15.46	244.88	8.19524	110.425	0	1
28	8	29	2011	3	0.61	19.46	252.95	5.65799	123.465	1	1
29	8	29	2011	6	0.65	19.45	253.36	4.25027	131.566	1	2
30	8	29	2011	9	0.62	19.35	254.88	1.67287	101.377	1	3
31	8	29	2011	12	0.59	18.94	254.52	1.52712	23.5434	1	4
32	8	29	2011	15	0.57	17.99	245.08	0.657343	76.8092	0	4
33	8	29	2011	18	0.56	17.8	246.79	0.559464	155.725	0	4
34	8	29	2011	21	0.54	17.74	249.22	2.92775	211.736	0	4
35	8	30	2011	0	0.52	17.7	250.16	4.80021	187.422	0	4
36	8	30	2011	3	0.51	17.67	251.34	4.50821	164.299	0	4
37	8	30	2011	6	0.5	17.62	251.62	2.98453	136.086	0	3
38	8	30	2011	9	0.49	17.5	252.32	2.37952	207.535	0	2

- Model: Lighter Topside (Scenario #1)
- Heading: #1. Toward Sea+10deg.
- Data: 1 year (Aug.2011 – Jul.2012)
- Recovery time: 24 hours/event
- # of total downtime event: 14
- Total downtime: 480 hours = 20 days

No.	Month	day	year	hour	Hs(m)	Tp(s)	WaveDir	WindS	WindDir	index1*	index2**
39	8	30	2011	12	0.47	17.21	252.19	2.55033	221.503	0	1
40	9	9	2011	21	0.74	19.51	254.33	6.71662	104.926	1	1
41	9	10	2011	0	1.11	19.42	253.78	10.8228	99.9495	1	2
42	9	10	2011	3	1.59	19.42	254.7	10.841	90.7926	1	3
43	9	10	2011	6	1.91	19.38	253.63	8.19525	83.9762	1	4
44	9	10	2011	9	2.02	19.06	253.72	6.89701	67.6739	1	5
45	9	10	2011	12	2.04	17.87	249.93	5.52254	76.0642	1	6
46	9	10	2011	15	1.96	17.72	250.26	5.04026	81.9019	1	7
47	9	10	2011	18	1.81	17.7	249.51	6.54047	93.2428	1	8
48	9	10	2011	21	1.7	17.7	249.45	10.2192	116.063	1	9
49	9	11	2011	0	1.75	17.65	249.23	9.67512	102.657	1	9
50	9	11	2011	3	1.94	17.37	250.07	10.5326	93.756	0	8
51	9	11	2011	6	2.1	16.57	245.97	8.37225	84.2415	0	7
52	9	11	2011	9	2.09	16.33	245.98	6.04003	71.2649	0	6
53	9	11	2011	12	1.99	16.28	245.78	5.26849	67.5724	0	5
54	9	11	2011	15	1.88	16.31	246.29	6.07787	79.1891	0	4
55	9	11	2011	18	1.83	16.36	246.68	8.78237	97.8531	0	3
56	9	11	2011	21	1.86	16.38	247.57	10.249	108.665	0	2
57	9	12	2011	0	1.97	16.34	248.04	10.8155	104.73	0	1
58	9	13	2011	6	2.21	17.02	251.63	11.4719	84.0457	1	1
59	9	13	2011	9	2.39	6.37	73.38	9.35183	69.8597	0	1
60	9	13	2011	12	2.44	7.01	68.49	9.05743	62.4446	0	1
61	9	13	2011	15	2.49	7.55	63.39	7.81703	58.7093	0	1
62	9	13	2011	18	2.42	7.64	63.76	6.06211	88.4874	0	1
63	9	13	2011	21	2.19	15.36	248.5	6.91868	117.083	0	1
64	9	14	2011	0	1.94	15.19	245.56	7.0578	112.932	0	1
65	9	14	2011	3	1.78	15.05	245.96	7.64519	96.2324	0	1
66	9	14	2011	6	1.72	14.89	246.1	7.73828	80.4036	0	1
67	9	23	2011	9	0.79	19.19	247.44	1.73612	189.951	1	1
68	9	23	2011	12	0.84	18.07	243.51	2.67081	202.917	1	2
69	9	23	2011	15	0.91	17.68	243.45	1.66208	211.969	0	2
70	9	23	2011	18	0.98	17.43	242.73	1.43339	255.867	0	2
71	9	23	2011	21	1.07	17.14	244.93	1.08074	267.879	0	2
72	9	24	2011	0	1.16	16.93	247.81	1.73669	256.684	0	2
73	9	24	2011	3	1.23	16.39	239.97	0.800812	195.946	0	2
74	9	24	2011	6	1.27	16.03	240.9	1.46014	203.405	0	2
75	9	24	2011	9	1.32	15.92	243.71	1.93414	228.564	0	2
76	9	24	2011	12	1.36	15.89	246.12	2.48171	257.196	0	1
77	10	4	2011	21	1.37	17.97	243.44	3.71442	212.578	1	1
78	10	5	2011	0	1.38	17.75	242.7	4.06503	196.875	1	2

- Model: Lighter Topside (Scenario #1)
- Heading: #1. Toward Sea+10deg.
- Data: 1 year (Aug.2011 – Jul.2012)
- Recovery time: 24 hours/event
- # of total downtime event: 14
- Total downtime: 480 hours = 20 days

No.	Month	day	year	hour	Hs(m)	Tp(s)	WaveDir	WindS	WindDir	index1*	index2**
79	10	5	2011	3	1.38	17.51	243.4	3.3754	196.878	1	3
80	10	5	2011	6	1.38	17.16	244.55	3.09627	212.202	0	3
81	10	5	2011	9	1.38	16.62	239.94	3.38186	223.083	0	3
82	10	5	2011	12	1.37	16.22	239.7	4.32478	217.957	0	3
83	10	5	2011	15	1.36	15.96	239.9	4.03045	233.983	0	3
84	10	5	2011	18	1.34	15.77	240.06	3.52548	222.241	0	3
85	10	5	2011	21	1.31	15.61	241.09	3.02952	198.076	0	3
86	10	6	2011	0	1.29	15.48	242.05	4.43654	207.085	0	2
87	10	6	2011	3	1.27	15.38	243.3	4.91427	209.904	0	1
88	10	18	2011	3	1.07	17.77	244.15	4.17969	123.88	1	1
89	10	18	2011	6	1.03	17.52	243.23	1.89992	123.188	1	2
90	10	18	2011	9	0.99	17.36	243.27	1.60078	268.21	0	2
91	10	18	2011	12	0.97	16.99	242.72	1.61505	187.829	0	2
92	10	18	2011	15	0.95	16.1	240.14	1.33255	211.185	0	2
93	10	18	2011	18	0.94	15.94	239.81	3.96834	201.587	0	2
94	10	18	2011	21	0.94	15.83	239.96	4.39001	197.362	0	2
95	10	19	2011	0	0.95	15.7	239.68	3.48023	179.341	0	2
96	10	19	2011	3	0.95	15.46	239.8	2.85281	132.3	0	2
97	10	19	2011	6	0.93	15.04	237.55	2.14972	74.3473	0	1
98	6	3	2012	12	1.22	17.77	242.76	6.07119	75.2082	1	1
99	6	3	2012	15	1.26	17.59	242.71	6.13705	80.338	1	2
100	6	3	2012	18	1.32	16.58	239.66	7.10927	81.9951	0	2
101	6	3	2012	21	1.4	16.2	239.52	8.30167	86.9616	0	2
102	6	4	2012	0	1.49	16.09	239.36	9.56365	98.8416	0	2
103	6	4	2012	3	1.59	15.91	239.41	9.1437	88.3704	0	2
104	6	4	2012	6	1.65	5.63	72.63	8.43019	82.0908	0	2
105	6	4	2012	9	1.62	14.75	237.36	6.98928	74.6512	0	2
106	6	4	2012	12	1.56	14.63	237.28	5.86605	71.7193	0	2
107	6	4	2012	15	1.53	14.53	237.34	6.19752	69.8983	0	1
108	6	7	2012	15	1.56	17.53	250.32	7.6893	75.078	1	1
109	6	7	2012	18	1.61	17.43	250.95	8.63296	82.5455	0	1
110	6	7	2012	21	1.71	5.98	66.64	9.26311	91.4844	0	1
111	6	8	2012	0	1.78	6.03	68.1	9.20005	89.813	0	1
112	6	8	2012	3	1.8	6.08	68.96	8.61359	95.0617	0	1
113	6	8	2012	6	1.8	6.09	69.45	8.42813	92.5159	0	1
114	6	8	2012	9	1.74	6.18	68.87	7.26298	77.8389	0	1
115	6	8	2012	12	1.66	15.9	244.97	6.66053	72.4354	0	1
116	6	8	2012	15	1.59	6.41	66.04	6.69156	75.9013	0	1
117	6	11	2012	3	1.44	17.77	251.51	6.7743	86.2757	1	1
118	6	11	2012	6	1.38	17.49	252.04	5.3051	85.6756	0	1

- Model: Lighter Topside (Scenario #1)
- Heading: #1. Toward Sea+10deg.
- Data: 1 year (Aug.2011 – Jul.2012)
- Recovery time: 24 hours/event
- # of total downtime event: 14
- Total downtime: 480 hours = 20 days

No.	Month	day	year	hour	Hs(m)	Tp(s)	WaveDir	WindS	WindDir	index1*	index2**
119	6	11	2012	9	1.32	16.82	248.27	4.64812	95.0603	0	1
120	6	11	2012	12	1.27	16.32	249.09	3.38423	95.2555	0	1
121	6	11	2012	15	1.24	16.15	249.71	3.10852	71.6232	0	1
122	6	11	2012	18	1.23	15.99	249.67	3.64927	63.2944	0	1
123	6	11	2012	21	1.24	15.6	249.72	4.07413	63.309	0	1
124	6	12	2012	0	1.26	14.93	247.14	3.48811	71.0974	0	1
125	6	12	2012	3	1.28	14.71	247.3	4.01647	82.2732	0	1
126	6	20	2012	3	1.27	17.67	250.87	5.4159	118.931	1	1
127	6	20	2012	6	1.25	17.64	251.25	4.95556	81.4119	1	2
128	6	20	2012	9	1.23	17.56	252.09	4.5124	63.2644	1	3
129	6	20	2012	12	1.22	17.33	252.42	3.05408	52.7172	0	3
130	6	20	2012	15	1.2	16.41	247.79	1.49402	53.4368	0	3
131	6	20	2012	18	1.18	16.12	247.98	0.788923	120.465	0	3
132	6	20	2012	21	1.15	16.03	248.14	2.64322	152.756	0	3
133	6	21	2012	0	1.12	15.96	248.05	3.16893	155.78	0	3
134	6	21	2012	3	1.09	15.83	248.31	3.27452	150.146	0	3
135	6	21	2012	6	1.06	15.55	248.41	2.18874	162.724	0	2
136	6	21	2012	9	1.04	14.71	246.14	2.46398	176.742	0	1
137	7	15	2012	3	0.8	18.03	243.81	4.14673	64.7325	1	1
138	7	15	2012	6	0.7	17.85	245.79	5.0711	61.1099	0	1
139	7	15	2012	9	0.63	17.75	248.21	4.26298	55.8998	0	1
140	7	15	2012	12	0.57	17.68	249.72	3.26657	28.5264	0	1
141	7	15	2012	15	0.54	17.61	251.14	1.99251	49.2738	0	1
142	7	15	2012	18	0.57	17.53	251.92	2.5045	93.4334	0	1
143	7	15	2012	21	0.64	17.48	252.53	4.8848	104.463	0	1
144	7	16	2012	0	0.72	19.05	253.17	6.53471	124.273	1	2
145	7	16	2012	3	0.84	19.29	252.85	7.41659	98.7636	1	3
146	7	16	2012	6	0.95	19.31	250.91	5.93507	82.9347	1	3
147	7	16	2012	9	1	19.07	249.74	4.36835	58.3838	1	4
148	7	16	2012	12	1.07	17.98	247.88	3.79084	54.3392	1	5
149	7	16	2012	15	1.13	17.81	247.23	3.91261	68.0897	1	6
150	7	16	2012	18	1.14	17.76	246.27	4.05346	85.3301	1	7
151	7	16	2012	21	1.11	17.7	245.81	4.4419	91.6769	1	8
152	7	17	2012	0	1.06	17.56	245.51	5.43089	104.829	1	9
153	7	17	2012	3	1.01	17.33	245.52	6.17029	131.518	0	8
154	7	17	2012	6	0.99	17	245.39	5.1241	127.227	0	7
155	7	17	2012	9	0.99	16.42	241.28	3.73	132.501	0	6
156	7	17	2012	12	1.01	16.15	241.67	3.78308	135.321	0	5
157	7	17	2012	15	1.04	16.02	242.11	4.73001	126.748	0	4
158	7	17	2012	18	1.06	15.93	242	4.19395	113.019	0	3

- Model: Lighter Topside (Scenario #1)
- Heading: #1. Toward Sea+10deg.
- Data: 1 year (Aug.2011 – Jul.2012)
- Recovery time: 24 hours/event
- # of total downtime event: 14
- Total downtime: 480 hours = 20 days

No.	Month	day	year	hour	Hs(m)	Tp(s)	WaveDir	WindS	WindDir	index1*	index2**
159	7	17	2012	21	1.06	15.84	242.02	4.31771	112.466	0	2
160	7	18	2012	0	1.05	15.72	241.61	4.49484	139.15	0	1

APPENDIX 2

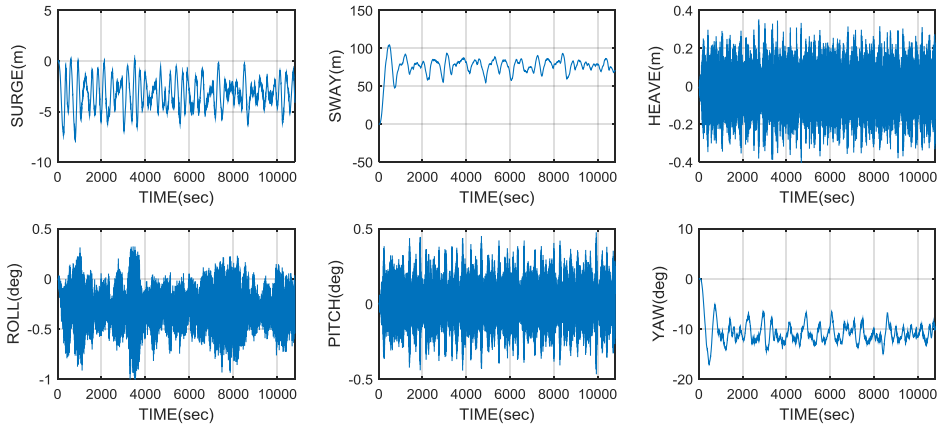

Figure 59. Test result: ZCG=5m under 1-year extreme condition (Part 1)

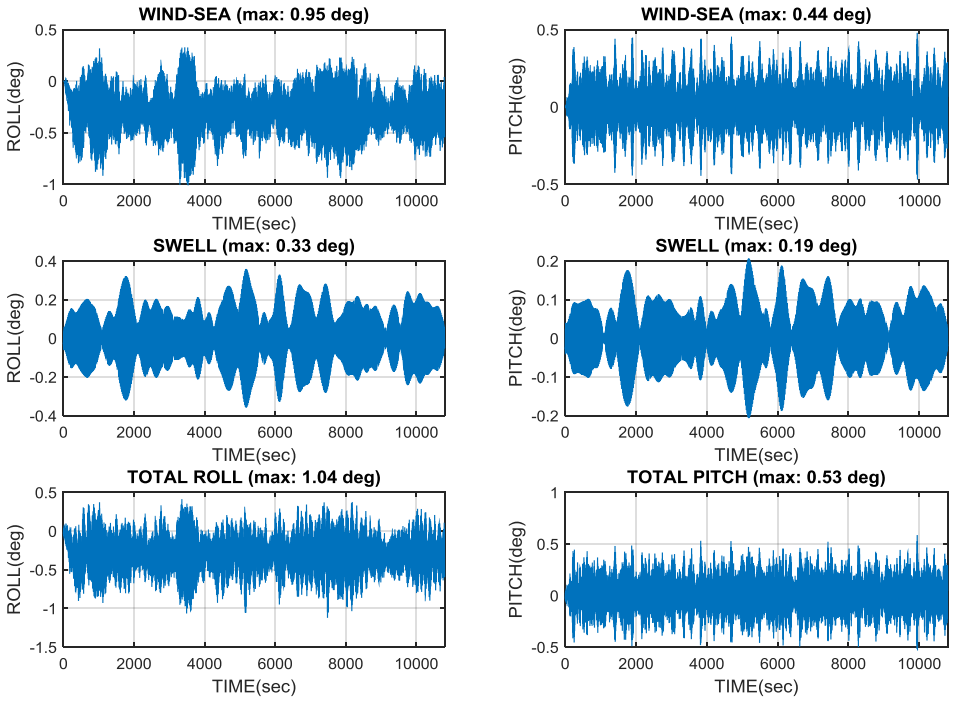

Figure 60. Test result: ZCG=5m under 1-year extreme condition (Part 1+ Part 2)

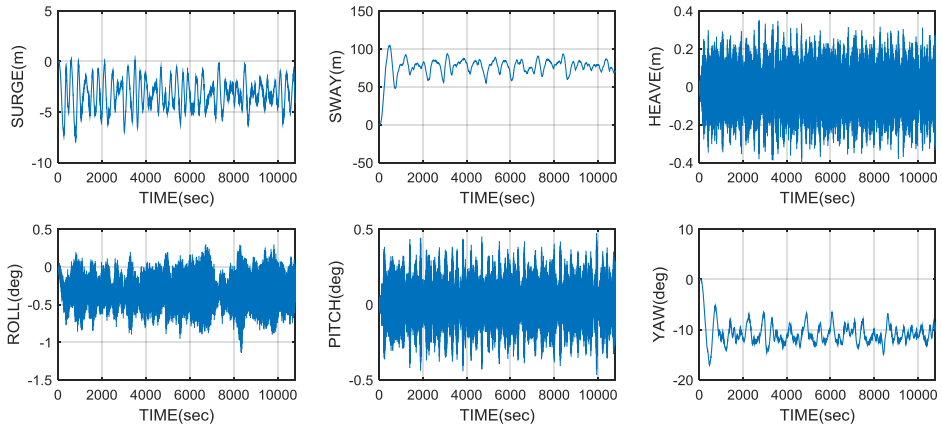

Figure 61. Test result: ZCG=6m under 1-year extreme condition (Part 1)

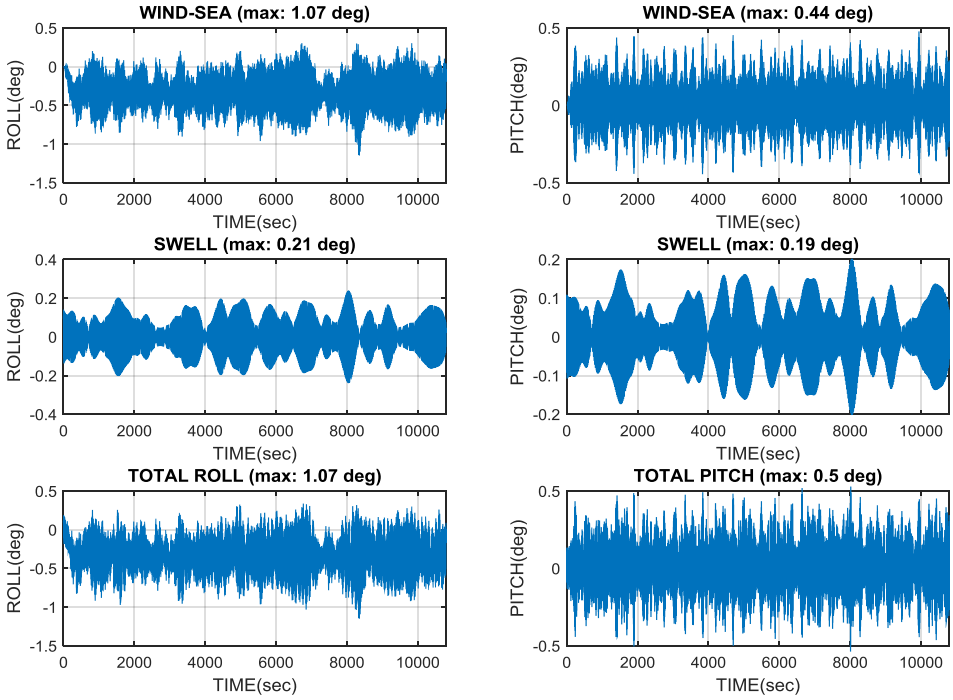

Figure 62. Test result: ZCG=6m under 1-year extreme condition (Part 1+ Part 2)

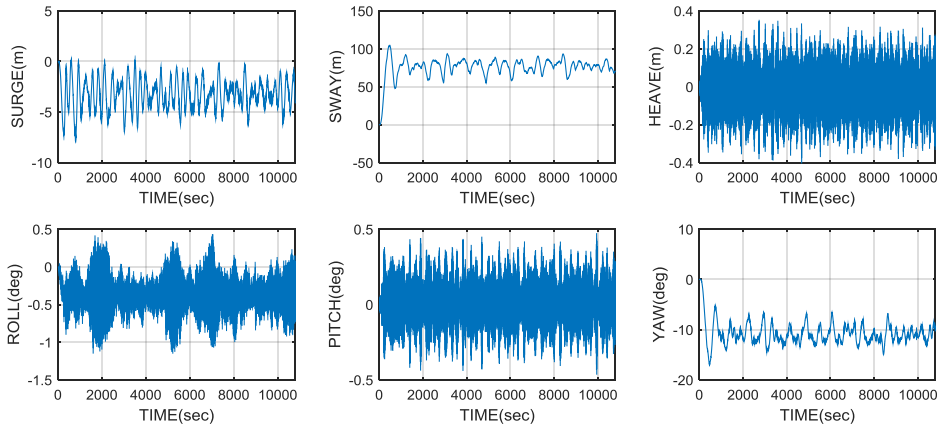

Figure 63. Test result: ZCG=7m under 1-year extreme condition (Part 1)

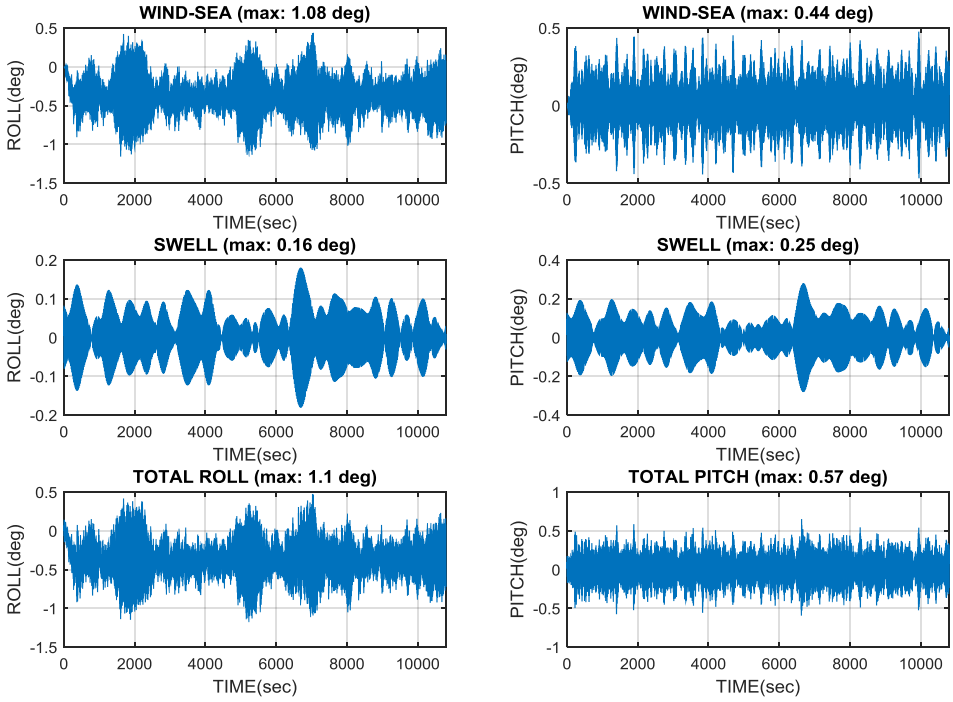

Figure 64. Test result: ZCG=7m under 1-year extreme condition (Part 1+ Part 2)

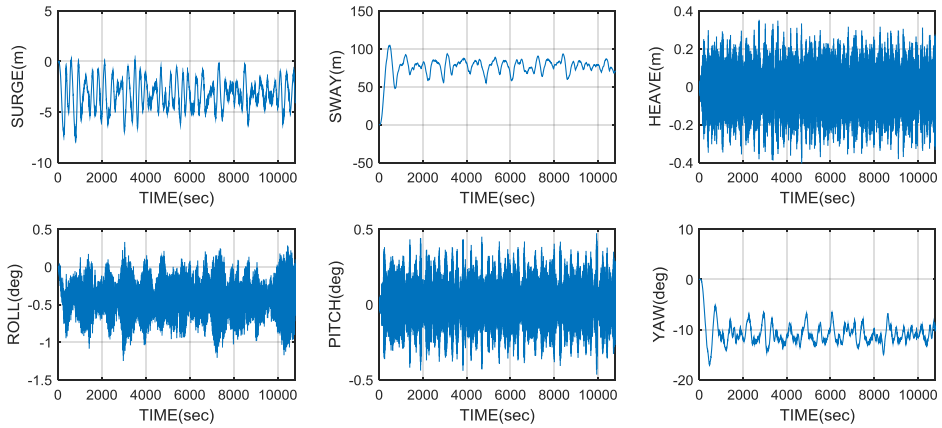

Figure 65. Test result: ZCG=8m under 1-year extreme condition (Part 1)

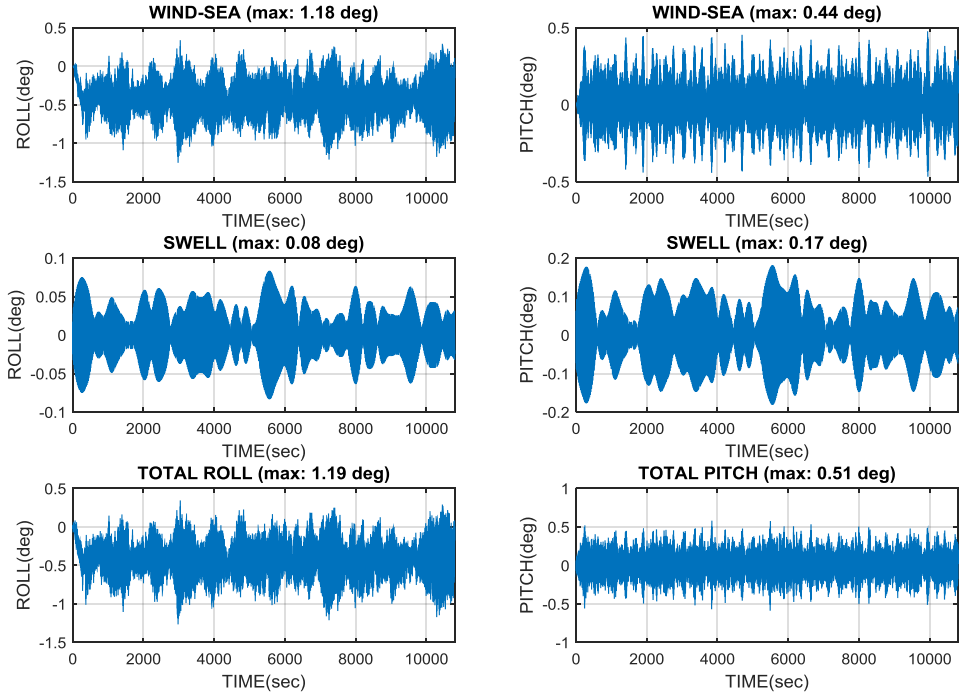

Figure 66. Test result: ZCG=8m under 1-year extreme condition (Part 1+ Part 2)

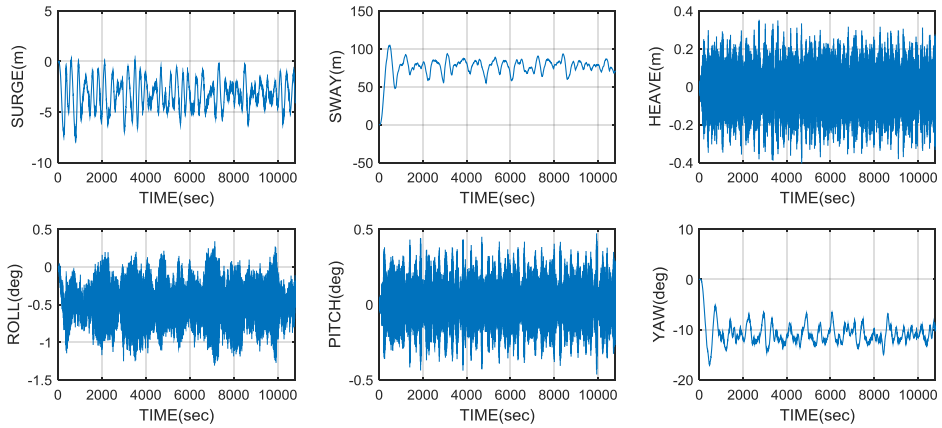

Figure 67. Test result: ZCG=9m under 1-year extreme condition (Part 1)

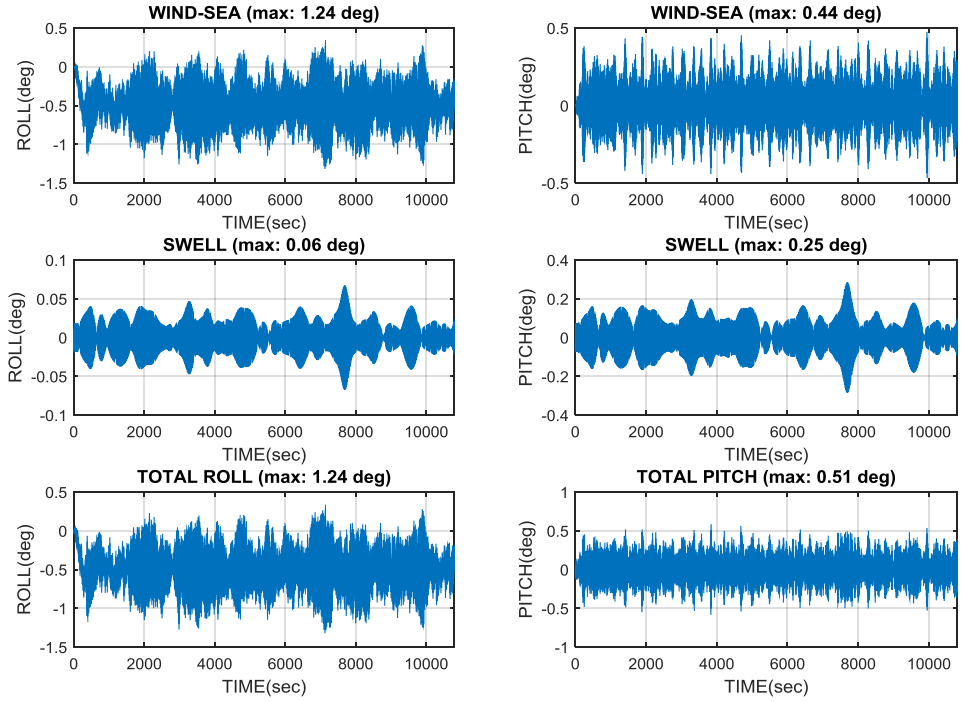

Figure 68. Test result: ZCG=9m under 1-year extreme condition (Part 1+ Part 2)

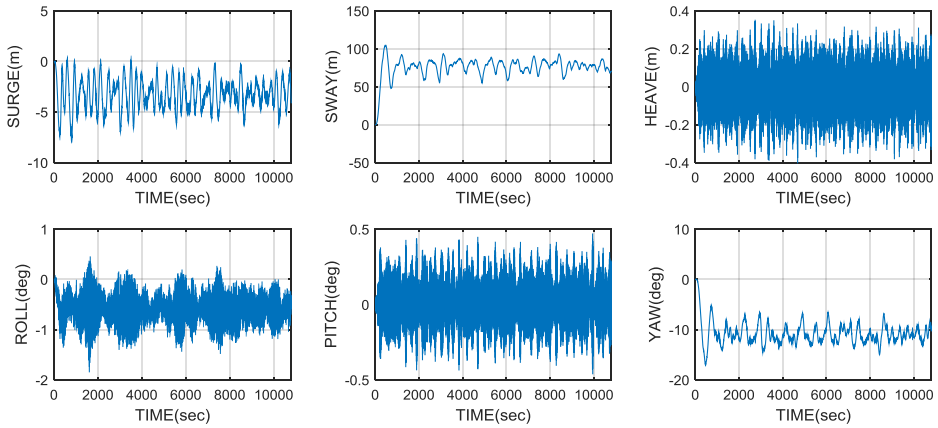

Figure 69. Test result: ZCG=10m under 1-year extreme condition (Part 1)

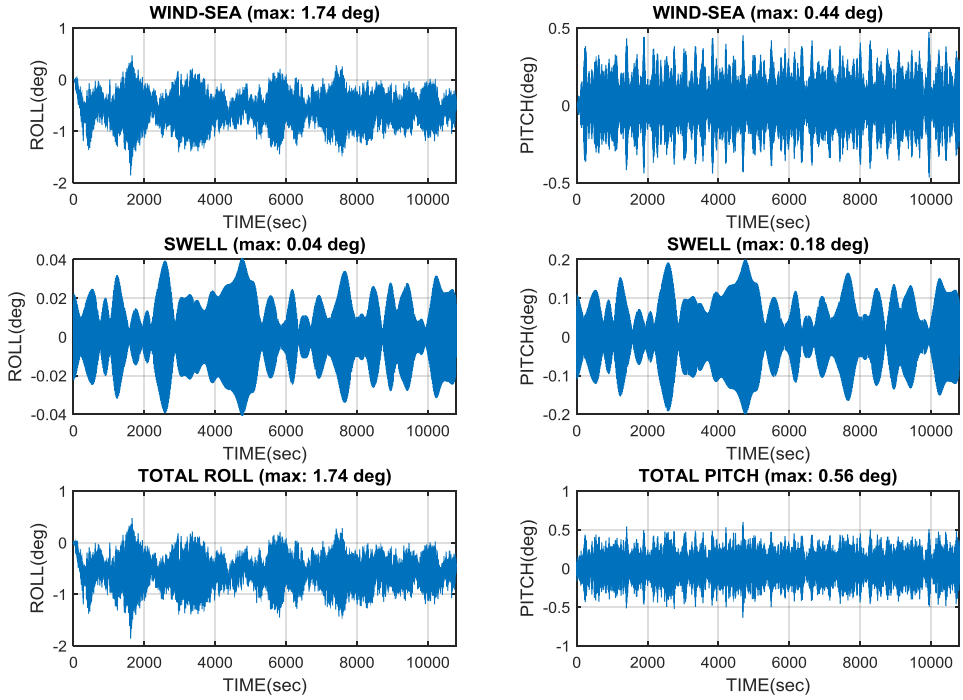

Figure 70. Test result: ZCG=10m under 1-year extreme condition (Part 1+ Part 2)

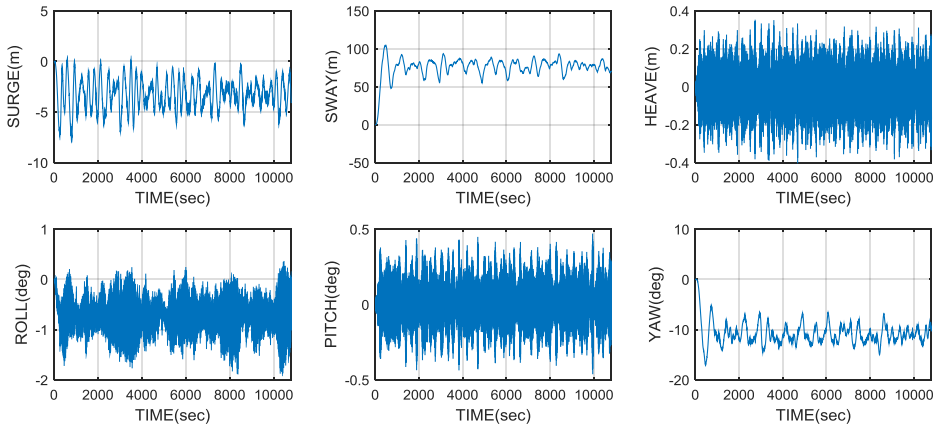

Figure 71. Test result: ZCG=11m under 1-year extreme condition (Part 1)

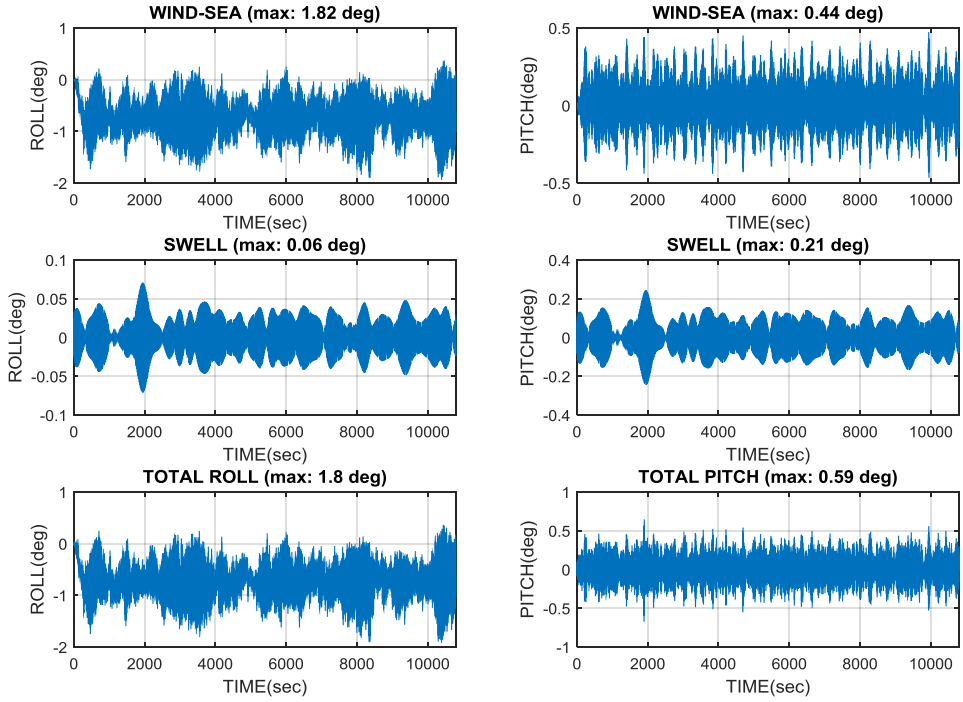

Figure 72. Test result: ZCG=11m under 1-year extreme condition (Part 1+ Part 2)

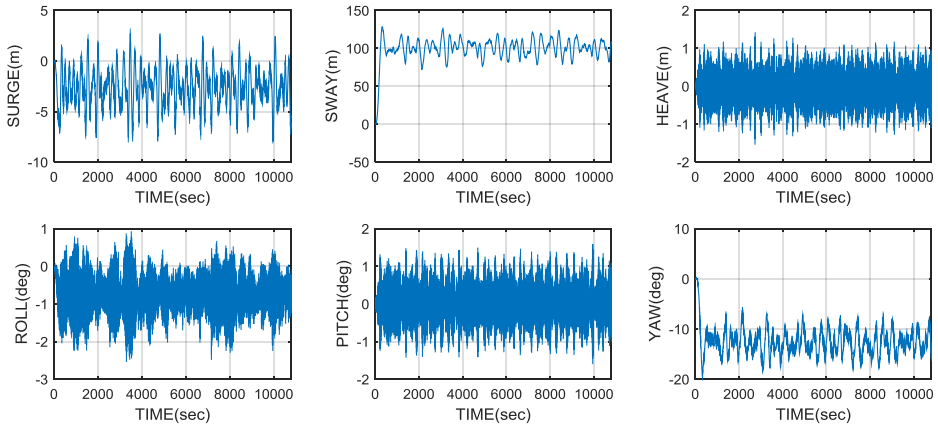

Figure 73. Test result: ZCG=5m under 10-year extreme condition (Part 1)

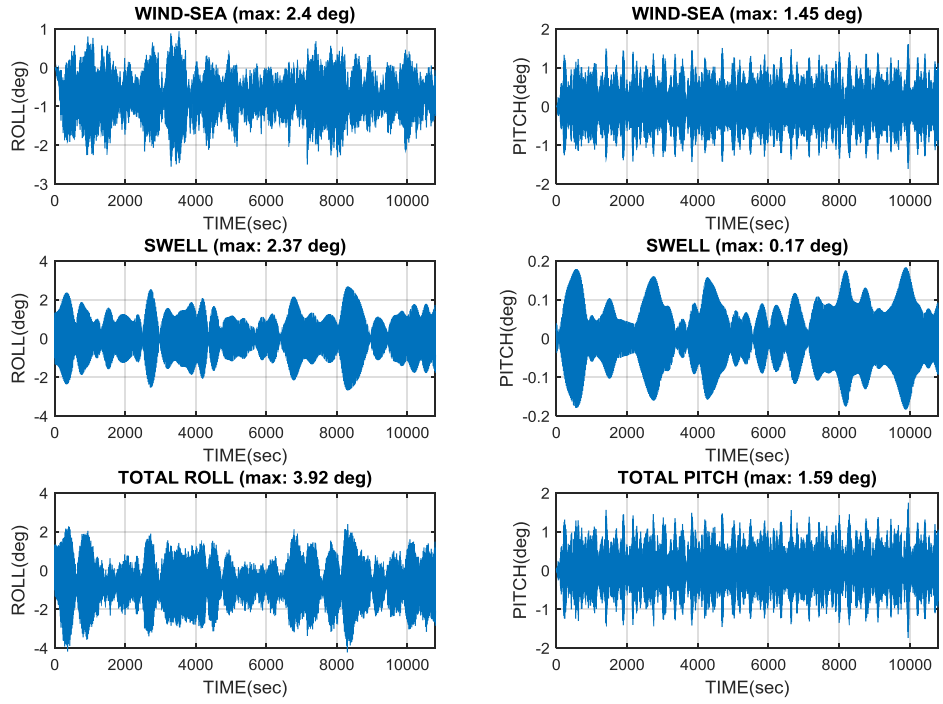

Figure 74. Test result: ZCG=5m under 10-year extreme condition (Part 1+ Part 2)

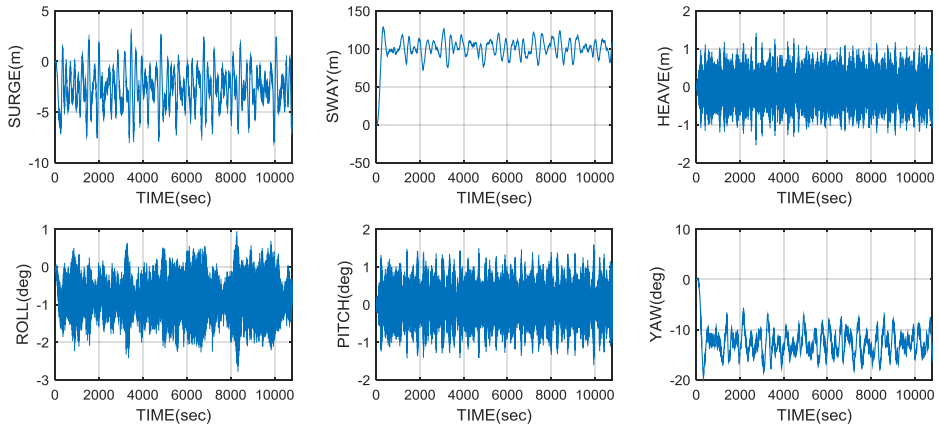

Figure 75. Test result: ZCG=6m under 10-year extreme condition (Part 1)

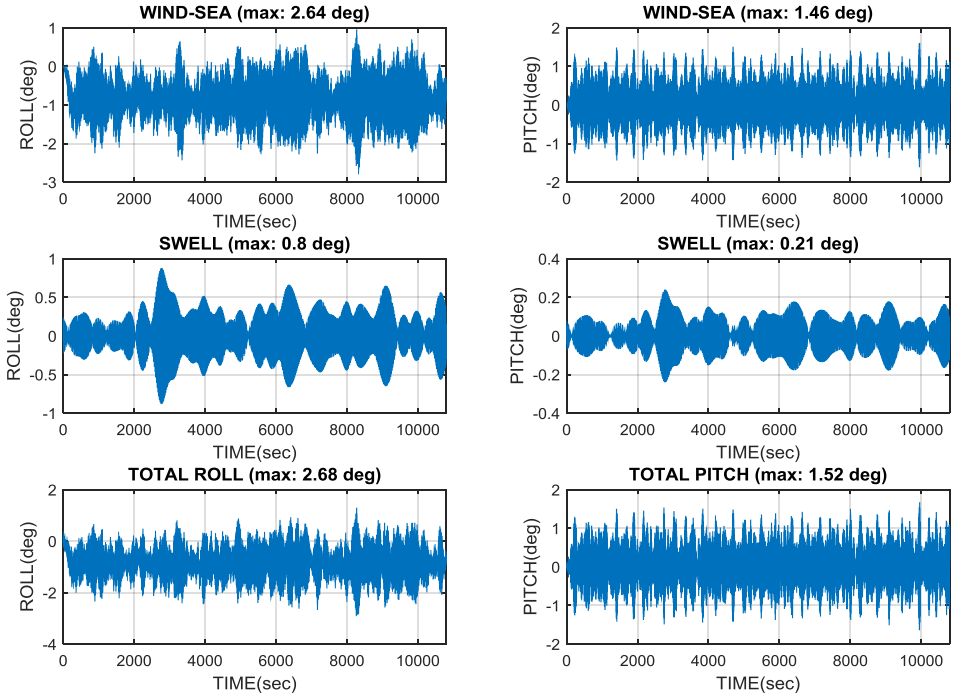

Figure 76. Test result: ZCG=6m under 10-year extreme condition (Part 1+ Part 2)

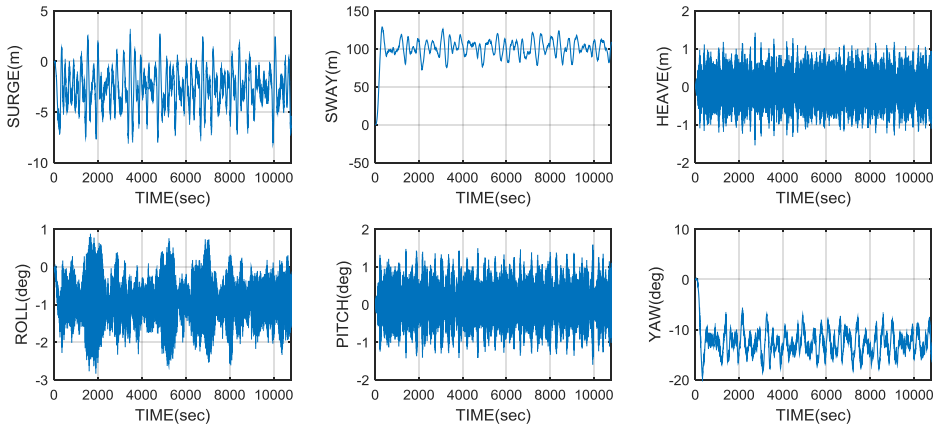

Figure 77. Test result: ZCG=7m under 10-year extreme condition (Part 1)

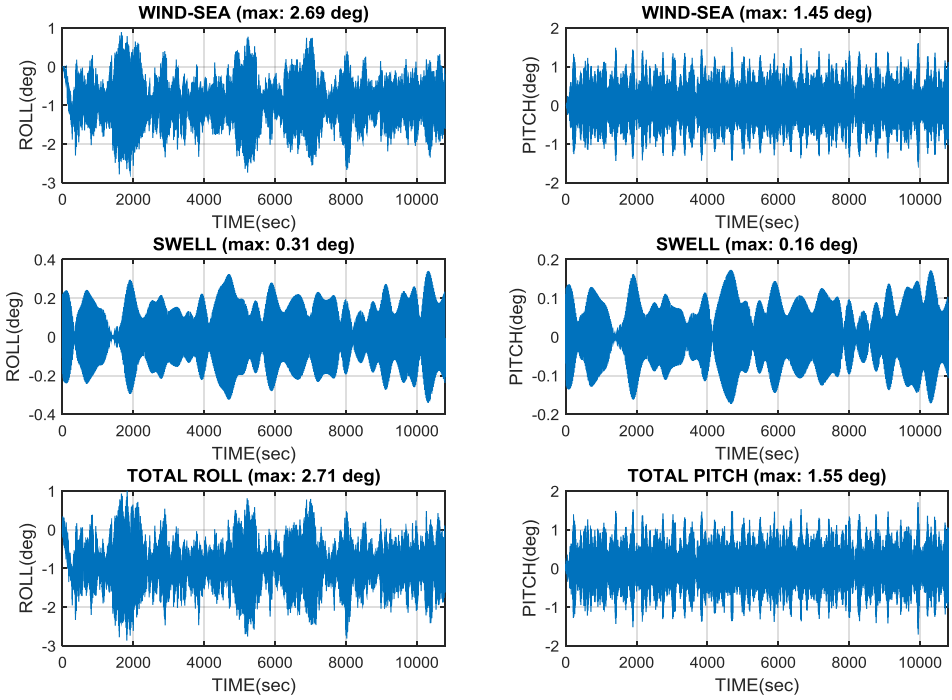

Figure 78. Test result: ZCG=7m under 10-year extreme condition (Part 1+ Part 2)

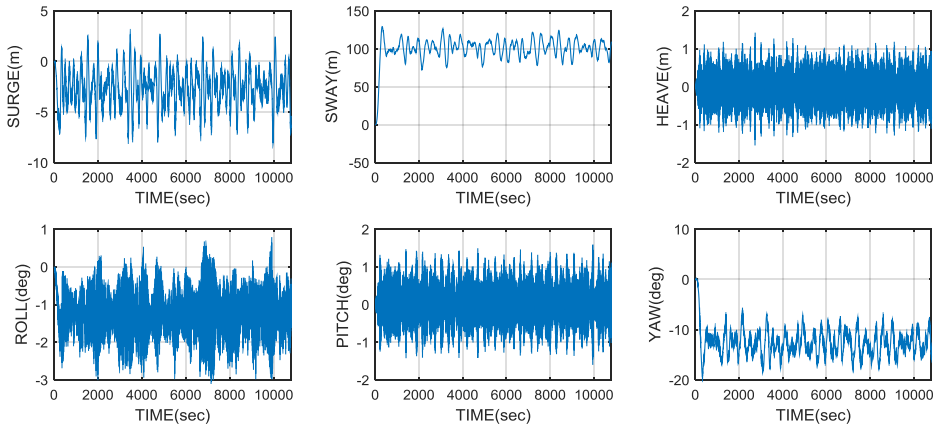

Figure 79. Test result: ZCG=9m under 10-year extreme condition (Part 1)

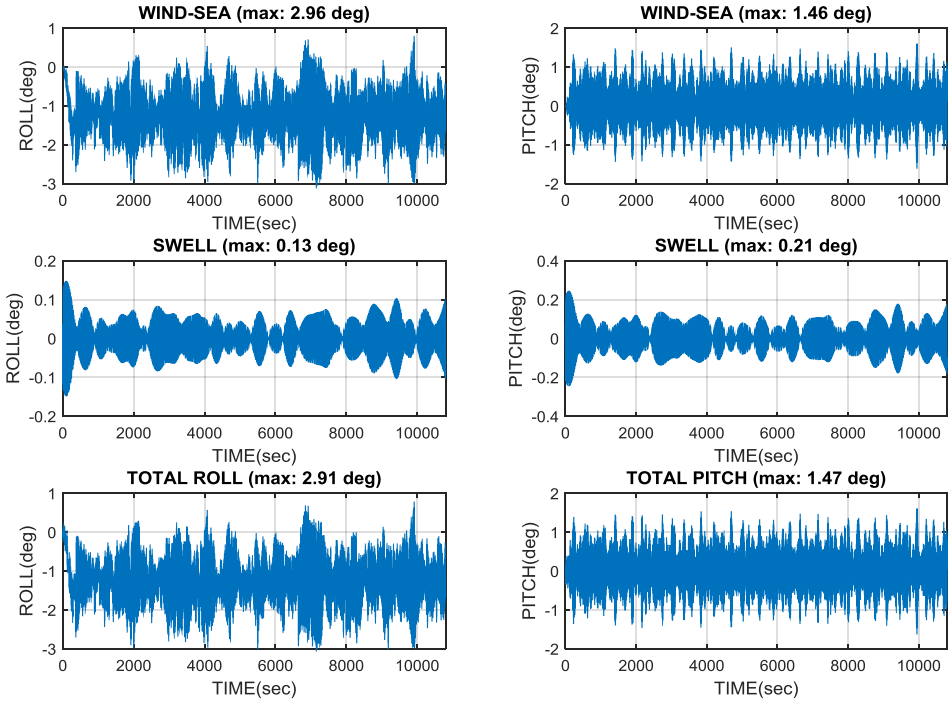

Figure 80. Test result: ZCG=9m under 10-year extreme condition (Part 1+ Part 2)

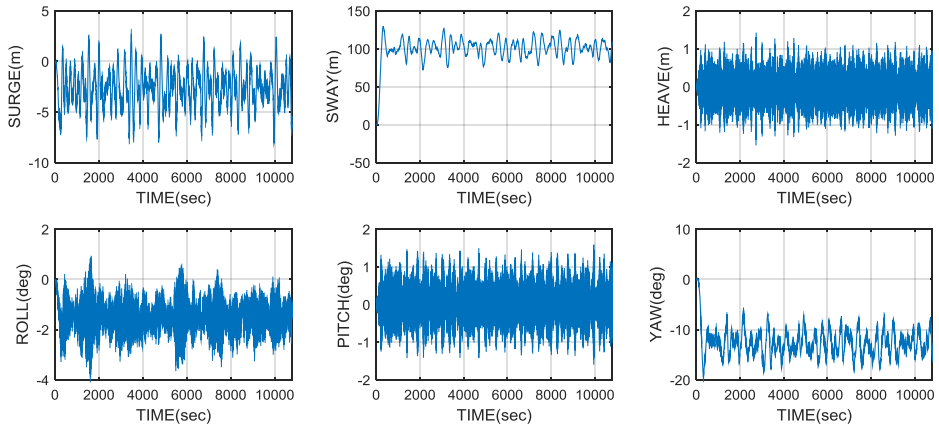

Figure 81. Test result: ZCG=10m under 10-year extreme condition (Part 1)

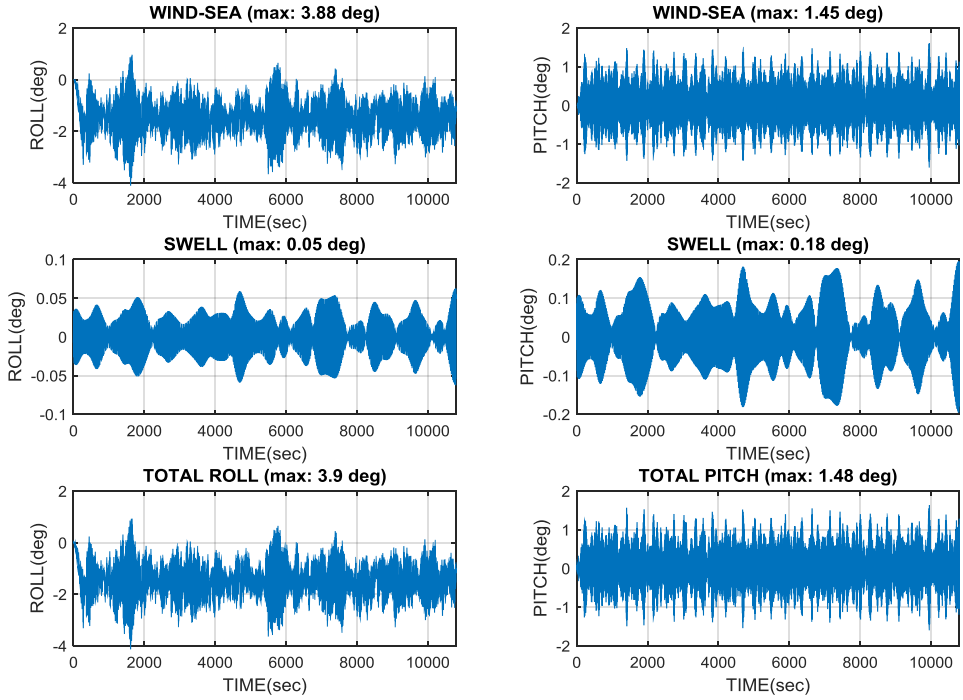

Figure 82. Test result: ZCG=10m under 10-year extreme condition (Part 1+ Part 2)

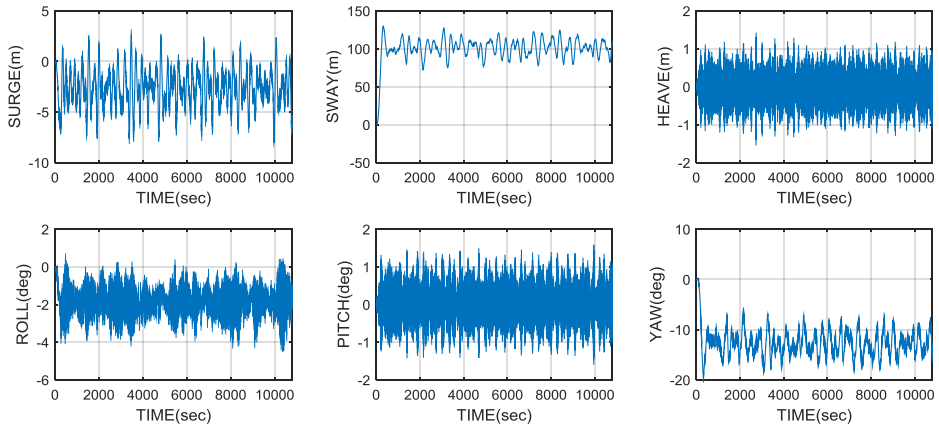

Figure 83. Test result: ZCG=11m under 10-year extreme condition (Part 1)

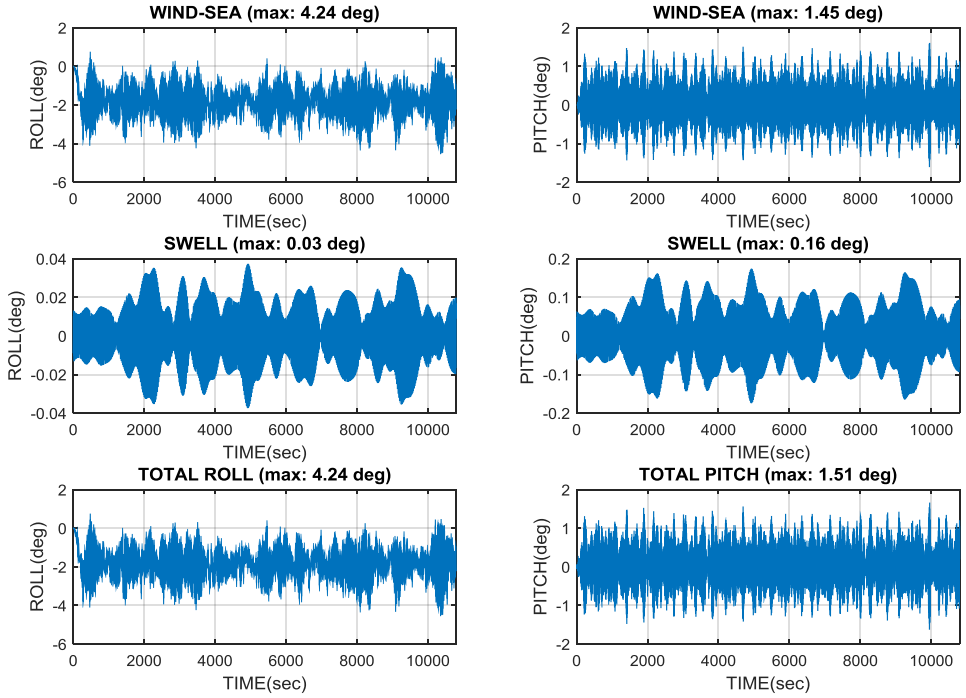

Figure 84. Test result: ZCG=11m under 10-year extreme condition (Part 1+ Part 2)

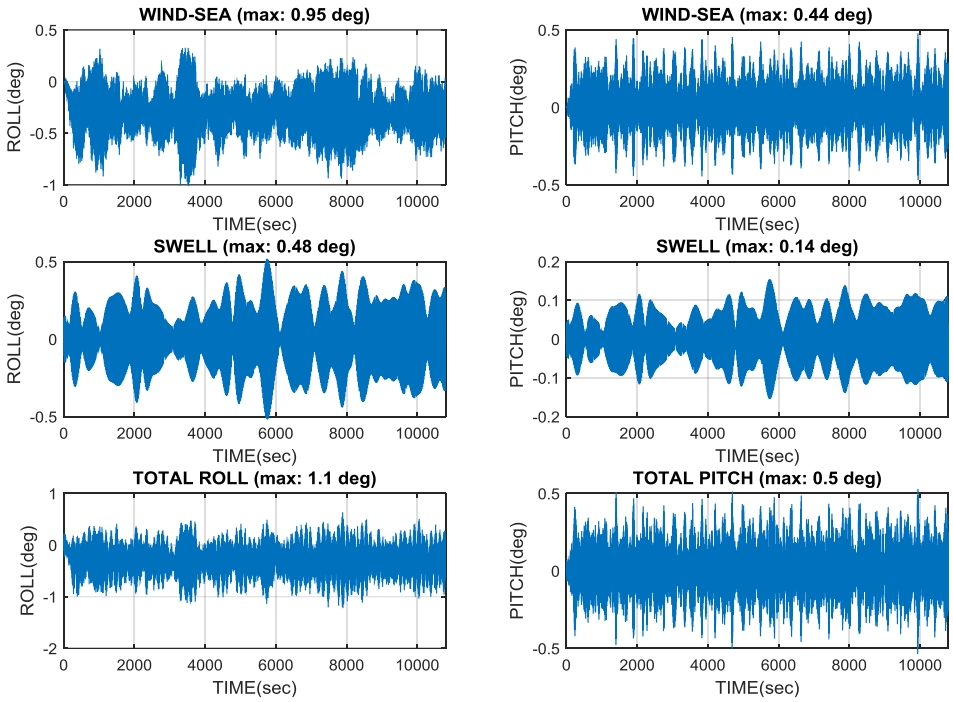

Figure 85. Test result: ZCG=5m under 1-year extreme condition (Swell BETA=250)

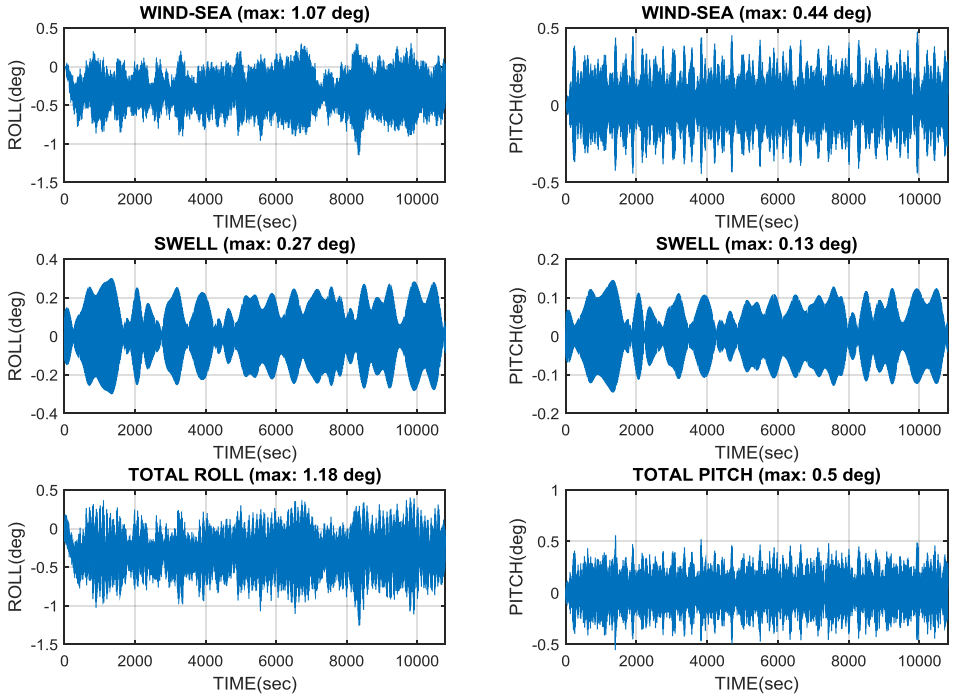

Figure 86. Test result: ZCG=6m under 1-year extreme condition (Swell BETA=250)

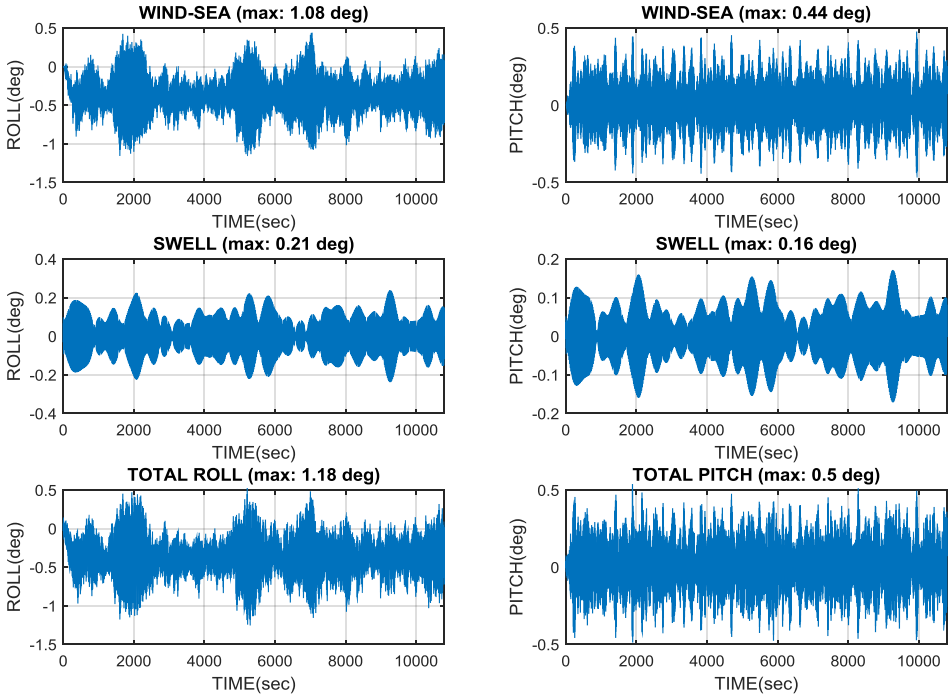

Figure 87. Test result: ZCG=7m under 1-year extreme condition (Swell BETA=250)

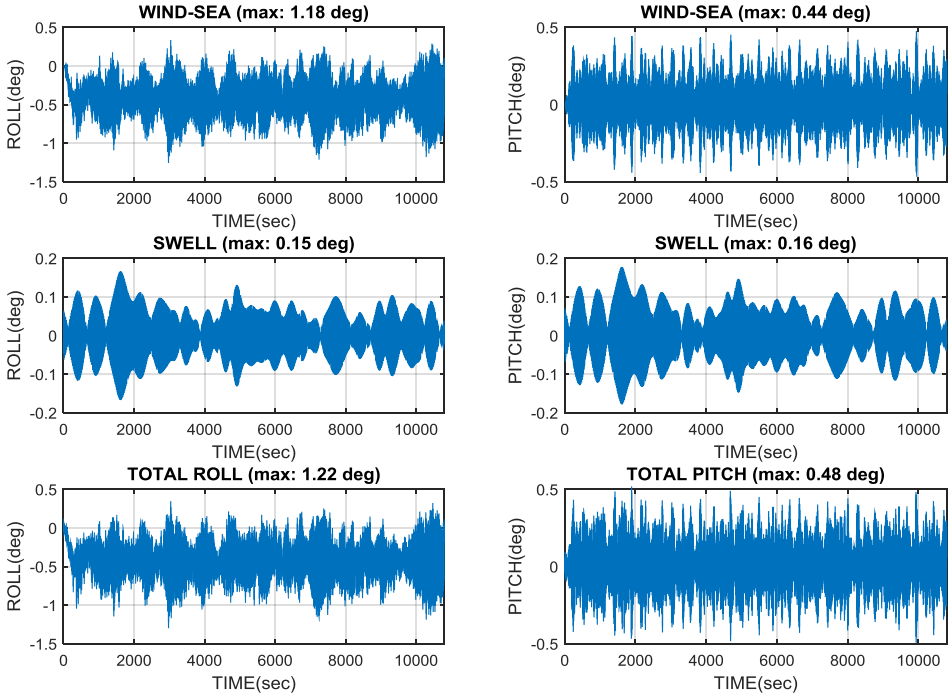

Figure 88. Test result: ZCG=8m under 1-year extreme condition (Swell BETA=250)

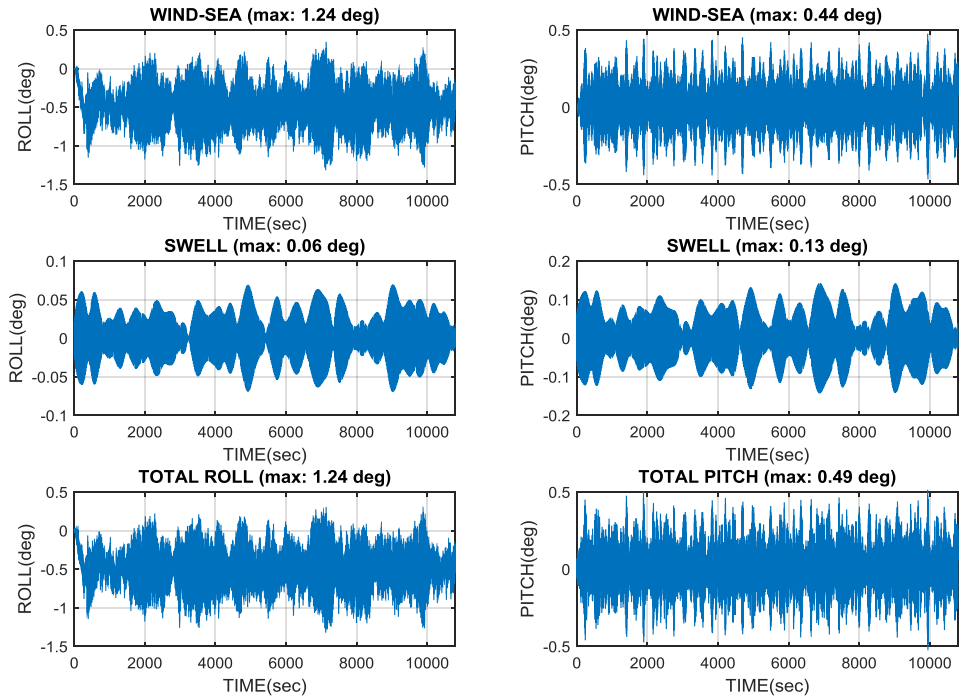

Figure 89. Test result: ZCG=9m under 1-year extreme condition (Swell BETA=250)

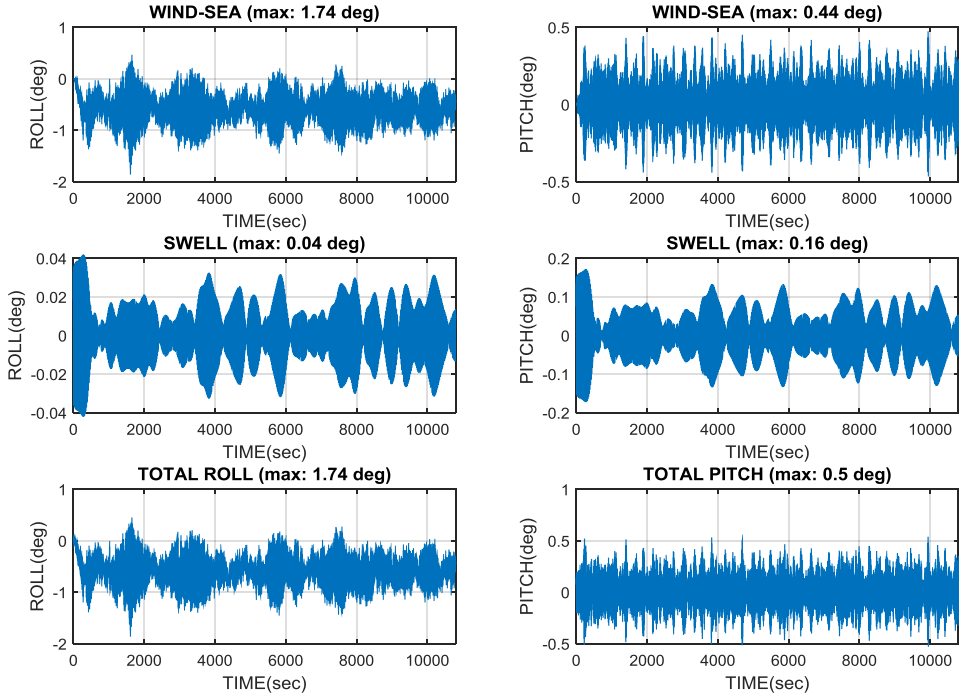

Figure 90. Test result: ZCG=10m under 1-year extreme condition (Swell BETA=250)

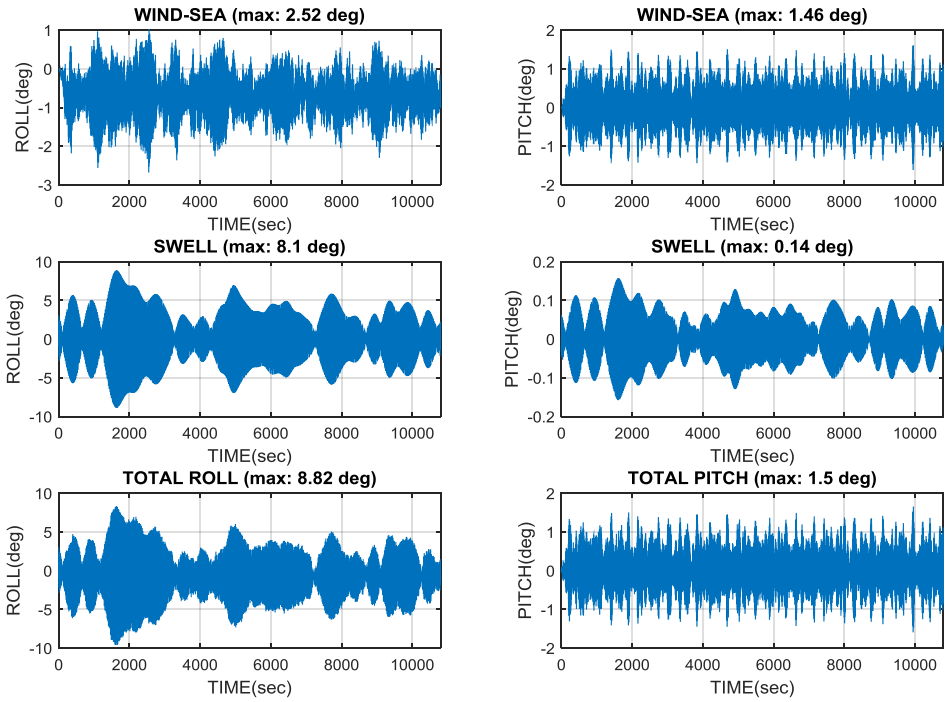

Figure 91. Test result: ZCG=4m under 10-year extreme condition (Swell BETA=250)

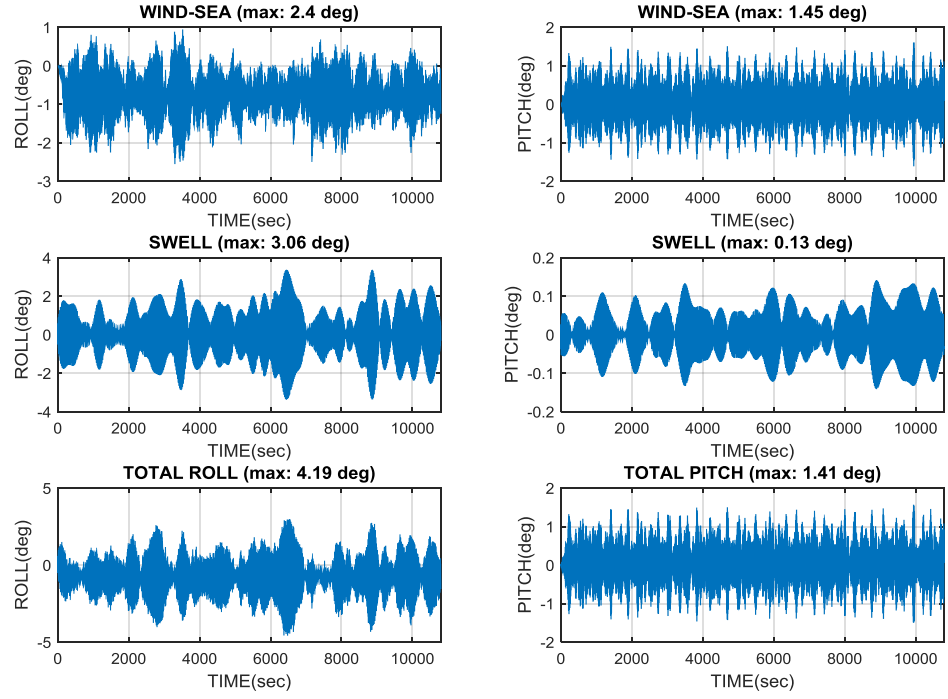

Figure 92. Test result: ZCG=5m under 10-year extreme condition (Swell BETA=250)

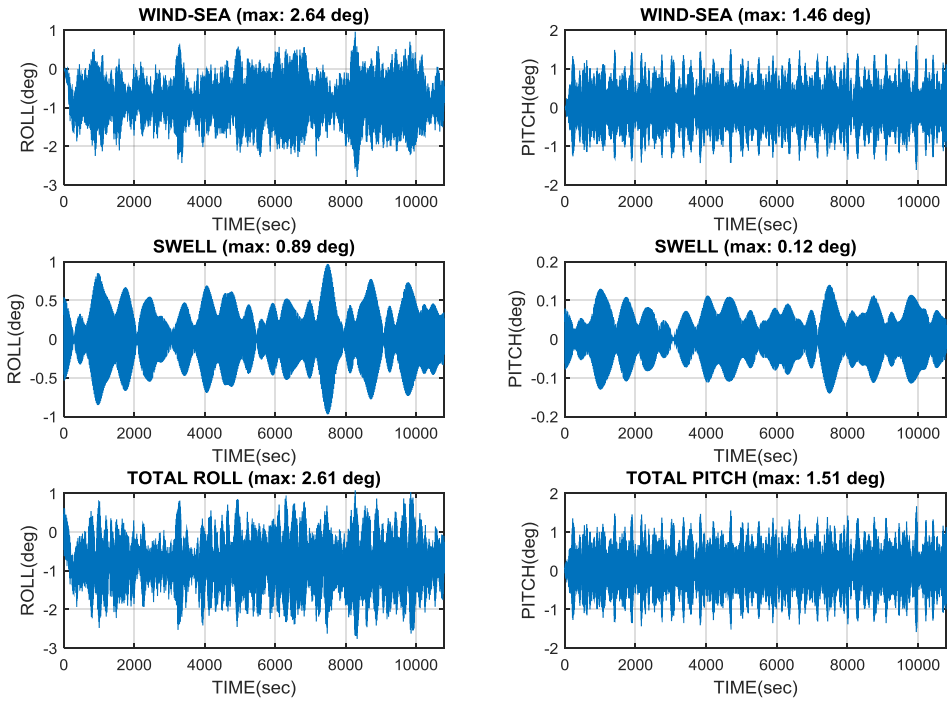

Figure 93. Test result: ZCG=6m under 10-year extreme condition (Swell BETA=250)

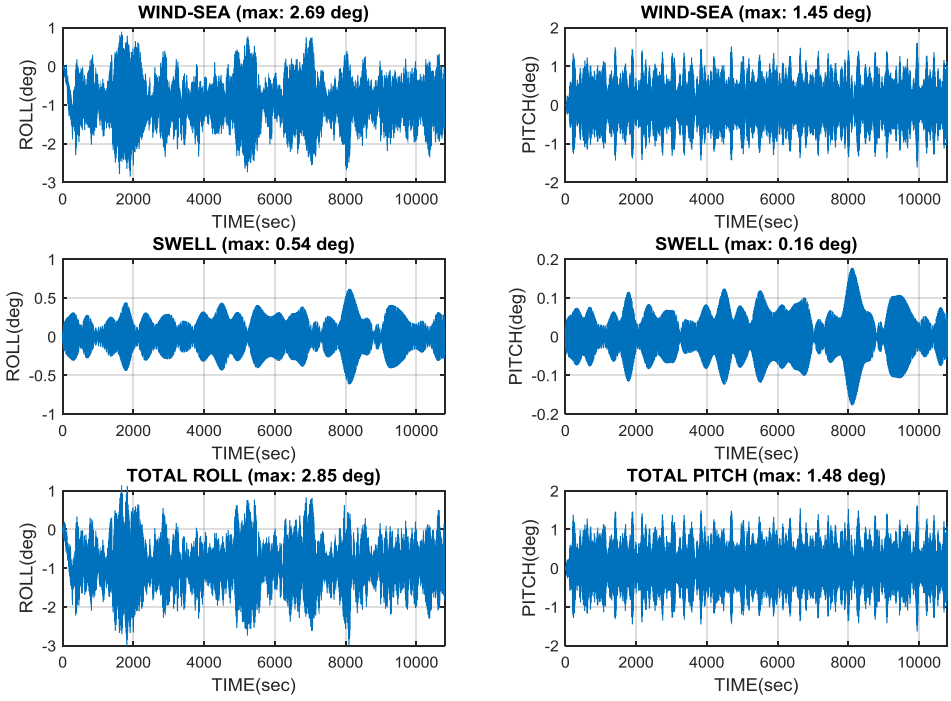

Figure 94. Test result: ZCG=7m under 10-year extreme condition (Swell BETA=250)

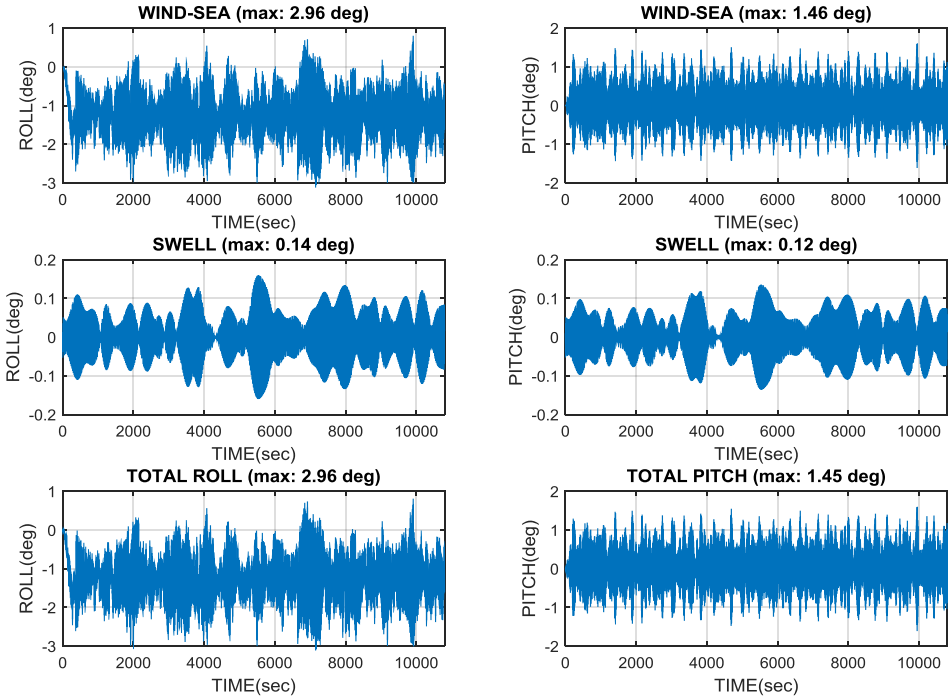

Figure 95. Test result: ZCG=9m under 10-year extreme condition (Swell BETA=250)

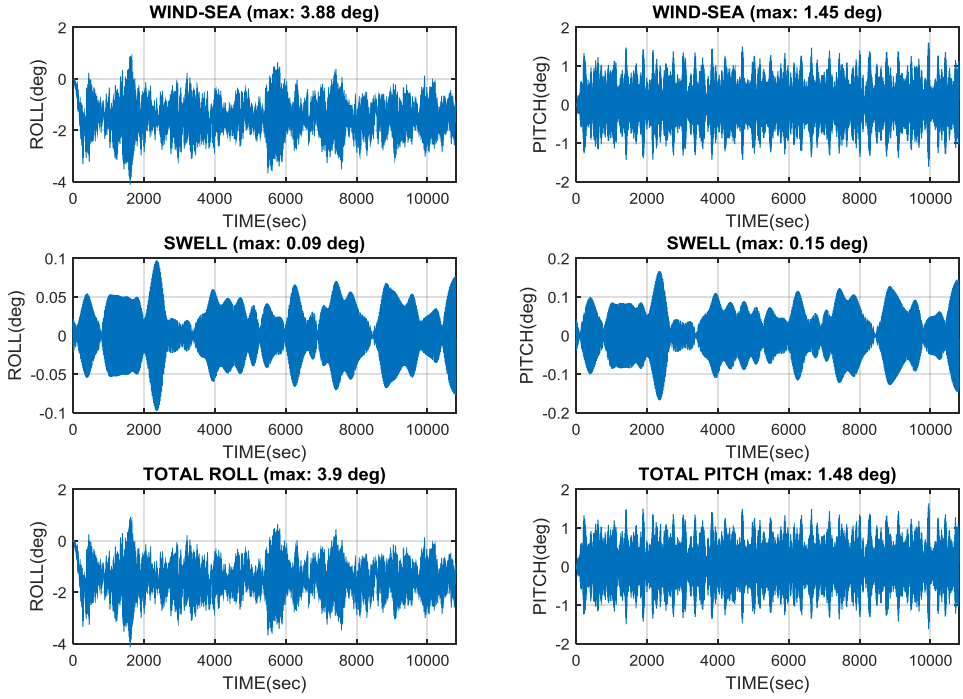

Figure 96. Test result: ZCG=10m under 10-year extreme condition (Swell BETA=250)